University of South-Eastern Norway

www.usn.no

FMH606 Master's Thesis 2020

Energy and Environmental Technology

# Cost-effective and safe oil production from existing and near-future oil fields

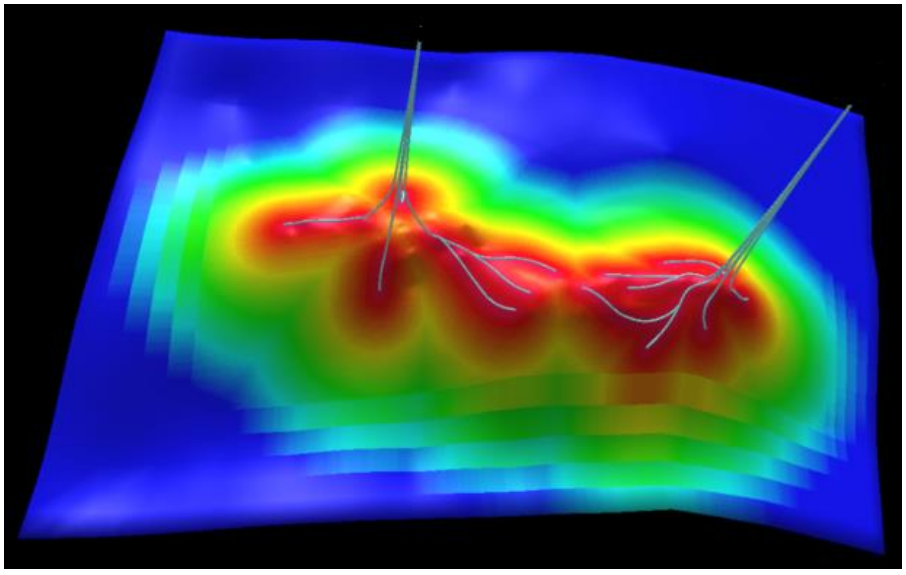

Ali Moradi

Faculty of Technology, Natural sciences and Maritime Sciences

Campus Porsgrunn

University of South-Eastern Norway

www.usn.no

**Course**: FMH606 Master's Thesis, 2020

**Title**: Cost-effective and safe oil production from existing and near-future oil fields

**Number of pages**: 153

**Keywords**: Near-well simulation, Horizontal well, EOR, OLGA, ROCX, ICD, AICD, RCP
Water breakthrough, Water coning, Heel-toe effect, Johan Sverdrup field

**Student:** Ali Moradi

**Supervisor:** Prof. Britt M. E. Moldestad

**External partner:** -

**Availability:** Open

*The University of South-Eastern Norway takes no responsibility for the results and conclusions in this student report.*

University of South-Eastern Norway

www.usn.no

**Summary:**

Despite the rapid progress in the area of renewable energy, fossil fuels will remain the world's most important energy source for the foreseeable future. Therefore, in order to meet future energy demands, increasing the efficiency of oil production and reducing carbon footprint from the oil and gas sector must be in the spotlight. One of the main principles of improving oil recovery is maximizing the reservoir contact, and long horizontal wells can be used for achieving this purpose especially in reservoirs with a thin oil column. However, there are some challenges related to horizontal wells like water coning towards the heel due to the heel-toe effect as well as early water breakthrough owing to heterogeneity along the well. In order to tackle these issues, well completion with passive inflow control devices (ICDs) and autonomous inflow control devices (AICDs) are widely used today. ICDs are able to balance the drawdown pressure along the horizontal well and as a result, postpone the early water breakthrough. By applying RCP valves, which are a special type of AICDs, water can be partially choked back in an autonomous way and the negative impacts of early water breakthrough will be attenuated.

The Johan Sverdrup field is a giant oil field located in the North Sea and it started production in October 2019. With the aim of obtaining maximum oil recovery and minimum environmental footprint, cutting-edge technologies have been applied in this field and further studies are needed to improve these technologies. The main objectives of this thesis are near-well simulation and study of oil production from a horizontal well with ICD and RCP completion. The simulations have been conducted based on the characteristics of the well number 16/2-D-12 in the Johan Sverdrup field by considering both homogeneous and heterogeneous reservoirs. OLGA in combination with ROCX has been used as a simulation tool. In this study, by using a new method based on developing a mathematical model and a control function for the RCP valves, the autonomous behavior of these valves has been implemented in OLGA.

The results showed that the well 16/2-D-12 with ICD and RCP completion can effectively handle the heel-toe effect and heterogeneity along the well, and consequently delay early water breakthrough and improve the oil recovery from this reservoir. Based on the simulation results, by using these inflow control devices for the well 16/2-D-12, the time of water breakthrough can be delayed by 253 days in the homogeneous reservoir and 255 days in the heterogeneous reservoir compared to the open-hole well. Moreover, it was observed that for the homogeneous and heterogeneous reservoirs, by completion of the well 16/2-D-12 with RCP valves, the accumulated water production can be reduced by 12.1% and 11.9% respectively during the first 750 days of production. Besides, using RCPs can reduce the flow rate of water production by 13.3% in the homogeneous and 13.4% in the heterogeneous reservoir after 750 days. For both homogeneous and heterogeneous reservoirs, by using RCP valves the outlet water cut can be reduced by 2.9% resulting in more cost-effective oil production. Furthermore, by evaluating the simulation results it can be concluded that using RCP valves has a negligible impact on both the accumulated oil production and the flow rate of oil production compared to using ICDs. Therefore, by completion of the well 16/2-D-12 with RCP valves more cost-effective oil production can be achieved.

*The University of South-Eastern Norway takes no responsibility for the results and conclusions in this student report.*

# Preface

This master's thesis presents the final outcome of the research work carried out in spring 2020 at the University of South-Eastern Norway (USN), Porsgrunn. It has been written to fulfill the graduation requirements of the Master of Science degree at USN.

The main objective of the thesis is to study and develop a simulation model for cost-effective and safe oil production from existing and near-future oil fields. The thesis description has been presented in Appendix A.

It was a highly valuable experience for me to be involved in this research project and to work under the close supervision of Prof. Britt Margrethe Emilie Moldestad.
First and foremost, I would like to express my sincere gratitude and appreciation to Prof. Britt M. E. Moldestad for her great support throughout this work. She always was available when I needed help and I benefited a lot from her knowledge and guidance to carry out this study.
I would also like to thank the staff of the IT department, especially Mr. Aleksander Svanberg for providing me with various technical supports related to the needed software.
Finally, I would like to thank my beloved wife Nastaran, who always was there for me during this journey, and encouraged me to do my best in completing this thesis.

Porsgrunn, May 25, 2020

Ali Moradi

# Contents


**1 Introduction ..... 17**

**1.1 Background of the study ..... 17**
**1.2 Problem description ..... 19**
**1.3 Objectives ..... 20**
**1.4 Thesis outline ..... 20**

**2 Literature review ..... 21**

**2.1 Cost-effective and enhanced oil recovery ..... 21**
***2.1.1 A brief description of EOR methods ..... 22***
***2.1.2 Potential of different EOR methods for Norwegian oil fields ..... 24***
***2.1.3 Geographical analysis of suitable EOR methods on NCS ..... 25***
***2.1.4 Cost estimation of different EOR methods ..... 26***
**2.2 Horizontal wells ..... 26**
***2.2.1 Characteristics of horizontal wells ..... 26***
***2.2.2 Gas and water coning ..... 27***
**2.3 Inflow control technologies ..... 29**
***2.3.1 Passive Inflow Control Devices ..... 29***
***2.3.2 Autonomous Inflow Control Devices ..... 30***
**2.4 Modeling and simulation of oil production ..... 33**

**3 Theoretical background ..... 34**

**3.1 Reservoir rock properties ..... 34**
***3.1.1 Porosity ..... 34***
***3.1.2 Absolute permeability ..... 35***
***3.1.3 Fluid saturation ..... 38***
***3.1.4 Wettability ..... 38***
***3.1.5 Capillary Pressure ..... 40***
***3.1.6 Relative Permeability ..... 41***
**3.2 Reservoir fluid properties ..... 42**
***3.2.1 Physical classification of crude oils ..... 43***
***3.2.2 Classification of reservoir fluids ..... 43***
***3.2.3 Black oil models ..... 45***
***3.2.4 Multiphase flow measurement terms ..... 46***
**3.3 Productivity index for horizontal wells ..... 47**
**3.4 Pressure drop in horizontal wells ..... 49**
**3.5 General mathematical models for ICDs and RCPs ..... 50**
***3.5.1 Passive inflow control devices (ICDs), orifice type ..... 50***
***3.5.2 Autonomous inflow control devices (AICDs), RCP type ..... 51***
**3.6 Linear regression ..... 54**

**4 Johan Sverdrup oil field ..... 55**

**4.1 Well 16/2-D-12 ..... 56**
**4.2 Characteristics of the reservoir near the well 16/2-D-12 ..... 56**
***4.2.1 Reservoir pressure and temperature ..... 57***
***4.2.2 Reservoir fluid properties ..... 57***
***4.2.3 Reservoir rock properties ..... 58***

**5 Methods and calculations ..... 64**

**5.1 Calculation of crude oil viscosity at the reservoir conditions ..... 64**
**5.2 Calculation of the permeability anisotropy ..... 65**

**5.3 Calculation of the horizontal length and production of the well 16/2-D-12 ..... 66**
***5.3.1 Calculation of the length of the horizontal section ..... 66***
***5.3.2 Estimation of the oil production ..... 67***
**5.4 Calculation of the frictional pressure drop ..... 67**
**5.5 Calculation of the productivity index for the well 16/2-D-12 ..... 67**
**5.6 Developing a mathematical model for RCP valves ..... 67**
***5.6.1 Extracting experimental data for the performance of the TR7 RCP valve ..... 68***
***5.6.2 Driving the mathematical equation for the TR7 RCP valve based on the experimental data ..... 69***
**5.7 Calculation of the average pressure drop across the TR7 RCP valve and the number of them for the well 16/2-D-12 ..... 72**
**5.8 Developing a control function for implementing RCP behavior in OLGA ..... 72**
**5.9 Estimation of the pressure drawdown for the well 16/2-D12 ..... 75**

**6 Development of the OLGA/ROCX model ..... 78**

**6.1 Development of the reservoir model in ROCX ..... 78**
***6.1.1 Determining the dimensions of the reservoir drainage area ..... 78***
***6.1.2 Grid setting and mesh sensitivity analysis ..... 80***
***6.1.3 Fluid property settings ..... 84***
***6.1.4 Reservoir property settings ..... 86***
***6.1.5 Relative permeability setting ..... 87***
***6.1.6 Initial condition settings ..... 87***
***6.1.7 Boundary condition settings ..... 88***
***6.1.8 Simulation settings ..... 88***
**6.2 Development of the well model in OLGA ..... 88**
***6.2.1 Case definition settings ..... 88***
***6.2.2 Compositional settings ..... 88***
***6.2.3 Flow component settings ..... 88***
**6.3 Simulated cases ..... 91**

**7 Results and discussion ..... 92**

**7.1 Fluid flow distribution and time of water breakthrough ..... 92**
**7.2 Performance of the implemented RCP valve in OLGA for choking the water ..... 98**
**7.3 Comparing the functionality of the ICDs and RCP valves in the homogenous reservoir ..... 100**
***7.3.1 Accumulated oil and water production ..... 100***
***7.3.2 Oil and water flow rate ..... 101***
***7.3.3 Outlet water cut ..... 103***
**7.4 Comparing the functionality of the ICDs and RCP valves in the heterogeneous reservoir ..... 104**
***7.4.1 Accumulated oil and water production ..... 104***
***7.4.2 Oil and water flow rate ..... 106***
***7.4.3 Outlet water cut ..... 107***
**7.5 Discussion ..... 108**
***7.5.1 Effect of the grid resolution on the simulation results ..... 108***
***7.5.2 Effect of the width of the drainage area on the simulation results ..... 109***
***7.5.3 Impact of heel-toe effect on oil production ..... 109***
***7.5.4 Impact of heterogeneity on oil production ..... 109***
***7.5.5 Performance of the implemented RCP valve in OLGA ..... 109***
***7.5.6 Accuracy of the calculated pressure drawdown used in developing the OLGA/ROCX model ..... 110***
***7.5.7 Functionality of ICDs and RCPs in enhancing oil recovery from the well 16/2-D-12 ..... 110***

**8 Conclusion ..... 111**

**References ..... 114**

**Appendicies …….. 119**

# Nomenclature

## Symbols and expressions

| | | |
|---|---|---|
| $a$ | Width of the near-well reservoir | m |
| $A$ | Area | $m^2$ |
| $a_{AICD}$ | RCP valve strength parameter | - |
| $A_{vc}$ | Vena Contracta area | $m^2$ |
| $b$ | Length of the near-well reservoir | m |
| $C_D$ | Discharge coefficient | - |
| $C_H$ | Babu and Odeh model parameter | - |
| $D, d$ | Diameter | m |
| $f$ | Mody friction factor | - |
| $h$ | Thickness of the near-well reservoir | m |
| $I_{AH}$ | Amott-Harvey wettability index | - |
| $J$ | Productivity index | bbl/psi/day |
| $k$ | permeability | D (Darcy) |
| $k_H$ | Horizontal permeability | - |
| $k_i$ | Permeability in the *i*-directions | - |
| $k_{ro}$ | Relative permeability for oil | - |
| $k_{rowc}$ | Relative permeability of oil at irreducible water saturation | - |
| $k_{rw}$ | Relative permeability for water | - |
| $k_{rwoc}$ | Relative permeability of water at residual oil saturation | - |
| $k_v$ | Vertical Permeability | - |
| $L$ | Length | m |
| $n_i$ | Number of cells in the *i*-direction in the grid setting | - |

| | | |
|---|---|---|
| $n_{ow}$ | Corey coefficients for oil | - |
| $n_w$ | Corey coefficient for water | - |
| $P_b$ | Bubble point pressure | Pa |
| $P_c$ | Capillary pressure | Pa |
| $P_{cgo}$ | Gas-oil capillary pressure | Pa |
| $P_{cgw}$ | Gas-water capillary pressure | Pa |
| $Q,\ \dot{Q}$ | Volumetric flow rate | $m^3/s$ |
| $R$ | Radius | m |
| Re | Reynolds number | - |
| $R_{sb}$ | Solution gas-oil ratio | - |
| $r_w$ | Radius of wellbore | m |
| $S_g$ | Gas saturation | - |
| $S_o$ | Oil saturation | - |
| $S_{or}$ | Residual oil saturation | - |
| $S_{ow}$ | Oil-water interface tension | Pa |
| $S_r$ | Babu and Odeh model parameter | - |
| $S_w$ | Water saturation | - |
| $S_{wc}$ | Connate (irreducible) water saturation | - |
| $T$ | Temperature | ˚C, K |
| $v$ | Fluid velocity | m/s |
| $V_{sh}$ | Volume fraction of shale | - |
| $x$ | RCP coefficient | - |
| $y$ | RCP coefficient | - |
| $\rho$ | Fluid density | $kg/m^3$ |

| | | |
|---|---|---|
| $\rho_{cal}$ | Calibration density | kg/m$^3$ |
| $\rho_{mix}$ | Mix density | kg/m$^3$ |
| $\mu_{mix}$ | Mix viscosity | cP |
| $\mu_{cal}$ | Calibration viscosity | cP |
| $\Delta P$ | Differential pressure | Pa |
| $\phi$ | Porosity | - |
| $\phi_e$ | Effective porosity | - |
| $\theta_{ow}$ | Water-oil contact angle | ° |
| $\gamma_o$ | Specific gravity of crude oil | - |
| $\gamma_g$ | Specific gravity of gas | - |
| $\varepsilon$ | Pipe roughness | m |
| $\Delta P_{friction}$ | Frictional pressure drop | Pa |
| $\alpha_i$ | Volume fraction of phase *i* | - |

## Abbreviations

| | |
|---|---|
| AICD | Autonomous Inflow Control Device |
| AICV | Autonomous Inflow Control Valve |
| API | American Petroleum Institute |
| bbl | barrels 159 liter |
| EOR | Enhanced Oil Recovery |
| EOS | Equation-Of-States |
| GI | Gas Injection |
| GLR | Gas-Liquid Ratio |

| | |
|---|---|
| GOR | Gas Oil Ratio |
| ICD | Inflow Control Device |
| JSF | Johan Sverdrup Field |
| mD | milli Darcy |
| MD | Measured Depth |
| NCS | Norwegian Continental Shelf |
| NPD | Norwegian Petroleum Directorate |
| PVT | Pressure-Volume-Temperature |
| RCP | Rate Controlled Production |
| scf | standard cubic foot |
| stb | stock tank barrel |
| TVD | True Vertical Depth |
| WAG | Water Alternating Gas |
| WC | Water Cut |

# Overview of tables and figures

## List of Figures

Figure 1.1: World primary energy supply by source [2]. ....17

Figure 1.2: Resource overview for the 27 fields on the NCS [3]. ....18

Figure 2.1: Resource overview and EOR potential on the 27 largest NCS oil fields [3]. ....21

Figure 2.2: A simplified presentation of the difference between (a) water and (b) polymer flooding [9]. ....22

Figure 2.3: Schematic of challenges and benefits of (a) gas injection, (b) water alternating gas injection, and (c) water+surfactant alternating gas injection [10]. ....24

Figure 2.4: Mid-range estimates and uncertainty ranges for the potential of EOR in the fields on NCS [3]. ....25

Figure 2.5: Suitable EOR methods for different areas on the NCS [3]. ....25

Figure 2.6: Horizontal well categories based on the buildup rate [18]. ....27

Figure 2.7: Schematic of gas and water coning. ....28

Figure 2.8: Heel-to effect in the homogeneous reservoir [20]. ....28

Figure 2.9: Liquid production from different zones in a heterogeneous reservoir [4]. ....29

Figure 2.10: Application of ICDs in mitigation of the early water breakthrough [22]. ....30

Figure 2.11: Statoil's RCP valve and its schematic sketch [23]. ....31

Figure 2.12: Volume flow of oil (460 cp), water and gas through RCP as a function of differential pressure [23]. ....31

Figure 2.13: Oil/water and oil/gas ratios as a function of differential pressure for oil with a viscosity of 460 cP [23]. ....32

Figure 2.14: Schematic of well completion with RCP valves in a heterogeneous reservoir [25]. ....32

Figure 3.1: Conceptual representation of different types of pores in a reservoir rock [35]. ....34

Figure 3.2: Darcy experiment expressed by a schematic representation of fluid flow through a core plug [35]. ....35

Figure 3.3: Radial flow system for the characterization of fluid flow into the wellbore [35]. 36

Figure 3.4: Horizontal well drainage pattern [36]. ....37

Figure 3.5: Schematic representation of water-wet and oil-wet pore spaces [35]. ....39

Figure 3.6: Typical oil-wet rock relative permeabilities (left) versus water-wet rock relative permeabilities. (right) [42]. ....42

Figure 3.7: Pressure-temperature phase diagram for a single-compound system [45]. ....44

Figure 3.8: Phase envelope for a hydrocarbon mixture [45]. ....45

Figure 3.9: Phase envelope of a typical black oil [35]. ..... 46
Figure 3.10: Well and reservoir geometry, and nomenclature used in the Babu and Odeh model [52]. ..... 48
Figure 3.11: Schematic model of orifice ICDs [55]. ..... 50
Figure 3.12: Schematic of a thin orifice plate in the middle of a pipe. ..... 50
Figure 3.13: RCP flow pass [58]. ..... 52
Figure 3.14: Schematic of the simplified RCP valve for analytical solving [59]. ..... 53
Figure 4.1: Johan Sverdrup field map [5]. ..... 55
Figure 4.2: Drilling information and the location of the well 16/2-D-12 in the Johan Sverdrup oil field [64]. ..... 56
Figure 4.3: West to east cross-section of the JSF [67]. ..... 58
Figure 4.4: Composite well log displays from well 16/2-8 [66]. ..... 59
Figure 4.5: Calculated porosity of the well 16/2-8 by using different methods [66]. ..... 60
Figure 4.6: Median permeability for individual wells in the JSF [68]. ..... 61
Figure 4.7: Relative permeability curves for the Johan Sverdrup reservoir. ..... 63
Figure 5.1: Estimation of crude oil viscosity of JSF at the reservoir temperature. ..... 65
Figure 5.2: Schematic figure of measured depth and total depth [73]. ..... 66
Figure 5.3: Experimental results for the performance of the TR7 RCP valve under single-phase fluid flow[57]. ..... 68
Figure 5.4: Mathematical model of the TR7 RCP valve compare to the experimental values. ..... 71
Figure 5.5: Valve opening versus water cut for the TR7 RCP valve under JSF conditions. ..... 74
Figure 5.6: Implementation of autonomous behavior of the TR7 RCP valve by using the Table Controller. ..... 75
Figure 5.7: Schematic of the pressure variation in for the well 16/2-D-12. ..... 76
Figure 6.1: Analysis of oil production from a well with different width of the drainage area. ..... 79
Figure 6.2: Schematic geometry of the drainage area. ..... 79
Figure 6.3: Pressure drop near an open hole oil production well [45]. ..... 80
Figure 6.4: Grid setup for mesh sensitivity analysis in the (a) *z*-direction and (b) *y*-direction. ..... 81
Figure 6.5: Sensitivity of oil and water production to the number of grids in the *z*-direction. 82
Figure 6.6: Sensitivity of oil and water production to the number of grids in the *y*-direction. 83
Figure 6.7: Y-Z, X-Z and 3D view of the grid resolution and the well position in the Y-Z plane. ..... 84

Figure 6.8: Permeability distribution in (a) homogeneous reservoir (b) heterogeneous reservoir. ....86

Figure 6.9: Initial water saturation in the reservoir.....87

Figure 6.10: Simplified representation of a single production zone. ....89

Figure 6.11: Representation of the RCP valve control setup in OLGA.....90

Figure 7.1: Outlet water cut from the well 16/2-D-12 for the open-hole conditions.....93

Figure 7.2: Oil saturation distribution after 10 days for open-hole well in (a) Homogeneous reservoir (b) Heterogeneous reservoir. ....94

Figure 7.3: Outlet water cut from the well 16/2-D-12 for the simulation cases. ....95

Figure 7.4: Wellbore water cut along the well 16/2-D-12 at the 265$^{th}$ day of production for the homogeneous and heterogeneous reservoir. ....96

Figure 7.5: Oil saturation distribution for (a) Homogeneous reservoir and (b) Heterogeneous reservoir, right after water breakthrough in the homogeneous reservoir. ....97

Figure 7.6: Performance of the RCP valve located in the toe and heel sides of the well in the homogeneous reservoir. ....98

Figure 7.7: Performance of the RCP valve located in the low permeable and high permeable zones in the heterogeneous reservoir. ....99

Figure 7.8: Accumulated oil and water form the well 16/2-D-12 with ICD and RCP completion in the homogeneous reservoir. ....101

Figure 7.9: Flow rate of oil and water for the well 16/2-D-12 with ICD and RCP completion in the homogeneous reservoir. ....102

Figure 7.10: Outlet water cut as well as water cut along the production tubing after 750 days for the well 16/2-D-12 in the homogeneous reservoir. ....103

Figure 7.11: Accumulated oil and water from the well 16/2-D.12 with ICD and RCP completion in the heterogeneous reservoir. ....105

Figure 7.12: Flow rate of oil and water for the well 16/2-D-12 with ICD and RCP completion in the heterogeneous reservoir. ....106

Figure 7.13: Outlet water cut as well as the water cut along the production tubing after 750 days for the well 16/2-D-12 in the heterogeneous reservoir. ....107

# List of Tables

Table 3.1: Quiec's wettability classification based on the Amott-Harvey wettability index, $I_{AH}$ [35]. ....40

Table 3.2: Basic characteristics of the five types of reservoir fluids [35]. ....44

Table 3.3: Conditions for using the Lasater model [32]. ....46

Table 4.1: NPD's current resource estimations for the Johan Sverdrup oil field [61].....55

Table 4.2: Crude oil properties in the JSF. ....57

Table 4.3: Thickness of the net pay zone, average water saturation, and shale volume for the well 16/2-8 [66]. ..... 59

Table 4.4: End points and Corey parameters for calculation of relative permeability in the Frøy field [70]. ..... 62

Table 5.1: Results from the permeability anisotropy calculation. ..... 66

Table 5.2: Extracted experimental results for the performance of the TR7 RCP valve from Figure 5.3 ..... 69

Table 5.3: Calculated values of RCP coefficients for the mathematical model of RCP valves. ..... 71

Table 5.4: The number of required TR7 RCP valves and the pressure drop across each valve. ..... 72

Table 5.5: Cross-sectional area and diameter of the equivalent orifice hole for each joint in the well 16/2-D-12. ..... 73

Table 5.6: Control signal table for controlling the TR7 RCP valve in the JSF conditions. ..... 75

Table 5.7: Pressure drawdown and outlet pressure of the tubing for the well 16/2-D-12. ..... 77

Table 6.1: Drainage area dimensions of the test cases for the determination of the width of reservoir. ..... 78

Table 6.2: Number of cells and their sizes for the grid setting in ROCX. ..... 84

Table 6.3: Reservior oil properties used in developing the OLGA/ROCX model. ..... 85

Table 6.4: Oil and water feed components. ..... 85

Table 6.5: Values for the parameters of the Corey and Stone II model ..... 87

Table 6.6: Specifications of the components used in the zonal production setup in OLGA. ..... 89

Table 6.7: Flow path boundary conditions. ..... 90

Table 6.8: Description of the main simulated cases. ..... 91

Table 7.1: Water breakthrough time for the open-hole well and well with inflow control devices ..... 96

Table 7.2: Performance of the RCP valve under different conditions after 750 days of production. ..... 100

Table 7.3: Values of accumulated oil and water in the homogeneous reservoir after 750 days. ..... 101

Table 7.4: Values of volumetric flow rates of oil and water in the homogeneous reservoir after 750 days. ..... 103

Table 7.5: Outlet water cut from the well 16/2-D-12 in the homogeneous reservoir after 750 days. ..... 104

Table 7.6: Values of accumulated oil and water in the heterogeneous reservoir after 750 days. ..... 105

Table 7.7: Values of volumetric flow rates of oil and water in the heterogeneous reservoir after 750 days. ..... 107

Table 7.8: Outlet water cut from the well 16/2-D-12 in the heterogeneous reservoir after 750 days. ..... 108

# 1 Introduction

This thesis focuses on the study and simulation of new technologies for improving oil recovery. In this chapter, the background, problem description, objectives, and outline of the thesis will be presented.

## 1.1 Background of the study

Since 1859 when the first commercial oil was produced in Pennsylvania [1], oil has been a crucial element of human life and playing an important role in improving the living standards of modern society. According to DNV GL's Energy Transition Outlook 2019 [2], 55% of today's energy consumption is supplied by oil and gas. Also, it is expected that 46% of world energy supply will come from oil and gas in 2050 whereas the share of wind and solar is only 24% at that time. Moreover, world energy demand will reach its peak in 2030. These data indicate that despite rapid progress in the area of renewable energy, oil and gas will remain the most important source of energy for the years to come and there is an urgent need to increase oil and gas production to meet future energy demands. The historical and forecast contribution of various primary energy sources in supplying energy has been illustrated in Figure 1.1.

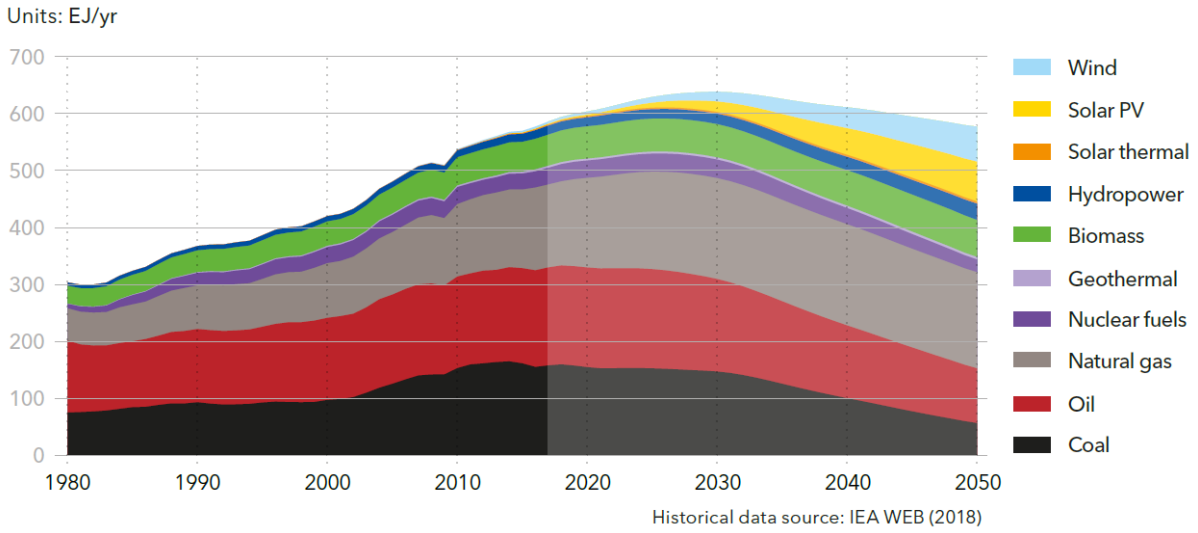


Figure 1.1: World primary energy supply by source [2].

Increasing oil production requires massive investments to explore and develop new oil fields. If the oil price is close to the cost of extraction, most companies will stop their new investments. Therefore, in order to stimulate new investments in the oil industry, new technologies and methods must be applied for increasing the efficiency of oil production and achieving maximum profit per barrel of oil. Besides, since the cost of energy production from renewable sources is relatively high, accelerating the use of sustainable alternatives to fossil fuels needs huge funding. Improving oil recovery and achieving more cost-effective oil production can encourage oil companies and countries with huge oil revenues to provide needed funding for promoting renewable energies.

Figure 1.2 shows the resource overview for the 27 of the largest fields on the Norwegian Continental Shelf (NCS). The gray bar represents the amount of oil that has already been extracted and the dark green bar is showing the oil that will be produced by the time of planned field cessation. Besides, the light green bar illustrates the remaining resources that are not recoverable under current production plans due to the high cost, lack of technology, etc. As can be seen in the figure, more than half of the existing oil in Norway's oil fields, will not be recovered by using current methods and technologies. Therefore, there is great potential for increasing oil production by developing new methods and technologies for enhancing oil recovery.

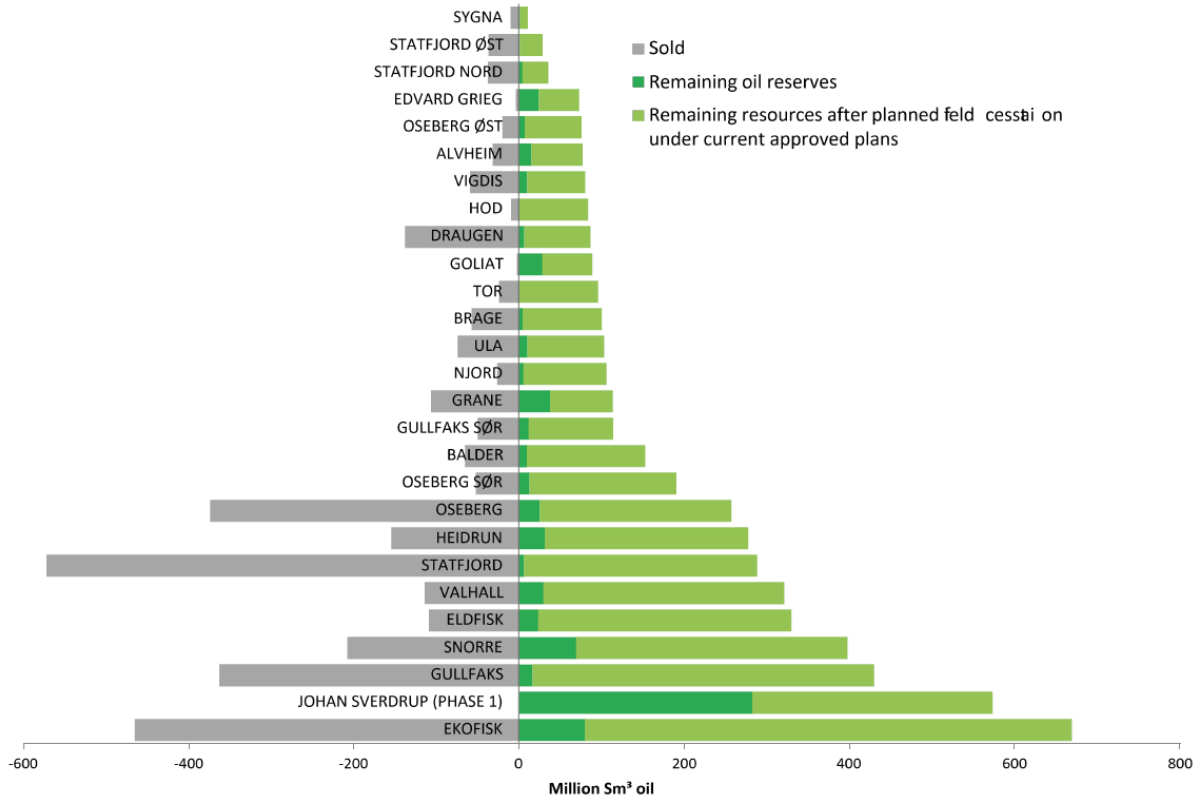


Figure 1.2: Resource overview for the 27 fields on the NCS [3].

In order to develop new technologies for enhancing oil recovery, one of the main principles that should be considered is maximizing the reservoir contact and long horizontal wells can be used for attaining this purpose especially in reservoirs with a thin oil column. However, there are some challenges related to horizontal wells like water coning towards the heel due to the heel-toe effect as well as early water breakthrough owing to heterogeneity along the well. In order to tackle these issues, well completion with passive inflow control devices (ICDs) and autonomous inflow control devices (AICDs) are widely used today. ICDs are able to balance the drawdown pressure along the horizontal well and as a result, postpone the early water breakthrough. By applying AICDs, in addition to postponing the early water breakthrough, water can be partially choked back autonomously and the negative impacts of early water breakthrough will be attenuated [4].

Safe and cost-effective oil production requires a successful design of the oil production system. To fulfill a suitable design of a long horizontal well with ICDs or AICDs completion, a detailed understanding of multiphase flow behavior from reservoir pore to the wellbore and production tubing is needed. In order to achieve this, in the first step, the characteristics of the reservoir should be investigated. In the next step, based on the obtained characteristics and using a reservoir modeling and a dynamic multiphase flow simulator software, a comprehensive model of multiphase flow from the reservoir to the production tubing should be prepared. Finally, this model can be used for the simulation of oil production and it can be a great help in suitable designing of the specification of the horizontal well, choosing the appropriate inflow control valves, determining the required number of valves and distribution of them along the horizontal well, etc. This model also will be used for improving technology, optimizing production, minimizing risk, and reducing costs for any further developments in the future.

## 1.2 Problem description

The Johan Sverdrup field is a giant oil field located in the North Sea and it started production in October 2019. With the aim of obtaining maximum oil recovery and minimum environmental footprint, cutting-edge technologies in the area of long horizontal wells and inflow control devices have been applied in this field [5]. Since there is a plan for developing this oil field in the near future, and a few studies have been done on this filed so far, further studies are needed to promote technologies and obtain more cost-effective oil recovery in this field. Therefore, the thesis focuses on making a model for near well simulation of oil production from the well 16/2-D-12 in the Johan Sverdrup field.

OLGA in combination with ROCX is a robust tool for creating a model of the oil production system. However, preparing a realistic model for simulation of oil production from the well 16/2-D-12 in the Johan Sverdrup field with OLGA/ROCX needs to know the realistic characteristics of this field. Since the extraction of oil from the Johan Sverdrup field has just started, there is limited information available in the literature describing the characteristics of this field. As a result, determining some characteristics of the field like the viscosity of the oil in the reservoir, anisotropy of permeability, wettability and relative permeability, etc. is not straightforward and needs curve-fitting on existing data, calculation by using general equations or some close to the mark assumptions. Moreover, due to the lack of information about the heterogeneity of the reservoir along the well, the model should be prepared for both homogeneous and heterogeneous reservoirs. Besides, since there is no predefined tool in OLGA for implementation of the autonomous behavior of RCP valves, creating a model of oil production by considering well completion with RCPs in OLGA is challenging. To tackle this problem, firstly, based on available experimental data, a mathematical model describing the performance of RCP valves should be prepared. Then, in order to implement the performance of RCPs in OLGA, a control function based on the mathematical model of RCPs must be created and introduced to OLGA. In addition, since the pressure drawdown has a direct impact on the oil production and there is no available data for determining the value of that, the other challenge that must be overcome is the estimation of the pressure drawdown. To achieve a realistic model, this parameter must be estimated as accurately as possible based on the expected oil production from the well, the frictional pressure drop along the well, and the pressure drop across the ICDs or RCPs.

## 1.3 Objectives

The main objective of the thesis is to study, modeling, and simulation of cost-effective and safe oil production from existing and near-future oil fields. To fulfill the main purpose of this project, the following goals will be pursued:

- Studying enhanced and cost-effective oil recovery by applying long horizontal wells with passive or autonomous inflow control devices.
- Investigating the characteristic of the Johan Sverdrup field near the well 16/2 D-12 in this field.
- Preparing a mathematical model describing the autonomous behavior of RCP valves.
- Creating a control function for implementing the performance of RCP valves in OLGA.
- Estimating the pressure drawdown.
- Developing a dynamic model of oil production from the well 16/2 D-12 by using OLGA in combination with ROCX.
- Conducting the near-well simulation of oil production by considering well completion with ICDs and RCPs for both homogeneous and heterogeneous reservoirs.
- Predicting the water breakthrough time.
- Comparing the functionality of ICDs and RCPs in improving oil recovery.
- Analyzing the performance of the implemented model of RCPs in OLGA.
- Evaluating the effects of heterogeneity in the reservoir on oil production.

## 1.4 Thesis outline

This report contains 8 chapters. The first chapter describes the background of the study, problem description, and the objectives of the thesis. Chapter 2 gives an overview of the previous works related to modeling and simulation of oil production as well as the new technologies for improving oil recovery including long horizontal wells and different types of inflow control devices. The required theories, principles, and equations for the study are introduced in Chapter 3. In the next chapter, the fluid and rock properties of the Johan Sverdrup field near the well 16/2 D-12 are investigated. Chapter 5 contains all methods, procedures, and calculations for finding the unknown parameters needed for developing the OLGA/ROCX model. In Chapter 6, the development of the model in OLGA/ROCX and the conduction of simulations for different cases will be explained step by step. The simulation results are presented and discussed in Chapter 7 and the last chapter gives the conclusion of the study and some suggestions for future works.

# 2 Literature review

In this chapter, based on the study of literature and previous researches, an overview of new methods and technologies for enhancing oil recovery as well as modeling and simulation of oil production, is presented.

## 2.1 Cost-effective and enhanced oil recovery

The process of oil recovery can be divided into three main stages, called primary, secondary, and enhanced oil recovery. During the primary recovery stage, natural mechanisms contribute to displacing oil from the reservoir to the surface. In this stage, the reservoir pressure is sufficient to force the oil to move towards the wellhead. Typically, the recovery factor of oil is 5% to 15% in this stage. During the lifetime of the well, the reservoir pressure drops and it is not sufficient anymore for displacing the oil. As a result, some external energy must be applied to maintain reservoir pressure. During the secondary or improved oil recovery stage, the required external energy to force the oil move towards the surface is provided by injecting water or gas into the reservoir as well as using gas lift. The typical recovery factor of using secondary recovery techniques is about 30%, depending on the characteristics of the reservoir rock and the oil properties. On average, it can be expected that 35% to 45% of oil in the reservoir will be recovered after primary and secondary oil recovery. Enhanced oil recovery (EOR) or tertiary recovery, is the extraction of crude oil from an oil field by increasing the mobility of the oil. By applying EOR methods, another 5% to 15% of the reservoir's oil can be recovered. Therefore, about 40% to 60% or more of the reservoir's oil, will be recovered using primary, secondary, and enhanced oil recovery [6-8].

Today, different methods of improving oil recovery including water and/or gas injection for maintaining pressure and sweeping oil in the reservoir are used on most Norwegian oil fields. However, a huge amount of immobile oil and resources in tight reservoirs of the Norwegian continental shelf (NCS) cannot be extracted profitably by using current methods. To avoid losing a considerable proportion of resources on the NCS, new methods of enhancing oil recovery must be developed and applied in a suitable time. Resources overview and the technical EOR potential on the NCS have been represented in Figure 2.1[3].

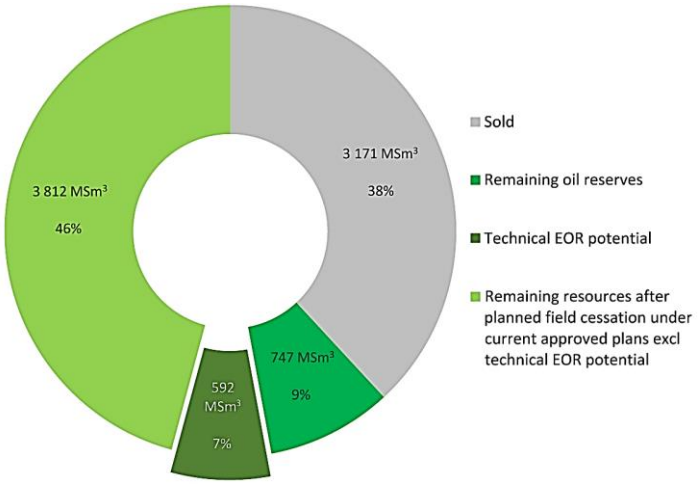


Figure 2.1: Resource overview and EOR potential on the 27 largest NCS oil fields [3].

Norwegian Petroleum Directorate (NPD) has conducted a screening study on 27 of the largest fields on the NCS which contain about two billion $Sm^3$ of immobile oil to estimate the technical potential for EOR. According to this study [3], there is a strong technical potential to recover 320 to 860 million $Sm^3$ of oil from these fields by applying different methods of EOR. It should be mentioned that in this study only the technical EOR potential has been estimated and the environmental, financial, and operational conditions must be taken into account as well. However, even if only 10 % of the technical EOR potential leads to commercial production, it will make almost 150 billion NOK more revenues by assuming an oil price of 50 USD /barrel and an exchange rate of 8 NOK to the USD.

### 2.1.1 A brief description of EOR methods

The primary techniques of EOR can be categorized into three general groups as gas injection, thermal injection, and chemical injection. In the gas injection technique or miscible flooding which is the most common method in EOR, natural gas, nitrogen, or $CO_2$ is injected into the reservoir in order to maintain the reservoir pressure and increase the mobility of the reservoir's oil. The thermal injection is widely used in the heavy oil fields and in this method, heat through steam is injected in the reservoir for decreasing the viscosity of oil and increasing the ability of oil for displacement. The injection of various chemicals like polymers, usually as dilute solutions for improving the effectiveness of water flooding is one of the recent methods of EOR and called chemical injection [7].

Norwegian Petroleum Directorate has assessed thirteen different EOR methods in order to find the ones, which have the biggest potential for increasing oil recovery from 27 fields on the Norwegian continental shelf. The results have shown that seven different EOR methods have the highest potential for increasing the recovery factor from these fields [3]. These methods will be described briefly in the following subchapters.

#### 2.1.1.1 Low salinity/polymer flooding

In this method, a combination of low salinity water and polymers is injected into the reservoir. Since the viscosity of water is increased by adding polymers, oil can be displaced in a stable manner [9]. Figure 2.2 schematically illustrates the difference between water and polymer flooding.

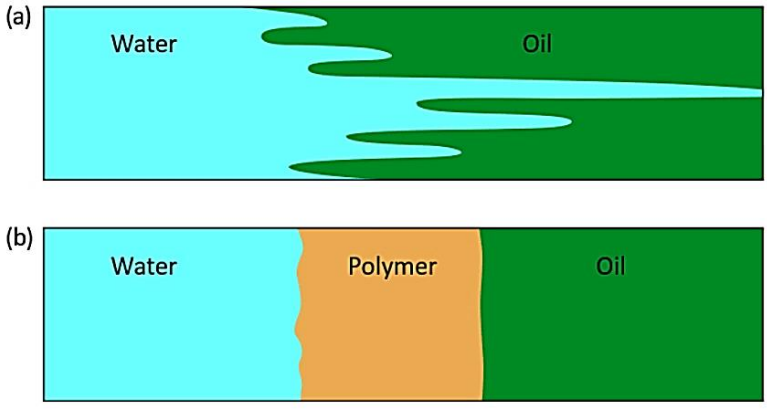


Figure 2.2: A simplified presentation of the difference between (a) water and (b) polymer flooding [9].

Low salinity water, which is water with reduced salt content, can change the wetting state of the rock. As a result, the interfacial tension of oil-water decreases, and the mobility of oil increases. Using this method not only improves the recovery of immobile oil but can also reduce the risk of downhole deposition of precipitated chemicals and acidification in the reservoir. Besides, by using this method the amount of required polymer to achieve suitable viscosity for the injected fluid can be reduced [9].

#### 2.1.1.2 Miscible WAG injection with CO2

Miscible $CO_2$ water alternating gas (WAG) injection can be used as an effective EOR method. By dissolving oil and $CO_2$ in each other in the miscible condition, which depends on the composition of oil and reservoir temperature and pressure, a single-phase fluid with lower viscosity is formed. This can help the oil to be displaced more easily from the reservoir pore to the surface. Besides, by alternating injection of $CO_2$ and water, the $CO_2$ consumption can be reduced while also the benefits of water injection like displacement and pressure support are provided. From an environmental point of view, the other asset of using this method is that part of the $CO_2$ is left behind in the reservoir forever and this can be combined with the carbon capture projects as an effective solution for preserving the environment [9, 10].

#### 2.1.1.3 Miscible WAG with hydrocarbon gas

This method is similar to miscible $CO_2$ WAG except using hydrocarbon gases instead of $CO_2$. Compare to miscible $CO_2$ WAG this method has some disadvantages like more difficult miscibility of hydrocarbons and oil as well as much higher cost of providing hydrocarbon gases. However, despite the advantages of using $CO_2$, in most of the offshore WAG projects, hydrocarbon gases are applied because of the availability of them in the production site [9, 10].

#### 2.1.1.4 Low salinity flooding

Applying the low salinity flooding technique is gaining popularity for both sandstone and carbonate reservoirs today. In this technique, the salinity of the injected water is reduced by changing its chemical composition. Using the low salinity water can alter the wettability of the reservoir rock from the mixed wet state toward more water-wet conditions. This can help to increase the mobility of immobile oil in the reservoir rock and improve oil production. It can also lead to reducing the risk of downhole deposition of precipitated chemicals and acidification in the reservoir [9, 11].

#### 2.1.1.5 Combined surfactant and polymer flooding

In this technique, in order to enhance oil recovery, a combination of surfactants and polymers is injected into the reservoir. Adding surfactants can significantly reduce the interfacial tensions between oil and formation water, decrease capillary forces, alter wetting properties of the reservoir rock and consequently mobilize oil. The main purpose of polymer injection is to reduce the mobility ratio between oil and water by increasing the viscosity of the aqueous phase. This can help to increase the vertical and areal sweep efficiencies allowing for a more stable and even displacement of the oil [9, 12]. In Figure 2.3, schematically shows the effect of adding surfactants to increase the sweep efficiency.

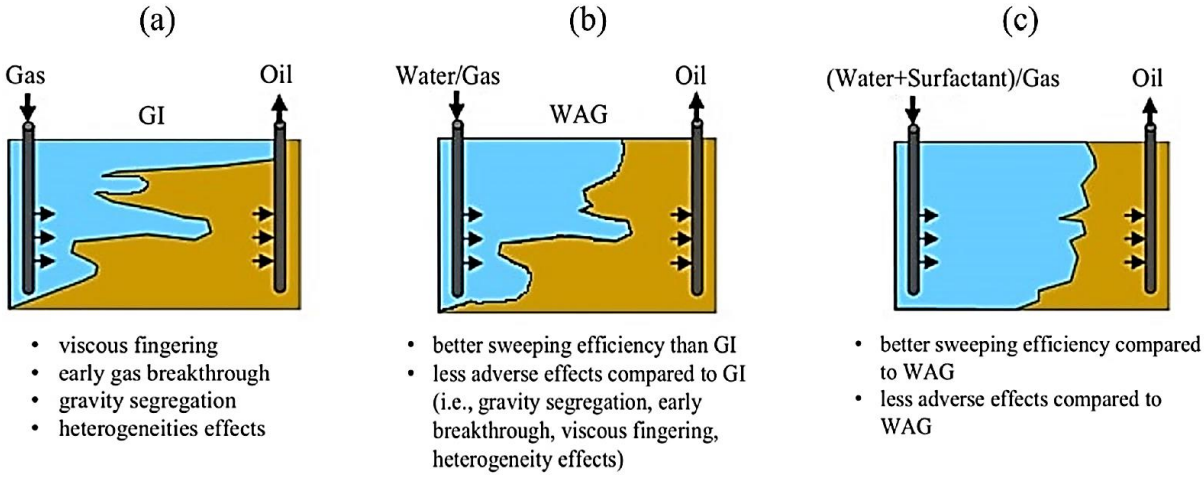


Figure 2.3: Schematic of challenges and benefits of (a) gas injection, (b) water alternating gas injection, and (c) water+surfactant alternating gas injection [10].

#### 2.1.1.6 Gel treatment

In heterogeneous reservoirs, which have some highly permeable zones, the injected water for improving oil recovery may flow through these zones to the production well. This can result in increasing the water cut and decreasing the efficiency of oil recovery. The main idea in the gel treatment method is setting a plug of gel in the highly permeable zones in heterogeneous reservoirs in order to seal these areas for stopping the penetration of water from these zones to the production well. Using this technique can improve the sweep efficiency of water injection in heterogeneous reservoirs [9, 13].

#### 2.1.1.7 Alkaline flooding

In the alkaline flooding method, alkaline substances like sodium carbonate and sodium hydroxide are added to the injection water. These substances react with the organic acids of crude oil and create in situ surfactants (soaps) that can reduce the interfacial tension between the formation water and oil. As a result, the wettability of the reservoir is changed, and the oil recovery is triggered. This method is only applicable for the reservoirs with high-acid crude oil and has a great potential for enhancing the recovery of oil with low and medium viscosity. Moreover, in the carbonate reservoirs due to the abundance of calcium and the potential for producing hydroxide precipitation by adding alkaline chemicals, this method can not be used [9, 14].

### 2.1.2 Potential of different EOR methods for Norwegian oil fields

Based on NPD's assessment of the technical potential of different EOR methods for 27 fields on the Norwegian continental shelf, low salinity/polymer flooding, miscible WAG injection with $CO_2$ or hydrocarbon gas have the highest technical potential for enhancing oil recovery in these fields. Figure 2.4 illustrates the mid-range estimates and uncertainty ranges for the technical potential of different EOR methods assessed by NPD for the fields on NCS.

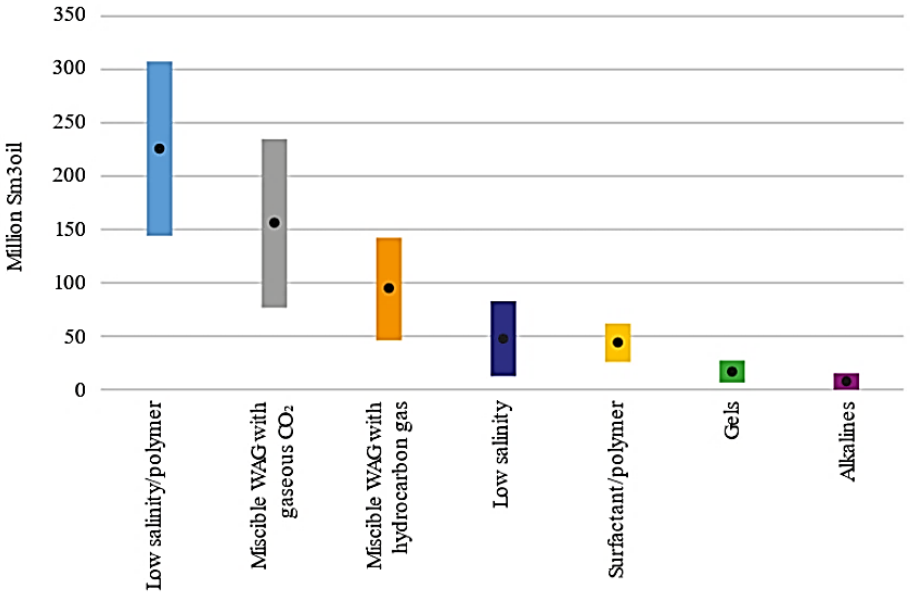


Figure 2.4: Mid-range estimates and uncertainty ranges for the potential of EOR in the fields on NCS [3].

### 2.1.3 Geographical analysis of suitable EOR methods on NCS

According to NPD's geographical analysis of the technical EOR potential [3], on the chalk fields at the southern part of Norway's North Sea sector, using the miscible WAG injection with $CO_2$ or hydrocarbon gas has the highest technical potential for improving oil recovery. On the Utsira High and the surrounding area, the best method of EOR can be the injection of low salinity/polymer flooding. Another technically feasible alternative with the almost same potential for this area is combined surfactant and polymer flooding. Furthermore, different EOR methods can be applied in the Tampen area of the northern North Sea. However, miscible WAG injection would have the largest potential for some fields, while water-based EOR solutions would be best for the others. Figure 2.5 depicts the suitable EOR methods for different areas on the Norwegian continental shelf.

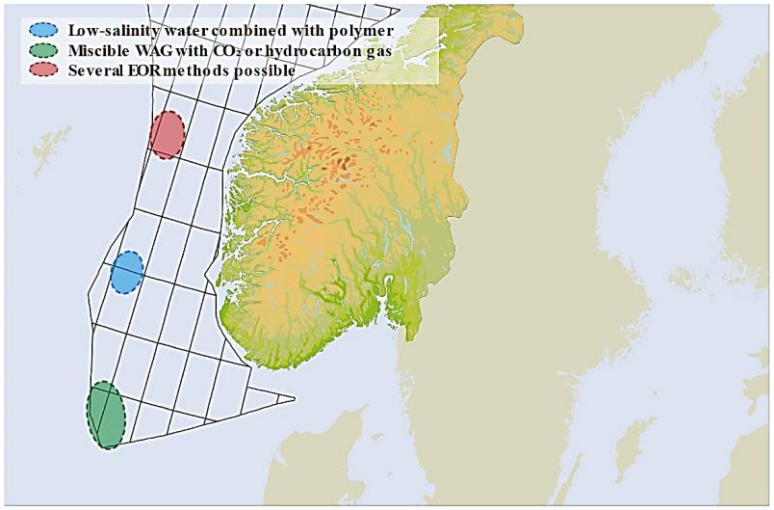


Figure 2.5: Suitable EOR methods for different areas on the NCS [3].

### 2.1.4 Cost estimation of different EOR methods

Implementation of offshore EOR projects has a huge capital cost but compared to conventional methods, extra oil recovery can be yielded later on. The total capital cost of different EOR methods depends on several factors. As an example, in most cases, in order to identify uncertainties related to the recovery potential and technical feasibility of the EOR project, various pilot tests are needed before large-scale implementation of the project. Therefore, the cost of pilot tests must be assessed and added to the capital cost. However, it can be roughly said that the EOR methods that need $CO_2$ or low salinity water injection have the highest capital cost. Besides, it can be considered that the operational cost of injecting polymers, surfactants, gels, and alkalines is higher. Therefore, choosing the most cost-effective method of EOR for each oil field requires doing a comprehensive cost estimation by assessing different aspects of technical, financial, and operational conditions [3].

## 2.2 Horizontal wells

In recent years, the advancement of horizontal well technology has played a major role in making oil production economically feasible from many reservoirs. Wells with an inclination greater than 85° are called horizontal wells and since the late 1990s, horizontal wells have been widely used as an alternative to vertical wells specially in oil production from the reservoirs with a thin oil column, tight formation, lenticular sands, and fault blocks. Vertical wells can only be exposed to a small portion of the oil layers. Therefore, in most cases, several vertical wells are required to achieve effective oil production from the reservoir. However, by using horizontal wells the contact with the reservoir drainage area is maximized. As a result, although the capital cost of drilling horizontal wells is higher than vertical wells, much higher oil production can be achieved from horizontal wells because of the larger capacity for producing oil at the same drawdown [15].

In general, the advantages of horizontal wells can be summarized as [16, 17]:

- To delay water and gas breakthrough because of lower pressure drawdown for a given production rate.
- To increase well productivity due to the greater wellbore length exposed to the pay zone.
- To decrease the pressure drop around the wellbore as a result of lower pressure drawdown.
- To reduce fluid velocities around the wellbore due to lower pressure drawdown.
- To reduce sand production because of lower pressure drop and fluid velocities around the wellbore.
- To achieve a larger and better drainage pattern leading to improved overall reserves recovery.
- To minimize the footprint on the surface by reducing the required number of offshore platforms.
- To make it possible to reach difficult targets since several reservoirs are located under residential areas where drilling is impossible.

### 2.2.1 Characteristics of horizontal wells

Typically, horizontal wells are characterized by their build rate, which is the positive change in inclination over a normalized length (e.g., 5°/100 ft.). Based on this, horizontal wells are

classified into three groups of long-radius, medium-radius, and short-radius as shown in Figure 2.6 [17].

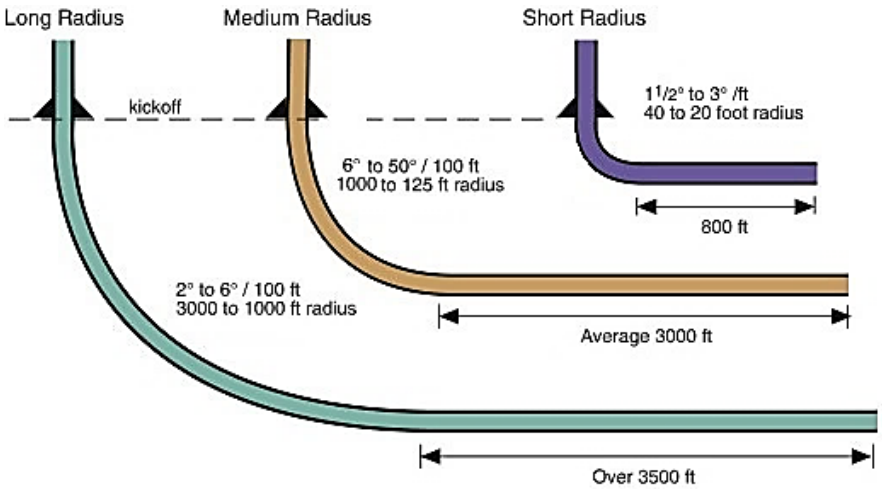


Figure 2.6: Horizontal well categories based on the buildup rate [18].

Horizontal wells with build rates of 2 to 6°/100 ft, which results in radii of 1000 to 3000 ft are classified as long-radius horizontal wells. The lateral section for this type of well is drilled up to 8000 ft. A medium horizontal well is characterized by build up rates of 6 to 50°/100 ft, radii of 125 to 1000 ft, and an average lateral section of 3000 ft. Short-radius wells have build rates of 1.5 to 3°/ft or radii of 20 to 40 ft and a lateral section drilled between 200 and 900 ft [17].

### 2.2.2 Gas and water coning

One of the major problems that can reduce the efficiency of using horizontal well is gas and water coning. To describe the mechanism underlying the upward movement of water and downward movement of gas into the wellbore, the term *coning* is used. Water and gas conning can significantly reduce the well productivity, and delaying water and gas breakthrough is one of the main measures that must be taken to maximize the field's ultimate oil recovery [19].
The fluid flow distribution around the well is affected by three main forces, which are capillary forces, gravity forces, and viscous forces. At any given time, the balance between these forces determines the distribution of fluid flow around the well. The fluid movement towards the well occurs when there is enough pressure gradient between the well and reservoir that create viscous forces for overcoming gravitational and capillary forces. As a result, when the pressure gradient is large enough, water or gas tends to move towards the well. On the other hand, because of different densities and maintaining gravity equilibrium, gas has a tendency for remaining above the oil zone, and water tends to be below the oil zone. Consequently, these opposite tendencies reshape the gas-oil and water-oil contact into a conical shape as shown in Figure 2.7 and this phenomenon called gas or water coning [19].

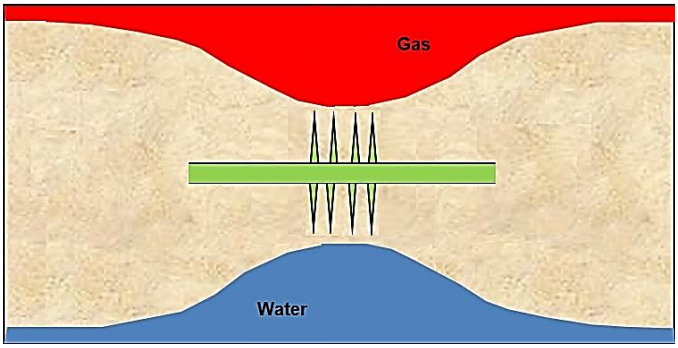


Figure 2.7: Schematic of gas and water coning.

#### 2.2.2.1 Early water coning owing to the heel-toe effect

One of the main changes related to using horizontal wells is early water breakthrough due to the heel-toe effect. When a horizontal well is used for oil production, owing to the frictional pressure drop, the pressure difference between the well and reservoir, called pressure drawdown, will be uneven along the well. The pressure drawdown reaches its maximum value at the heel of the well and its value is significantly higher compared to that of the toe. The higher the pressure drawdown, the higher the driving force for moving the reservoir fluids towards the well. Consequently, the water cone will grow much faster and breaks into the well much sooner at the heel compared to the toe of the well. This phenomenon called the heel-toe effect and is shown in Figure 2.8 [4].

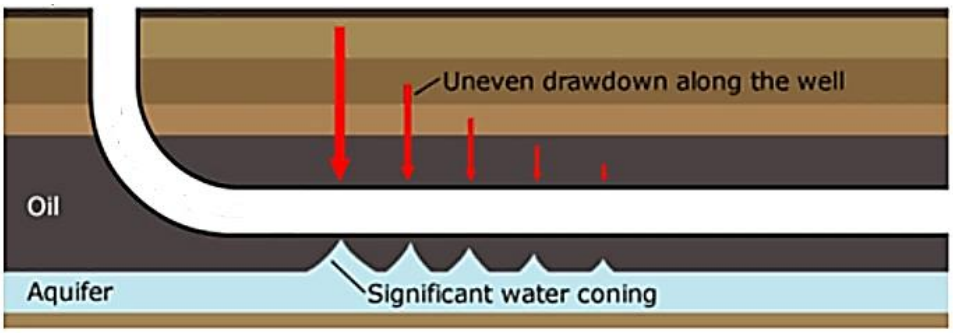


Figure 2.8: Heel-to effect in the homogeneous reservoir [20].

#### 2.2.2.2 Early water coning as a result of heterogeneity along the well

In the heterogeneous reservoirs, the reservoir characteristics are different from one location to another. Oil production is significantly affected by the permeability of the reservoir, and for a horizontal well in heterogeneous reservoirs, the permeability varies along the well. Based on Darcy's law, because of the lower flow resistance in the high permeable zones or fractures, the inflow to the well is higher than the other zones. This brings about an uneven inflow profile along the well. The water cone grows faster in places with higher inflow and consequently, the early water breakthrough occurs in the high permeable zones and fractures [4]. Figure 2.9 shows the early water coning in a heterogeneous reservoir with a very high permeable zone.

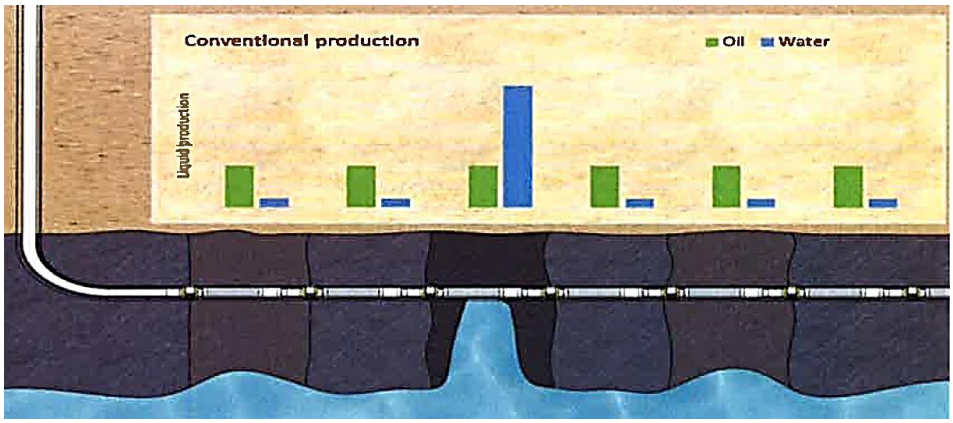


Figure 2.9: Liquid production from different zones in a heterogeneous reservoir [4].

## 2.3 Inflow control technologies

Horizontal wells are wildly used for increasing the efficiency of oil recovery but there are some challenges related to using this technology that needs to be overcome. One of the major challenges is early water coning due to the heel-toe effect and heterogeneity along the well. This problem gives rise to an uneven inflow profile along the well. Inflow control technologies are used to counteract the non-uniform inflow and balance inflow throughout the length of the well leading to improve the well performance and efficiency.

### 2.3.1 Passive Inflow Control Devices

One of the mature technologies that have been developed since the early 1990s for managing the early water breakthrough in horizontal wells is passive Inflow Control Devices (ICDs). A passive ICD is a flow restrictor device with no moving part installed as a part of the sandface completion hardware. ICDs are used for chocking the flow by adding extra pressure drop and thereby even out the flow influx along a horizontal well. Passive ICDs has been developed by four main companies including Baker Hughes, Halliburton, Schlumberger, and Weatherford and they can be classified into three different types as [21]:

a) Channel-type ICD: the required flow restriction is created by a number of helical channels with preset diameter and length.
b) Nozzle-type ICD: the desired pressure drop is generated in the device as fluid flows and passes through several nozzles
c) Orifice-type ICD: each ICD includes several orifices with a suitable diameter and the additional pressure resistance is adjusted by varying the number of open orifices.

Horizontal wells are completed with many ICDs distributed along the well. The pressure drop across an ICD is a function of flow rate, the geometry of ICD, and the fluid density but it does not depend on the fluid viscosity. The flow restriction in a well with ICDs completion leads to lower oil production initially compared to an open-hole well. However, As Figure 2.10 is showing, ICDs can delay the early water breakthrough by balancing the inflow along the well and as a result, increasing the oil production significantly later on.

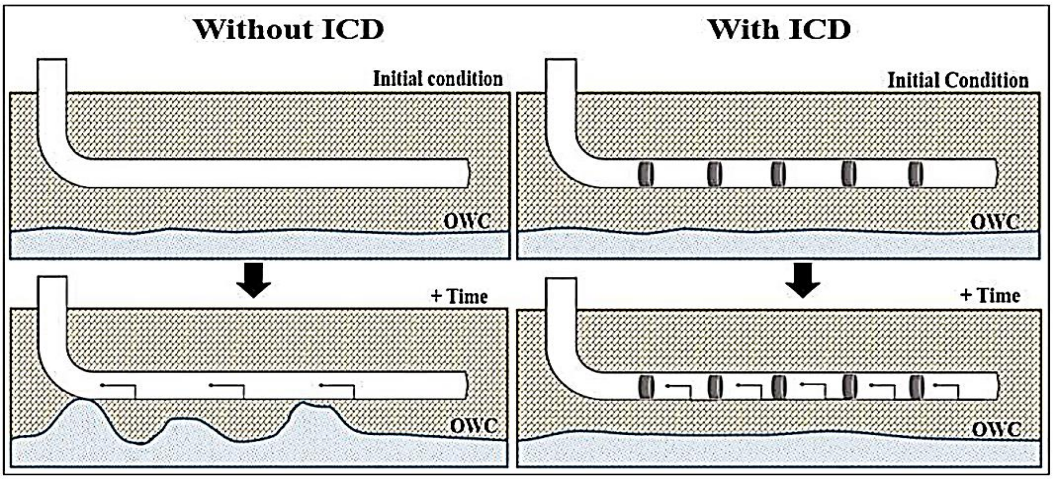


Figure 2.10: Application of ICDs in mitigation of the early water breakthrough [22].

One of the main drawbacks of passive ICDs is that they are not able to choke the water back after breakthrough. In this condition, the well must be shut in to avoid increasing the water cut more than the capacity of the separation facilities and it leads to the reduction of oil production [4].

### 2.3.2 Autonomous Inflow Control Devices

Since passive ICDs have no ability to choke the water or gas back after breakthrough, Autonomous Inflow Control Devices (AICDs) have been developed as a robust alternative in recent years. AICDs have a moveable disk and they can be partially closed for low viscous fluids compared to oil like water and gas. As a result, in addition to delaying the water or gas breakthrough, AICDs can reduce the production of water or gas after breakthrough autonomously with no need to control form the surface and increase oil production compare to passive ICDs [4].

AICDs are available with different designs and one of the most widely used types of AICDs called Rate Control Production (RCP) has been developed by Norsk Hydro and Statoil. As Figure 2.11 shows, this type of AICD consists of three parts, which are the valve body, nozzle, and free-floating disk. The valve is designed based on the fluid properties in such a way that when oil passes through the valve, the pressure at the inlet is higher and the disk rests at the seat. Thus, the maximum flow area is obtained and as a result, the maximum amount of oil passes through the valve. Besides, the position of the moveable disk can vary based on the fluid properties and flow conditions. Owing to the special design of this valve, when low viscous fluids like water or gas enter the valve, the pressure at the inlet becomes lower. Consequently, based on Bernoulli's equation the total force acting on the disk pulls it towards the inlet, and the flow area is partially closed. Therefore, RCPs can minimize the flow rate of unwanted fluids like water or gas autonomously [23, 24].

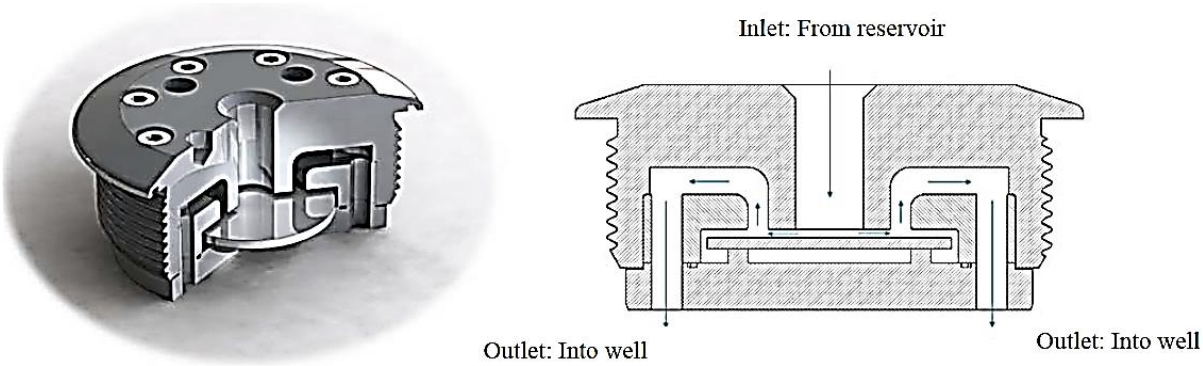


Figure 2.11: Statoil's RCP valve and its schematic sketch [23].

Since RCPs have a choking effect on the low viscous fluids after breakthrough, they can be effectively used for reducing the gas production in the reservoirs with light oil, as well as reducing both the gas and water production in the reservoirs with heavy oil. In the wells with passive ICDs completion, when the water or gas breakthrough takes place, the pressure drawdown must be reduced in order to minimize the production of unwanted fluids. When the pressure drawdown is reduced, the low permeable zones are not able to produce oil like the initial condition and as a result, the oil production decreases significantly. By using the RCPs, the unwanted fluid production is minimized and besides the initial pressure drawdown can be sustained. This results in higher production from low permeable zones and improving the oil recovery [24]. Figure 2.12 represents the flow rate of gas, water, and heavy oil through an RCP valve as a function of the differential pressure across the valve based on the experiments performed in the Statoil's multiphase flow laboratory.

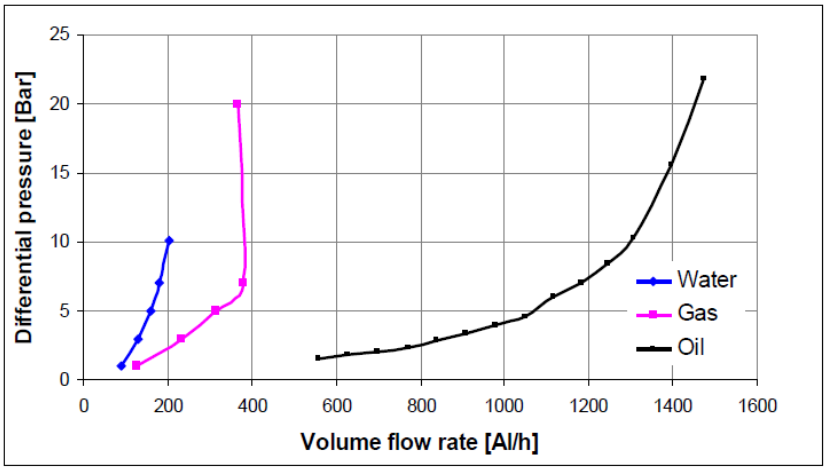


Figure 2.12: Volume flow of oil (460 cp), water and gas through RCP as a function of differential pressure [23].

According to the results given in Figure 2.12, the values of the oil/gas ratio and oil/water ratio based on differential pressure are calculated and illustrated in Figure 2.13.

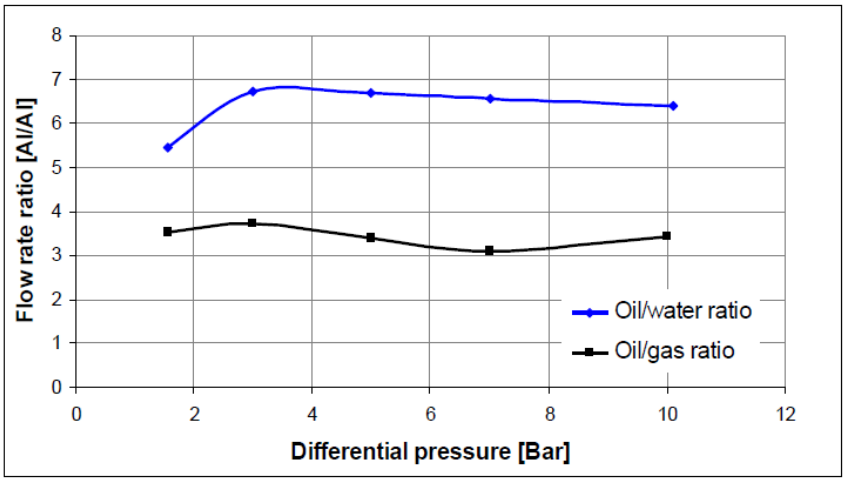


Figure 2.13: Oil/water and oil/gas ratios as a function of differential pressure for oil with a viscosity of 460 cP [23].

As can be seen in Figure 2.13, the oil/gas ratio is approximately 6.5 and the oil/water ratio is about 3.5 for heavy oil with the viscosity of 460 cp. This can show the suitable performance of RCPs for choking low viscous fluids in the reservoirs with heavy oil [23]. Moreover, based on Halvorsen et al [25], RCPs have been successfully tested and implemented in some of the wells at the Troll field with light oil and gas cap. Based on the evaluation of oil and gas production, after 1.5 years of production, the GOR in the well with RCP completion was almost 1/3 compared to the well with ICDs completion. Besides, the oil production from the well with RCP completion was about 20% higher. This indicates that RCPs can act effectively for reducing gas production and improving oil recovery from the reservoirs with light oil and gas cap.

The schematic of well completion with RCP valves in a heterogeneous reservoir is shown in Figure 2.14. The reservoir fluids pass through the sand screen at first, and then it passes into the inflow chamber where the RCP is installed. Practically, one RCP valve is mounted for each screen but based on the condition, up to four RCPs may be installed for each screen section [23].

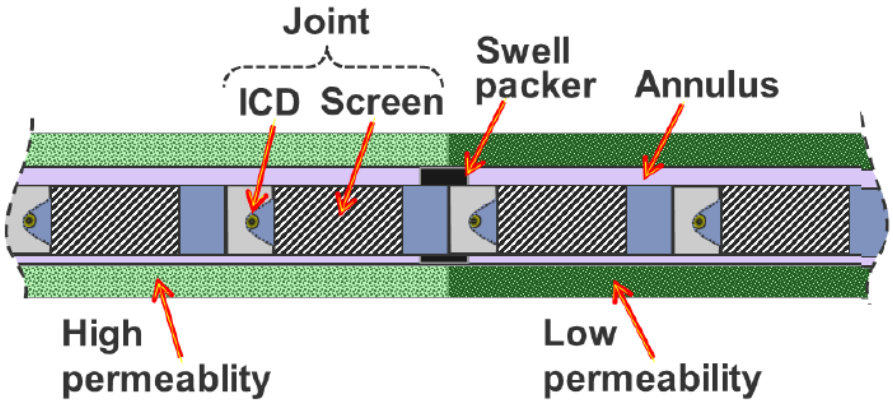


Figure 2.14: Schematic of well completion with RCP valves in a heterogeneous reservoir [25].

When the reservoir is heterogeneous, some zonal isolations are necessary. The early water or gas breakthrough occurs in the heel of the well or high permeability zones owing to the higher inflow than the rest of the reservoir. Therefore, these zones must be isolated for stopping the flow of unwanted fluids through the annulus soon after the early breakthrough. If there is no zonal isolation, the low viscous fluids fill the annulus and all RCPs will be partially closed and as a result, the oil production decreases significantly. In fact, by using zonal isolation, the water or gas production zones will be isolated and the oil production from the rest of the well will be continued which leads to improving oil recovery from the well [23].

## 2.4 Modeling and simulation of oil production

Today, oil and gas modeling and simulation software packages are widely used for creating a realistic representation of reservoirs, wells, and production equipment. Using these types of software packages helps oil and gas companies for making better decisions by evaluating risks and profitability based on simulation results. In the area of modeling and simulation of oil production, several free and commercial software products have been developed in recent years. Coupling a multiphase flow simulator software with a reservoir simulator software like OLGA+ROCX/ECLIPSE or LedaFlow+ECLIPSE is commonly used in industry for modeling and simulation of oil production. There is also some software products with special application like NETool which is a simulator for designing and modeling advanced well completion [26, 27].

The Combination of OLGA with ROCX creates one of the leading and robust tools for modeling and simulation of multiphase flow behavior from the reservoir pore to the production pipe and process facilities. OLGA is a dynamic multiphase flow simulator and ROCX is a reservoir simulator that can be coupled to OLGA as a plug-in. For the simulation of three phases (oil/gas/water) flow near the wellbore in three dimensions, the wellbore pressure information is calculated and sent by OLGA simulator to ROCX. Then the flow rate for each phase of the reservoir fluids is determined and sent back by ROCX to OLGA. Moreover, an implicit scheme couples OLGA with ROCX based on the same PVT file. OLGA+ROCX combination can have a different application in modeling and simulation of liquid loading, wellbore slugging, well kick-off and cleanup, well testing, shut-in/start-up, dynamic water and gas coining, etc. [28].

So far, OLGA in combination with ROCX has been used for near-well simulation of oil production under different conditions in several studies. In [29] and [30], oil production from heavy oil reservoirs with water drive by considering well completion with ICD and AICV has been simulated by OLGA+ROCX. Using the same tool, the effect of relative permeability on oil production as well as the effect of using different types of control valves for managing the water production after breakthrough from heavy oil reservoirs with water drive have been simulated in [31]. Furthermore, Near-well simulation of oil production from light oil reservoirs with water drive and well completion with ICD and AICD has been performed by OLGA+ROCX in [32]. Besides, the oil production from heterogeneous oil reservoirs with a gas cap has been simulated in [33], in the same way. In addition to them, in [4] the application of AICV technology for improving oil recovery in different types of reservoirs has been modeled in OLGA+ROCX and NETool.

# 3 Theoretical background

Understanding the reservoir rock and fluid properties, as well as the principles of horizontal well completion design, are of key importance in modeling and simulation of oil production. In this chapter, the basic theories, principles, and equations needed for conducting the modeling and simulation of oil production will be described.

## 3.1 Reservoir rock properties

In petroleum engineering, a subsurface pool of hydrocarbon accumulated in porous or fractured rock formations is called a petroleum reservoir [34]. Reservoir rock properties significantly impact oil production and the most important of them will be described under the following subchapters.

### 3.1.1 Porosity

Even though a reservoir rock seems solid, a microscopic examination shows some small pores in the reservoir rock. The reservoir rocks were formed by the deposition of sediments during several years and as a result, different types of pores have been created in the reservoir rocks. As Figure 3.1 represents, almost every reservoir rock consists of rock grains and three basic types of pores that are interconnected pores, dead-end pores, and isolated or closed pores [35].

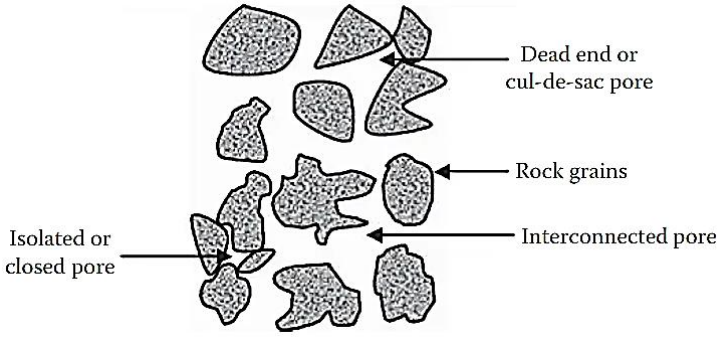


Figure 3.1: Conceptual representation of different types of pores in a reservoir rock [35].

The ratio of the pore volume to the total volume of the reservoir rock is one of the most important properties of the reservoir rock and can be determined by a parameter called *porosity* and expressed as a percentage. The *absolute porosity* is denoted by $\phi$ and defined mathematically as [35]:

$$\phi = \frac{\text{Total pore volume}}{\text{Total or bulk volume}} \qquad 3.1$$

Although a reservoir rock may have a very high total porosity, due to the lack of connection between the pores, a large portion of reservoir fluids may trap inside the isolated pores and hence immobile or unrecoverable. Therefore, it is useful to define a parameter that shows the

pore space that is occupied by mobile recoverable hydrocarbon fluids. To achieve this purpose, since isolated or closed pores are not able to contribute to producing any reservoir fluids, *effective porosity* is defined by the following relationship [35]:

$$\phi = \frac{\text{Vol. of interconnected pores + Vol. of dead-end pores}}{\text{Total or bulk Volume}} \qquad 3.2$$

## 3.1.2 Absolute permeability

The porosity parameter indicates the capacity of the reservoir rock to store fluids. However, in order to determine the potential of a petroleum reservoir to produce hydrocarbons fluids, the ability of fluids to flow through the reservoir rock must be considered as well. This is one of the most influential properties of the reservoir rock called *permeability* and denoted by *k*. The permeability of a reservoir rock saturated with a single fluid is different from that of the same reservoir saturated with more than one fluid. Therefore, *absolute permeability* of a reservoir rock is defined as the ability to flow or transmit fluids through a rock that is completely saturated with a single-phase fluid [35].

### 3.1.2.1 Mathematical expression of absolute permeability: Darcy's Law

Absolute permeability can be calculated by doing flow experiments in the porous medium and using a mathematical equation originated from Henry Darcy's experiments for the investigation of water flow through a cylindrical sand core plug. With a little difference, the Darcy experiment can be represented schematically by Figure 3.2 [35].

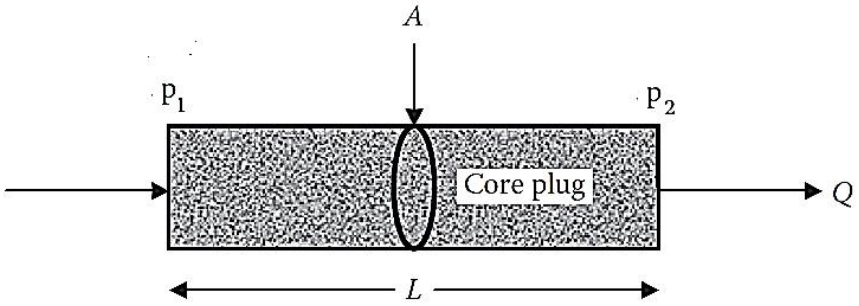


Figure 3.2: Darcy experiment expressed by a schematic representation of fluid flow through a core plug [35].

Darcy expressed the results of his experiments as a mathematical formula called Darcy's law and it can be written as the following equation [35]:

$$Q = -KA\frac{dP}{dL} \qquad 3.3$$

In Equation 3.3, $Q$ is the volumetric flow through the core plug (in $m^3/s$), $K$ is known as hydraulic conductivity (in m/s), $dP$ is the pressure difference between upstream and downstream of the core plug (in Pa), $A$ is the core plug cross-sectional area (in $m^2$) and $dL$ is the length of core plug (in m). It should be mentioned that Darcy's investigations were limited to the flow of water through core plugs that were saturated with only water. However, later studies prove that Darcy's law can be generalized to other fluids if $K$ is considered as the ratio

of $k/\mu$, where $\mu$ is the viscosity of the fluid (in N·s/m$^2$) and $k$ is the absolute permeability of porous medium (in m$^2$ which can also be converted to mD or D). Therefore, the general form of Darcy's law for the linear and single-phase flow can be expressed by Equation 3.4 [35].

$$Q = -\frac{k}{\mu} A \frac{dP}{dL} \tag{3.4}$$

As shown in Figure 3.3, by considering a radial flow system the flow of reservoir fluids from a cylindrical drainage area into a wellbore can be characterized [35].

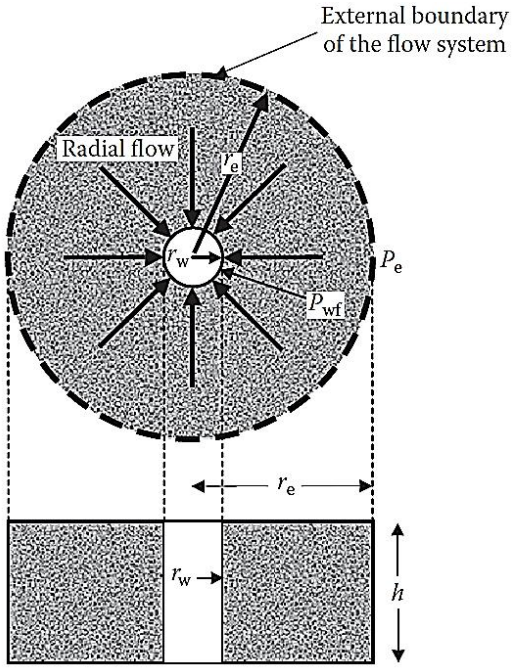


Figure 3.3: Radial flow system for the characterization of fluid flow into the wellbore [35].

For the radial flow system by replacing *dL* by *dr* and considering $A = 2\pi rh$, Darcy's law can be written as [35]:

$$Q = \frac{k}{\mu} A \frac{dP}{dr} \tag{3.5}$$

Based on the SI system, permeability has the unit m$^2$ but practically this unit is too large for measuring this parameter. Therefore, another unit called Darcy is commonly used in petroleum engineering for measuring permeability. A porous medium with a cross-sectional area of 1 cm$^2$ has a permeability of one darcy when a single-phase fluid with a viscosity of one centipoise (cP) that fills the porous medium, can flow through that at a rate of 1 cm$^3$/s under a laminar flow regime and a pressure gradient of 1 atm/cm. In order to convert m$^2$ to darcy, it can be written that [35]:

$$1 \text{ darcy} = 1 \text{ D} = 1000 \text{ mD} = \frac{(1 \text{ cm}^3/\text{s})(1 \text{ cP})}{(1 \text{ cm}^2)(1 \text{ atm/cm})} = 9.869 \times 10^{-13} \text{ m}^2 \tag{3.6}$$

### 3.1.2.2 Anisotropic permeability in petroleum reservoirs

Generally, in most reservoirs, the permeability is significantly different between the horizontal and vertical directions. This directional dependency is known as *anisotropy* and the ratio of vertical permeability to horizontal permeability ($k_v/k_H$) can be used for quantifying permeability anisotropy. Typically, the permeability in the *x*-direction is close to that of the *y*-direction. However, due to the fact that the reservoir rocks are created through the sedimentation process, permeability in parallel to layers of sedimentary rocks is generally higher than that of perpendicular to these layers. This means, in most cases, the horizontal permeability is higher than the vertical permeability in the petroleum reservoirs. Therefore, as Figure 3.4 illustrates, the drainage area for a horizontal well has an ellipsoidal shape and it highly depends on the permeability anisotropy [36, 37].

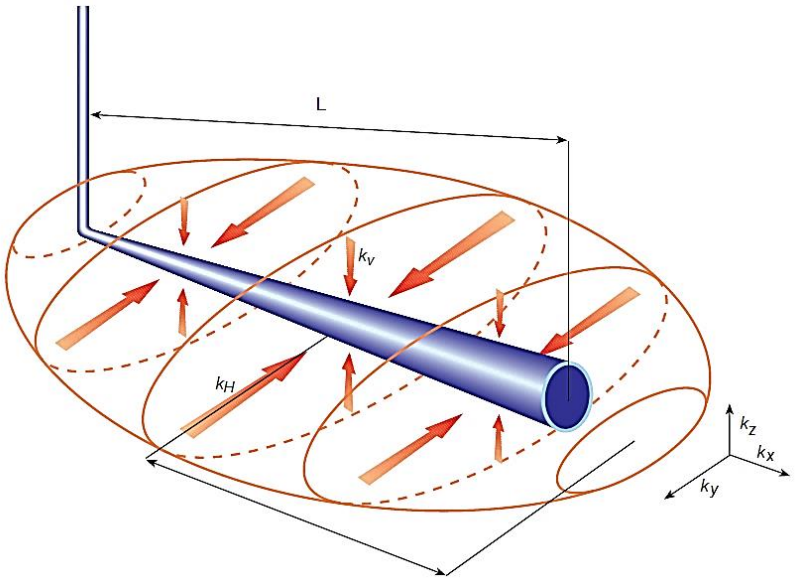


Figure 3.4: Horizontal well drainage pattern [36].

With some simplifications, the following equations can be used in order to determine the horizontal permeability ($k_H$) and average permeability ($k$) for a porous medium based on permeability in the *x*, *y* and *z* directions ($k_x$, $k_y$, $k_z$) [38, 39]:

$$k_H = \sqrt{k_x k_y} \tag{3.7}$$

$$k = \sqrt[3]{k_x k_y k_z} \tag{3.8}$$

In recent years, several empirical vertical-horizontal correlations have been proposed for different types of reservoirs. Based on experimental data from a sandstone reservoir in Nigeria, several correlations between horizontal and vertical permeability for sandstone reservoirs have been suggested by Iheanacho et al [40]. Equation 3.9 represents the correlation that has the best fit with experimental data proposed by Iheanacho with a correlation coefficient of 0.953.

$$k_v = k_z = 0.0718 \times \sqrt{\left[\frac{k_H(1-V_{sh})}{\phi_e}\right]^{2.0901}} \quad 3.9$$

where $V_{sh}$ is the volume of shale in the reservoir and $\phi_e$ is the reservoir effective porosity.

### 3.1.3 Fluid saturation

Porosity is a property that shows the maximum capacity of a reservoir rock to store fluids. However, this parameter does not give us any information about how much of this storage capacity, actually has been allocated to gas, oil, and water which are the three typical reservoir fluid phases. Therefore, another important parameter should be defined for quantifying the fractions of the total pore space that has been occupied by reservoir fluid phases. This can be done by introducing the parameter *fluid saturation* that is defined as the ratio of the volume of a fluid phase existing in a reservoir rock sample to the effective pore volume of the sample. Therefore, oil, gas, and water saturation are defined as follows and they can be expressed by a fraction or percentage [35]:

$$S_g = \frac{\text{Volume of gas}}{\text{Effective pore volume}} \quad 3.10$$

$$S_o = \frac{\text{Volume of oil}}{\text{Effective pore volume}} \quad 3.11$$

$$S_w = \frac{\text{Volume of water}}{\text{Effective pore volume}} \quad 3.12$$

Since all saturations are measured as a fraction (or percentage) of the pore volume, the summation of them must be always 1 (or 100%). Therefore [35]:

$$S_g + S_o + S_w = 1 \text{ (or } 100\%) \quad 3.13$$

### 3.1.4 Wettability

By definition, absolute permeability of a reservoir rock is measured when it is fully saturated by a single-phase fluid. However, such a simple single-phase fluid system rarely exists, and typically in a petroleum reservoir rock, the pore space is occupied by either two or three fluid phases. During the production process, reservoir fluids are always in contact with reservoir rock surfaces until they reach the production pipe. Therefore, to investigate petroleum production from a given reservoir, considering the interfacial forces between reservoir liquid phases and rock surfaces is highly important. For this purpose, the parameter *wettability* is defined for specifying the relative ability of a reservoir liquid phase (oil or water) to coat the reservoir rock surface in the presence of another liquid phase [35].

### 3.1.4.1 Classification of wettability

Wettability is one of the most important properties of a reservoir rock that can be classified to five main states as [35]:

- Water-wet: in this wettability state, the water phase has much more tendency to spread on all pore surfaces of the rock and as a result, the gas and oil will be positioned in the center of the pore.
- Oil-wet: opposite to the water-wet state, wettability is in an oil-wet state when all rock surfaces have a strong preference for oil state compare to water and in this condition, the water is located in the middle of the pore space. Figure 3.5 is a simple illustration of water-wet and oil-wet pore spaces.

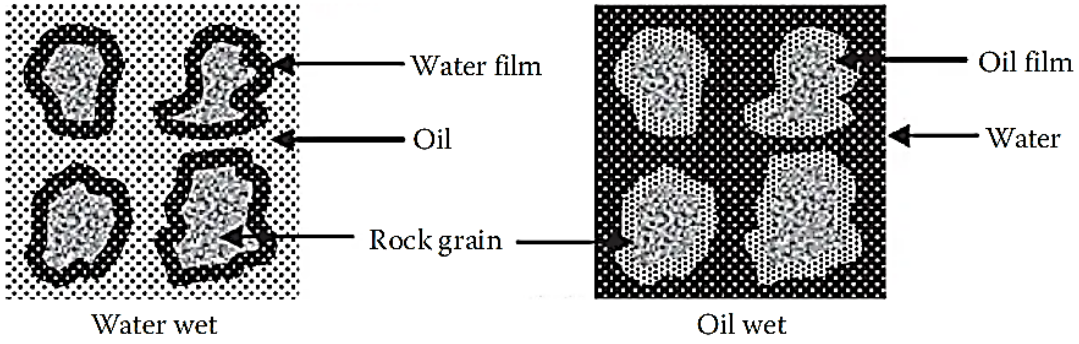


Figure 3.5: Schematic representation of water-wet and oil-wet pore spaces [35].

- Intermediate-wet: this state of wettability refers to a condition that pore surfaces have an equal preference for oil and water. Since in this state oil or water does not have any dominant tendency to coat the pore surfaces, it also can be considered as a neutral-wet state.
- Fractional-wet: in the state that some pore spaces are strongly water-wet while others are strongly oil-wet, wettability is classified as the fractional-wet state.
- Mixed-wet: this wettability state is a special type of the fractional-wet state in which larger pore spaces are oil-wet and smaller pore spaces are water-wet.

### 3.1.4.2 Measurement of wettability: Amott-Harvey test

Today, different qualitative and quantitative methods are used for evaluating reservoir rock wettability. The Amott-Harvey wettability test is the most common core analysis test for the measurement of the average wettability of a core sample based on the displacement properties of an oil-water-rock system. In this method by doing different displacement tests the Amott-Harvey wettability index, $I_{AH}$, is calculated as:

$$I_{AH} = \delta_w - \delta_o \qquad 3.14$$

Where $\delta_w$ is called *displacement by water ratio* and the value of that approaches 1 when the rock is strongly water-wet and 0 when it is strongly oil-wet. The term $\delta_o$ called *displacement by oil ratio* and unlike $\delta_w$, it approaches 1 when the rock is strongly oil-wet and 0 when it is

strongly water-wet. By doing the Amott-Harvey wettability test and using the relevant formulas, the values of $\delta_w$ and $\delta_o$ are calculated and he wettability of a core sample can be quantitively measured by calculation of $I_{AH}$ from Equation 3.14. Moreover, in order to classify wettability states based on the range of Amott-Harvey wettability index values, Table 3.1 has been proposed by Quiec that is widely used in petroleum engineering [35].

Table 3.1: Quiec's wettability classification based on the Amott-Harvey wettability index, $I_{AH}$ [35].

| $I_{AH}$ Range | Wettability |
|---|---|
| +0.3 to +1.0 | Water wet |
| +0.1 to +0.3 | Slightly water wet |
| −0.1 to +0.1 | Neutral |
| −0.3 to −0.1 | Slightly oil wet |
| −1.0 to −0.3 | Oil wet |

### 3.1.5 Capillary Pressure

When a porous medium is saturated with two or more immiscible fluids due to the interfacial forces between the fluids, the interface boundary between them is curved. This interfacial curvature leads to a difference in the pressure across the interface named *capillary pressure, $P_c$*. In a petroleum reservoir, the pressure of the none-wetting fluid is higher than that of the wetting fluid. Therefore, capillary pressure can be defined as the difference between the pressure of the nonwetting phase, $P_{nw}$, and the pressure of the wetting phase, $P_{w,}$ and it can mathematically be written as [35]:

$$P_c = P_{nw} - P_w \tag{3.15}$$

When an oil-gas or water-gas system considered, gas is the nonwetting phase and gas-oil capillary pressure, $P_{cgo}$, and gas-water capillary pressure, $P_{cgw}$, can be expressed by the following Equations [35]:

$$P_{cgo} = P_g - P_o \tag{3.16}$$

$$P_{cgw} = P_g - P_w \tag{3.17}$$

Since both water and oil can be the wetting phase, the capillary pressure of an oil-water system must be defined based on the reservoir rock wettability. In a water-wet reservoir, the oil-water capillary pressure, $P_{cow}$, is calculated by [35]:

$$P_{cow} = P_o - P_w \tag{3.18}$$

where $P_g$, $P_{o,}$ and $P_w$ are the pressures of gas, oil, and water phases respectively.

Since capillary forces depend on interfacial forces, reservoir rock wettability and pore sizes, Equation 3.19 that includes these properties can be used for calculating oil-water capillary pressure as [35]:

$$P_{cow} = \frac{2\delta_{ow}\,\mathrm{Cos}\,\theta_{ow}}{r} \qquad 3.19$$

where $\delta_{ow}$ is the oil-water interfacial tension, $\theta_{ow}$ is the contact angle, and $r$ is the capillary radius.

### 3.1.6 Relative Permeability

The general form of Darcy's law, Equation 3.4, has been developed based on the single-phase flow in a porous medium. However, since such a single-phase flow system rarely exists in the petroleum reservoirs, for various reservoir engineering calculations, further modifications of Darcy's law is necessary to cover multiphase flow systems as well. When two or three fluid phases flow through reservoir rock pores, the pore spaces are shared between them and the flow of one fluid phase interferes with the other. In order to consider this fact, a new parameter called *effective permeability*, $k_e$, comes into the picture instead of absolute permeability. Effective permeability depends on fluid saturations, wetting characteristics, and the geometry of pores and can be measured by doing some laboratory tests. Therefore, by having effective permeability of each phase and using it instead of absolute permeability, Darcy's equation is still valid and can be used. In order to evaluate the permeability of each phase in a multiphase flow system, based on the fluid saturation, a more straight forward parameter called *relative permeability*, $k_r$, is commonly used. This parameter is calculated through normalizing values of effective permeability by absolute permeability. Therefore, relative permeability is expressed as a fraction (or percentage) and it is calculated for the fluid phase *i* of a multiphase flow system by using Equation 3.20 as [35]:

$$k_{ri} = \frac{k_{ei}}{k} \qquad 3.20$$

where, $k_{ri}$ is the relative permeability and $k_{ei}$ is the effective permeability of fluid phase *i*, and $k$ is absolute permeability. In a reservoir that contains three phases of gas, oil, and water simultaneously, the relative permeability of these phases is denoted by $k_{rg}$, $k_{ro,}$ and $k_{rw}$ respectively. In this case, Equation 3.21 is valid [41].

$$k_{rg} + k_{ro} + k_{rw} < k \qquad 3.21$$

Relative permeability values are usually plotted as relative permeability versus fluid saturation curves. For a system, that has only oil and water, the fluid saturation on the *x*-axis varies from irreducible or connate water saturation ($S_{wc}$) to the residual oil saturation after water flooding ($S_{orw}$). Irreducible water saturation is the water saturation below that water is immobile or its relative permeability is zero, and residual oil saturation is the oil saturation below that oil is not mobile or the relative permeability of oil equals to zero. Figure 3.6 represents the relative permeability diagrams for both water-wet and oil-wet porous media contains oil and water. In this figure, $k_{rwro}$ is the maximum relative permeability of water taking place at the critical oil

saturation (where oil becomes mobile), and $k_{rocw}$ is the endpoint of oil relative permeability taking place at the critical water saturation (where water becomes mobile) [35, 41].

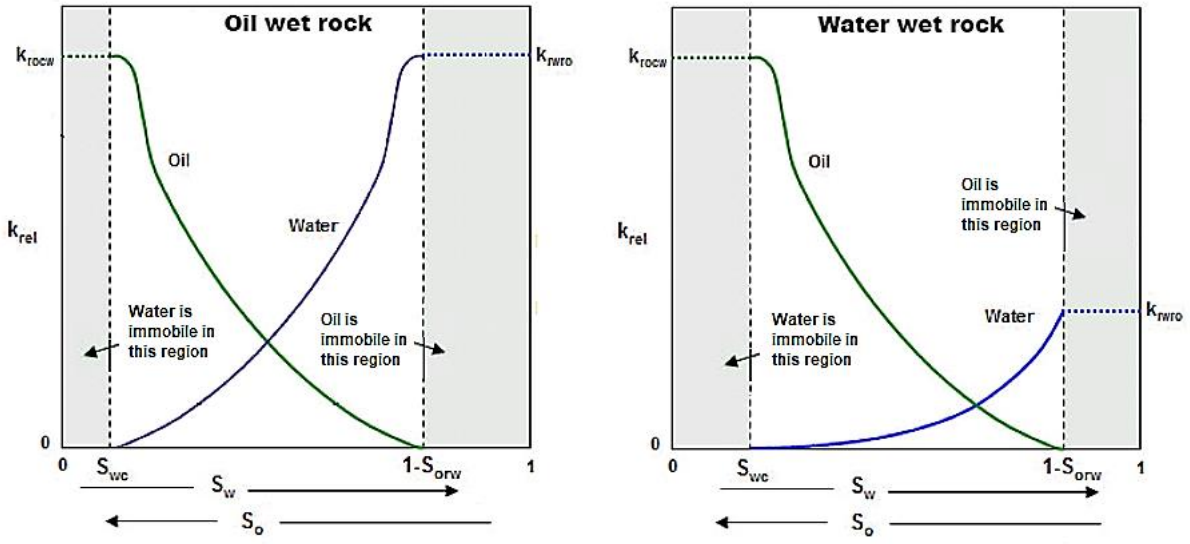


Figure 3.6: Typical oil-wet rock relative permeabilities (left) versus water-wet rock relative permeabilities. (right) [42].

#### 3.1.6.1 Mathematical models for relative permeability

In recent years, several mathematical models have been developed for the approximation of two-phase or three-phase relative permeability. One of the most accurate parametric models for the estimation of relative permeability for a two-phase system like gas-oil, gas-water, and oil-water systems is the Generalized Corey model. Based on this model, for an oil-water system, the relative permeability of oil and water can be estimated by the following functions [43]:

$$k_{ro} = k_{rocw}\left[\frac{1-S_w-S_{orw}}{1-S_{wc}-S_{orw}}\right]^{n_{ow}} \qquad 3.22$$

$$k_{rw} = k_{rwro}\left[\frac{S_w-S_{wc}}{1-S_{wc}-S_{orw}}\right]^{n_w} \qquad 3.23$$

where $S_w$ is the water saturation, $S_{wc}$ is the irreducible water saturation, $S_{orw}$ is the residual oil saturation, $n_{ow}$ and $n_w$ are the Corey exponents, $k_{rocw}$ and $k_{rwro}$ are the maximum relative permeability of oil and water respectively.

## 3.2 Reservoir fluid properties

In this subchapter, some of the most important physical properties of reservoir fluids used in this thesis are briefly explained.

### 3.2.1 Physical classification of crude oils

One of the most common physical properties used for the classification of crude oils is the specific gravity. The specific gravity of crude oil, $\gamma_o$, is a dimensionless number and defined as [35]:

$$\gamma_o = \frac{\rho_o}{\rho_w} \tag{3.24}$$

where $\rho_o$ and $\rho_w$ are the density of crude oil and water respectively at the standard condition of 60˚F and 14.7 psia.

Another scale widely used in the petroleum industry is the API gravity and it is defined based on the specific gravity as [35]:

$$°\text{API} = \frac{141.5}{\gamma_o} - 131.5 \tag{3.25}$$

API gravity indicates how heavy or light the crude oil is compared to water and based on that, crude oils can be classified into the four main groups as [44]:

- Light oil when API > 31.1˚
- Medium oil when 22.3˚ < API < 31.1˚
- Heavy oil when 10˚ < API < 22.3˚
- Extra-heavy oil when API < 10˚

### 3.2.2 Classification of reservoir fluids

Typically, produced fluids from a petroleum reservoir consist of several different compounds in two or three phases of gas, liquid, and solid (in some conditions wax, asphaltene, and hydrates which are in a solid phase may also exist). Besides, each compound has specific physical properties and phase behavior at different pressure and temperature conditions that are different from the other compounds. However, petroleum reservoir fluids can be classified into five main categories based on their physical properties and phase behavior as [35, 45]:

- Black oils
- Volatile oils
- Gas condensates or retrograde gases
- Wet gases
- Dry gases

Table 3.2 shows the basic characteristics of each category of reservoir fluids based on physical properties and chemical compositions.

Table 3.2: Basic characteristics of the five types of reservoir fluids [35].

| Reservoir Fluid | API Gravity (°) | Viscosity (cP) | Color of Stock Tank Liquid | Initial Producing GOR (scf/STB) | Mol% of $C_{7+}$ |
|---|---|---|---|---|---|
| Black oils | 15–40 | 2 to 3–100 and up | Dark, often black | 250–1,750 | >20.0 |
| Volatile oils | 45–55 | 0.25–2 to 3 | Brown, orange, or green | 1,750–3,200 | 12.5–20.0 |
| Gas condensates | Greater than 50 | In the range of 0.25 | Light colored or water white | >3,200 | <12.5 |
| Wet gases | Greater than 60 | In the range of 0.25 | Water white | >50,000 | May be present |
| Dry gases | No liquid is formed, hence the name "dry" | 0.02–0.05 | — | — | — |

As Figure 3.7 is showing, at a given pressure and temperature, and regardless of the melting, boiling, and sublimation boundaries, a single compound only exists in one phase of gas, liquid, or solid. However, since each compound has a special phase behavior and there is a mixture of compounds in a petroleum reservoir, both gas and liquid phases may exist in vapor-liquid equilibrium over a wide range of temperature and pressure conditions [45].

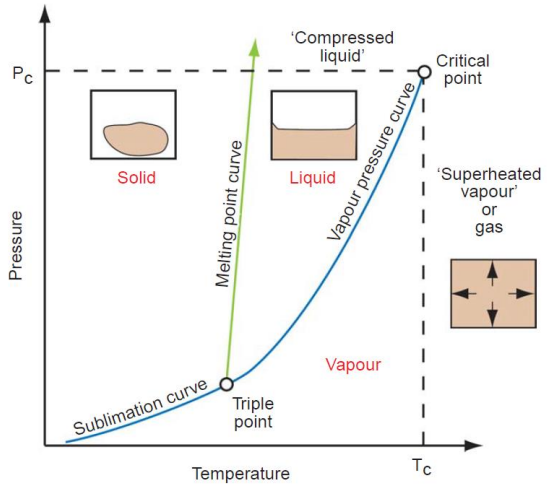


Figure 3.7: Pressure-temperature phase diagram for a single-compound system [45].

For a mixture of compounds, a mixture of phases may exist and one way of determining and representing the phase behavior of such mixtures is using the phase envelope diagrams. The phase envelope diagrams can be generated by either using pressure-volume-temperature (PVT) data which is obtained by laboratory tests or using equation-of-states (EOS) models. Figure 3.8 represents a phase envelope diagram for a hydrocarbon mixture. Besides, the approximate location of the initial pressure and temperature of the reservoir and separator for different types of reservoir fluids with respect to the given phase envelope diagram has been specified. The figure distinguishes the phase behavior of different types of reservoir fluids. As an example, it can be seen that compare to other reservoir fluid types, the black oils are liquid and well below their critical point at the reservoir pressure and temperature, and during their production by decreasing the pressure, a small portion of them will be evaporated [35, 45].

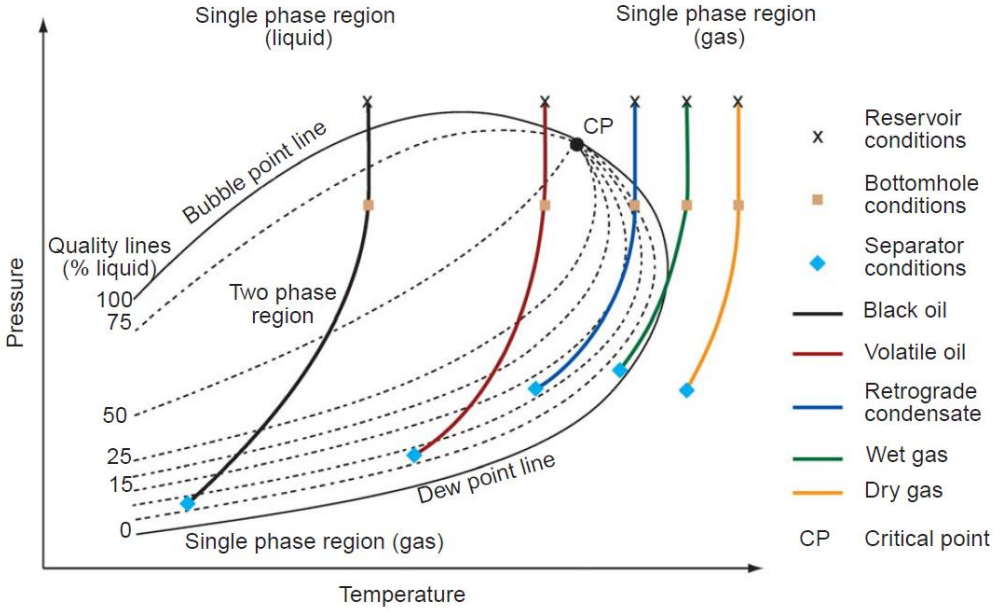


Figure 3.8: Phase envelope for a hydrocarbon mixture [45].

### 3.2.3 Black oil models

In order to simulate petroleum production from a reservoir, it is necessary to know the physical properties and the phase behavior of the reservoir fluids over a wide range of pressure and temperature. For achieving this goal, one way is using the PVT data, which is determined by the experiment. Another way is solving the equation-of-states (EOS) based on the temperature, pressure, chemistry, and overall composition of reservoir fluids and there are some commercial software packages (like PVTsim and Multiflash) available for doing that. Since doing laboratory tests for determining the PVT data is difficult and access to commercial soft may not be easy, several empirical correlations have been developed based on laboratory test results and available field data in recent years. Knowing the reservoir fluid composition is not required for using these empirical models due to the fact that in these models the reservoir fluids are considered as black oils. Therefore, these empirical correlations are called *black oil models.* Black oils are the most common type of reservoir fluids and generally, they contain more than 20% $C_{7+}$, which are considered as heavy hydrocarbons. Therefore, black oils have the widest phase envelope diagram among different types of reservoir fluids meaning they cover a wide range of temperatures. Figure 3.9 depicts the typical black oil phase envelope diagram. Point A is showing the initial reservoir pressure and condition and the ABC route represents the isothermal reduction of pressure in the reservoir. Anywhere along the AB path, the oil is a single-phase liquid and undersaturated, meaning that at the presence of gas oil can dissolve more gas. After point B, oil becomes saturated. Since black oil has a high critical temperature, the reservoir condition is located well to the left-hand side of the critical point leading to fairly low bubble point pressure. Furthermore, the separator condition is located in the two-phase region of the phase envelope diagram near a relatively high-quality liquid line which means that a large amount of oil remains liquid and reaches the surface [35, 45].

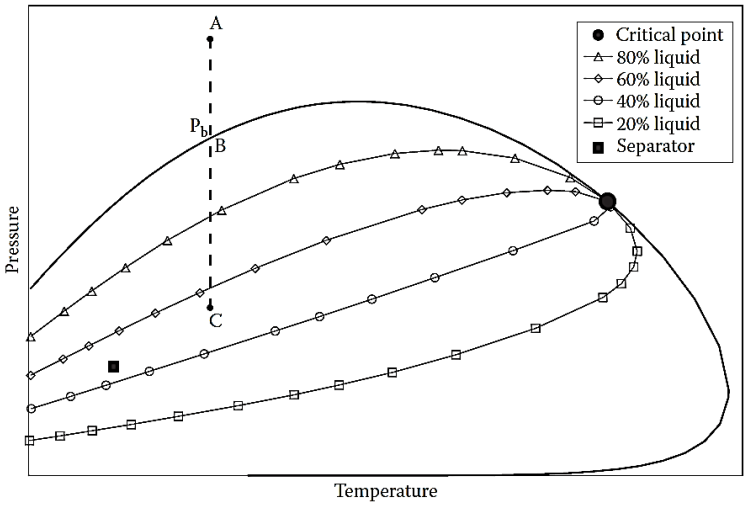


Figure 3.9: Phase envelope of a typical black oil [35].

#### 3.2.3.1 Lasater model

One of the appropriate black oil models widely used today is the Lasater model. The Lasater correlations can be used for the conditions given in Table 3.3 [46].

Table 3.3: Conditions for using the Lasater model [32].

| **Conditions** | **Units** |
|---|---|
| $17.9^\circ < \text{API} < 51.1^\circ$ | $^\circ$API |
| $48 < P_b < 5780$ | psia |
| $82 < T < 272$ | $^\circ$F |
| $3 < R_{sb} < 2905$ | scf/stb |
| $0.574 < \gamma_g < 1.223$ | $\gamma_{air} = 1$ |

where $P_b$ is the bubble point pressure, $T$ is the reservoir fluid temperature, $R_{sb}$ is the solution gas-oil-ratio, and $\gamma_g$ is the specific gravity of the gas.

### 3.2.4 Multiphase flow measurement terms

In this part, some commonly used multiphase flow measurement terms are described.

#### 3.2.4.1 Water cut

The ratio of the volume flow rate of water produced to the volume flow rate of total liquid produced is called *water cut* and is abbreviated with *WC*. It is a dimensionless number which can be presented as a percentage (or a fraction) with the following equation [47]:

$$WC = \frac{\dot{Q}_{water}}{\dot{Q}_{liquid}} = \frac{\dot{Q}_{water}}{\dot{Q}_{water} + \dot{Q}_{oil}} \times 100\% \qquad 3.26$$

#### 3.2.4.2 GOR

The ratio of the volume flow rate of gas produced to the volume flow rate of oil produced is called *GOR* which mathematically can be defined as [48].

$$GOR = \frac{\dot{Q}_{gas}}{\dot{Q}_{oil}} \qquad 3.27$$

GOR can be presented by either $sm^3/sm^3$ or scf/stb (standard cubic feet per stock tank barrel).

#### 3.2.4.3 GLR

The gas-liquid ratio or *GLR* is the ratio of the volume flow rate of gas produced to the volume flow rate of total liquid produced which is defined as [49]:

$$GOR = \frac{\dot{Q}_{gas}}{\dot{Q}_{liquid}} = \frac{\dot{Q}_{gas}}{\dot{Q}_{oil} + \dot{Q}_{water}} \qquad 3.28$$

## 3.3 Productivity index for horizontal wells

The potential or ability of a reservoir to deliver fluids to the wellbore is measured by a parameter called *productivity index*, *J*. In the other words, productivity index represent the volume of fluids that can be delivered by the reservoir to the wellbore per each unit of the pressure drawdown during a specific period of time and therefore it is commonly stated as bbl/psi/day. During recent years, several mathematical models have been proposed for calculating the productivity index both for vertical and horizontal wells. One of the best models that have proved useful in practice for estimating the productivity index of open-hole horizontal wells with a nearly rectangular drainage area and eccentric in the horizontal direction, has been introduced by Babu and Odeh. Equation 3.29 shows the general form of this model [45, 50]:

$$J = \frac{7.08 \times 10^{-3} \times b\sqrt{k_x k_z}}{B\mu(\ln(C_H \sqrt{ah} / r_w) - 0.75 + S_r} \qquad 3.29$$

where $J$ is productivity index (in stb/d/psi) $a$, $b$ and $h$ are geometric parameters (in ft) and shown in Figure 3.10, and $r_w$ is the radius of the wellbore (in ft). Moreover, $k_x$ and $k_z$ are the permeability of the reservoir in the $x$ and $z$ direction respectively (in mD). $B$ is the formation volume factor which is the ratio of gas volume at the reservoir condition to the gas volume at

the standard condition (in res. bbl/stb) and $C_H$ and $S_r$ are the Babu and Odeh model's parameters [51].

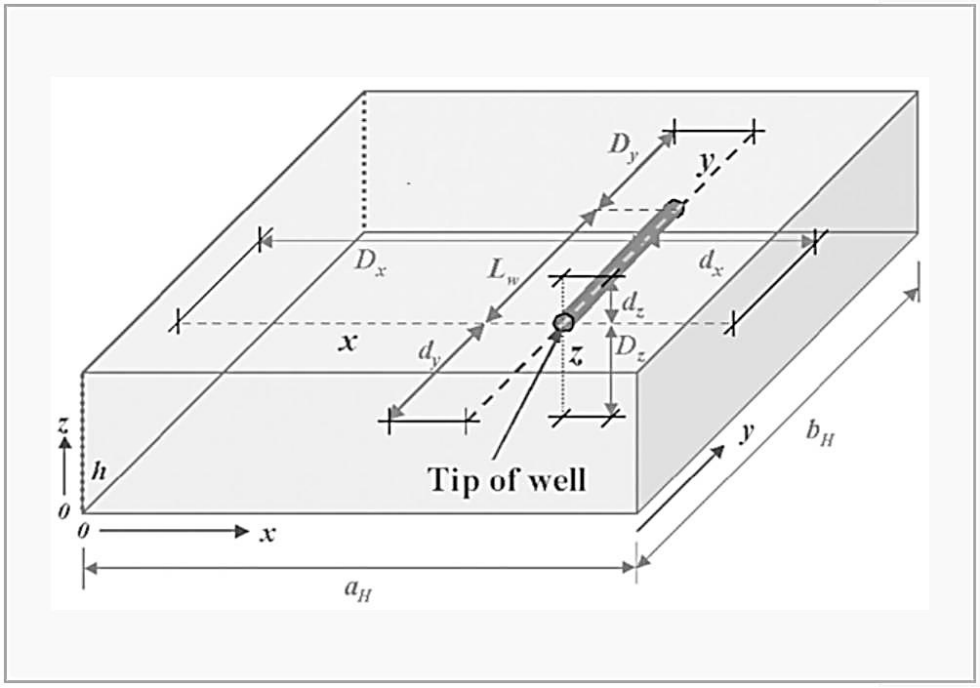


Figure 3.10: Well and reservoir geometry, and nomenclature used in the Babu and Odeh model [52].

In the Babu and Odeh model, some equations have been proposed for calculating the $C_H$ and $S_r$ parameters, which are the function of the geometry of the drainage area related to the location of the well and the permeability of the reservoir in the *x*, *y*, and *z* directions. Based on these formulas, if the conditions of Equation 3.30 are satisfied, Equations 3.31 and 3.35 can be used for the calculation of the $S_r$ and $C_H$ respectively [52].

$$\frac{b}{\sqrt{k_y}} > \frac{1.33a}{\sqrt{k_x}} \gg \frac{0.75h}{\sqrt{k_z}} \qquad 3.30$$

$S_r$ can be calculated by using the following equations:

$$S_r = P_{xyz} + P_y + P_{xy} \qquad 3.31$$

where:

$$P_{xyz} = \left(\frac{b}{L_w} - 1\right)\left\{\ln\left(\frac{h}{r_w}\right) + 0.25\ln\left(\frac{k_x}{k_z}\right) - \ln\left[\sin\left(\frac{\pi d_z}{h}\right)\right] - 1.838\right\} \qquad 3.32$$

and by considering $y_m = d_y + \frac{L_w}{2}$:

$$P_y = \frac{6.28b^2}{ah}\frac{\sqrt{k_x k_z}}{k_y}\left[(\frac{1}{3}-\frac{y_m}{b}+\frac{y_m^2}{b^2})+\frac{L_w}{24b}(\frac{L_w}{b}-3)\right] \quad 3.33$$

and also, when $d_x \geq 0.25a$:

$$P_{xy} = (\frac{b}{L_w}-1)(\frac{6.28a}{h}\sqrt{k_z/k_x})(\frac{1}{3}-\frac{d_x}{a}+\frac{d_x^2}{a^2}) \quad 3.34$$

Besides, Babu and Odeh proposed Equation 3.35 for calculating $C_H$ as:

$$\ln C_H = \frac{6.28a}{h}\sqrt{k_z/k_x}(\frac{1}{3}-\frac{d_x}{a}+\frac{d_x^2}{a^2})-\ln(\sin\frac{\pi d_z}{h})-0.5\ln\left[(a/h)\sqrt{k_z/k_x}\right]-1.088 \quad 3.35$$

## 3.4 Pressure drop in horizontal wells

One of the most important parameters that strongly affects oil production from a horizontal well is the frictional pressure drop along the well. Therefore, predicting the frictional pressure drop is highly important for achieving suitable modeling and simulation of oil production from a horizontal well. During oil production, fluid flow in the production tubing can be in a single-phase or multiphase state. When the fluid flow in a pipe is in the multiphase state, the pressure drop along the pipe is a function of several parameters and the calculation of that needs to use computer software. However, in order to calculate the frictional pressure drop in a pipe for a single-phase flow, several straightforward equations have been proposed in recent years. In general, for a single-phase flow the frictional pressure drop ($\Delta P_f$) in a pipe with a length of $L$ is a function of fluid density ($\rho$) and viscosity ($\mu$), as well as the diameter of the pipe ($d$) and a coefficient called *Mody frictional factor* ($f$). Frictional pressure drop is calculated by the Darcy–Weisbach equation which is represented by Equation 3.36 as [45, 53, 54]:

$$\frac{\Delta P_f}{L} = \frac{f\rho v^2}{2D} \quad 3.36$$

When the flow in the pipe is laminar the Mody frictional factor does not depend on the roughness of the pipe and $f$ is calculated by [45]:

$$f = \frac{64\mu}{\rho v d} \quad 3.37$$

where $v$ is the fluid velocity and $\rho vd/\mu$ is known as the Reynolds number (Re).

In most cases in oil production tubing the flow is turbulent and in this condition, $f$ is a function of pipe roughness ($\varepsilon$) and several equations are available for calculating this factor. One of the most commonly used equations, known as Colebrook–White equation is represented by Equation 3.38 as [45, 53]:

$$\frac{1}{\sqrt{f}} = 1.74 - 2\log\left(\frac{2\varepsilon}{d} + \frac{18.7}{\mathrm{Re}\sqrt{f}}\right) \qquad 3.38$$

## 3.5 General mathematical models for ICDs and RCPs

In the following subchapters, the mathematical equations governing the ICDs and RCPs are explained.

### 3.5.1 Passive inflow control devices (ICDs), orifice type

Base on the geometry of the orifice ICDs and the way of installation of them shown in Figure 3.11, they can be considered as a thin orifice plate for restriction of the fluid flow.

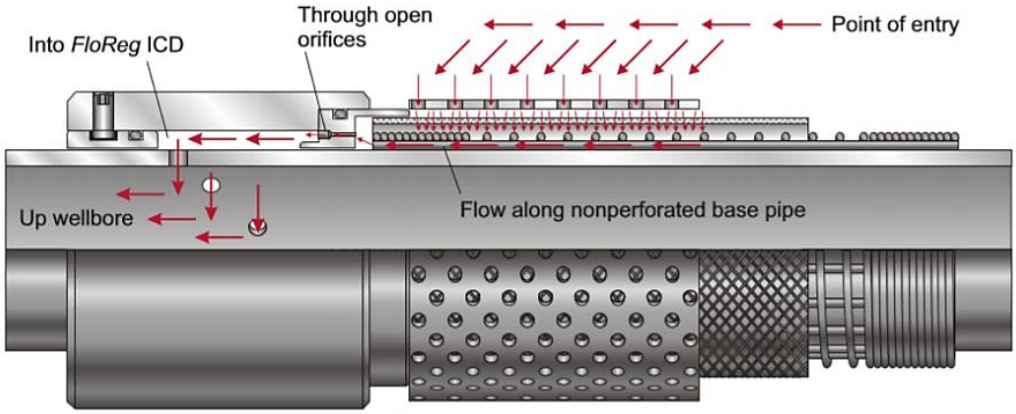


Figure 3.11: Schematic model of orifice ICDs [55].

The mathematical equation for an ideal thin orifice plate can be derived based on the continuity and Bernoulli's equations. Figure 3.12 shows a thin orifice plate in the middle of a pipe that restricts the fluid flow like an ICDs.

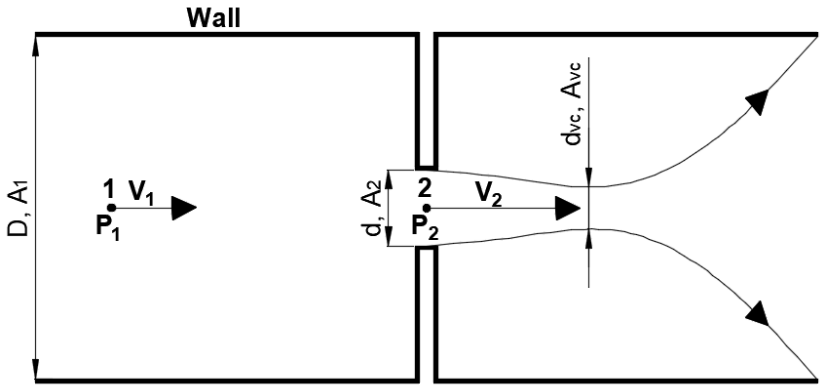


Figure 3.12: Schematic of a thin orifice plate in the middle of a pipe.

Points 1 and 2 are in the same height and the frictional losses can be neglected. By assuming steady-state, incompressible, and laminar fluid flow, as well as uniform velocity at points 1 and 2, Bernoulli's Equation, can be written as [56]:

$$P_1 + \frac{\rho v_1^2}{2} = P_2 + \frac{\rho v_2^2}{2} \qquad 3.39$$

Based on the continuity equation it can be concluded that:

$$\dot{Q} = v_1 A_1 = v_2 A_2 \Rightarrow v_1 = \frac{\dot{Q}}{A_1}, v_2 = \frac{\dot{Q}}{A_2} \qquad 3.40$$

By using Equation 3.39 and 3.40, Equation 3.41 is derived for calculating the flow rate passing through the orifice as:

$$\dot{Q} = A_2 \sqrt{\frac{2(P_1 - P_2)/\rho}{1-(A_2/A_1)^2}} \qquad 3.41$$

Equation 3.41 was derived for an ideal case. In practice, the flow rate $\dot{Q}$ is lower because of the geometry conditions. As a result, Equation 3.41 can be modified for the real cases by introducing the discharge coefficient, $C_D$, and changed as:

$$\dot{Q} = C_D A_2 \sqrt{\frac{1}{1-\beta^4}} \cdot \sqrt{\frac{2\Delta P}{\rho}} \qquad 3.42$$

Where $\dot{Q}$ is the volume flow rate of the fluid passing through the orifice plate (in $m^3$ /s), $\Delta P$ is the pressure drop over the orifice plate (in Pa), $\rho$ is the fluid density (kg/$m^3$) and $\beta = d / D$ . In Equation 3.42, $C_D = A_2 / A_{vc}$ in which $A_2$ is the cross-sectional area of the orifice hole (in m) and $A_{vc}$ is the minimum jet area just downstream of the orifice called *Vena Contracta* (in m). For orifice ICDs, the diameter of the orifice, *d*, is very small compared to the size of the annulus and production tubing which can be considered as *D*. Therefore, it can be assumed that $\beta = d / D \approx 0$ . If $0 \le a \le 1$ and the parameter *a*, represents the value of valve opening, equation 3.42 can be written as [56]:

$$\dot{Q} = a A_2 C_D \cdot \sqrt{\frac{2\Delta P}{\rho}} \qquad 3.43$$

Equation 3.43 represents the mathematical equation governing the behavior of orifice ICDs.

### 3.5.2 Autonomous inflow control devices (AICDs), RCP type

The RCP valves are designed in such a way that unwanted water and gas production is restricted autonomously. They have a levitating disc that regulates the flow path area and the position of that depends on the fluid viscosity and density. The levitating disc moves in response to the

static pressure, dynamic pressure, and frictional loss across the RCP valve. The picture of the RCP valve and the flow path through that is shown in Figure 3.13 [25, 57].

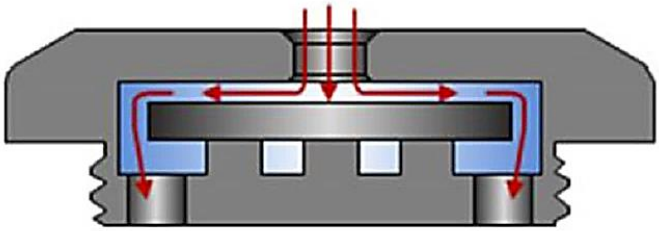

Figure 3.13: RCP flow pass [58].

The performance of the RCP valves is based on Bernoulli's equation. If the elevation and the compressible effect is neglected, the Bernoulli's equation for the valve can be expressed as [25]:

$$P_1 + \frac{\rho v_1^2}{2} = P_2 + \frac{\rho v_2^2}{2} + \Delta P_{friction\ loss} \qquad 3.44$$

where $P_1$ and $P_2$ are the static pressure in the reservoir side and well side respectively. The terms $\rho v_1^2/2$ and $\rho v_2^2/2$ are the dynamic pressure and $\Delta P_{friction\ loss}$ is the frictional pressure loss across the RCP valve. Equation 3.44 indicates that the sum of static pressure, dynamic pressure, and frictional pressure loss along the flow pass remains constant. Low viscous fluids like gas and water flow with higher velocity than oil. As a result, when gas or water flows through the RCP valve, the static pressure at the reservoir side of the valve will be lower. This creates a back pressure lifting the disc toward the inlet and consequently the flow of low viscous fluids like gas or water is restricted. When more viscous fluid passes through the RCP valve, due to the higher viscosity the frictional pressure loss increase resulting in decreasing the static pressure at the well side. Therefore, the total force acting on the disk depresses the disk and fully open the RCP valve, and allowing the fluid flows [25, 57].

#### 3.5.2.1 Analytical solution

By assuming incompressible fluid and after some simplification, Asheim et al have proposed an analytical solution for the pressure drop across the RCP valves as [24]:

$$\Delta p = \frac{\rho^3}{\mu^2} C_4 \dot{Q}^4 - \rho C_2 \dot{Q}^2 \qquad 3.45$$

where $\dot{Q}$ is the volumetric flow rate (in litter/s), $\rho$ is density (in kg/m$^3$ ), $\mu$ is viscosity (in cP) and $E$ is efficiency. $C_4$ and $C_2$ are the design parameters and depend on the RCP valve geometrical parameters, $r_e$ and $r_i$ (in mm) shown in Figure 3.14 and they can be calculated by the following equations:

$$C_4 = 357\frac{1}{r_i^6}\left[\frac{1}{4}\frac{r_i^2}{r_e^2}(1-E) + f_d \ln(\frac{r_e}{r_i}) f_d^2\right] \quad 3.46$$

$$C_4 = \frac{2.5}{r_i^4} \quad 3.47$$

$$f_d = \ln(r_e / r_i) - 0.5(1-E) \quad 3.48$$

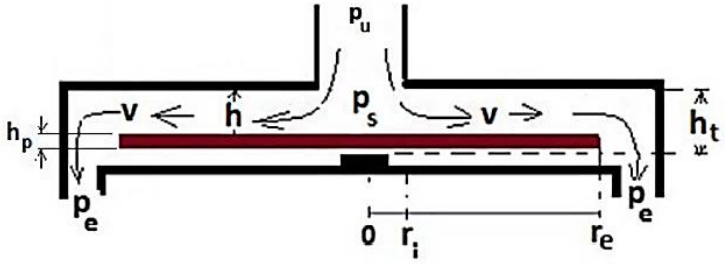


Figure 3.14: Schematic of the simplified RCP valve for analytical solving [59].

#### 3.5.2.2 Empirical function

The pressure drop across an RCP valve can be determined by Equation 3.49, which is an empirical mathematical function developed and validated by Statoil, and it is represented as:

$$\Delta P = f(\rho,\mu)\cdot a_{AICD}\cdot \dot{Q}^x \quad 3.49$$

where $\dot{Q}$ is the volumetric flow rate of fluid, and $a_{AICD}$ and $x$ are user-input parameters depending on the RCP design and fluid properties. $f(\rho,\mu)$ is an analytical function of fluid density and viscosity and defined as:

$$f(\rho,\mu) = \left(\frac{\rho_{mix}^2}{\rho_{cal}}\right)\cdot\left(\frac{\mu_{cal}}{\mu_{mix}}\right)^y \quad 3.50$$

where $y$ is a user-input parameter, and $\rho_{cal}$ and $\mu_{cal}$ are specified as calibration density and viscosity respectively. Moreover, $\rho_{mix}$ and $\mu_{mix}$ are the density and viscosity of the mixture of fluids passing through the RCP valve and are defined by:

$$\begin{aligned}\rho_{mix} &= \alpha_{oil}\rho_{oil} + \alpha_{water}\rho_{water} + \alpha_{gas}\rho_{gas}\\ \mu_{mix} &= \alpha_{oil}\mu_{oil} + \alpha_{water}\mu_{water} + \alpha_{gas}\mu_{gas}\end{aligned} \quad 3.51$$

where $\alpha_{oil}$, $\alpha_{water}$ and $\alpha_{gas}$ are the volume fraction of oil, water and gas in the mixture respectively.

## 3.6 Linear regression

Linear regression is a method of predicting the relationship between two sets of corresponding variables (dependent and independent variables) by fitting a linear model on them. One of the commonly used techniques for fitting linear regression models is the least square approach. Based on this method, if a function between two sets of corresponding variables, ($x_1$, $x_2$, …, $x_n$) and ($y_1$, $y_2$, …, $y_n$), can be described by a linear model as $y = \varphi^T(x) \cdot \theta$ where $\theta$ is the vector of unknown parameters of this model, $\theta^*$ which is the vector including the optimum values for the unknown parameters of the model, can be calculated by [60]:

$$\theta^* = (\phi^T \phi)^{-1} \phi^T Y \qquad 3.52$$

where:

$$\phi = \begin{bmatrix} \varphi^T(x_1) \\ \varphi^T(x_2) \\ \vdots \\ \varphi^T(x_n) \end{bmatrix}, \text{ and } Y = \begin{bmatrix} y_1 \\ y_2 \\ \vdots \\ y_n \end{bmatrix}$$

# 4 Johan Sverdrup oil field

The Johan Sverdrup is a giant oil field located in the central part of the North Sea, about 140 km west of Stavanger, Norway shown in Figure 4.1. The water depth in this field is between 110 and 120 m, and the depth of the main reservoir, which mostly contains oil in sandstone, is about 1900 m. The main reservoir has an excellent quality owing to its very high permeability. In this field water injection as well as gas lift are used as the pressure support. Oil is transported from the riser platform to the Mongstad terminal by a pipeline and gas is exported to Kårstø terminal with another pipeline [61, 62].

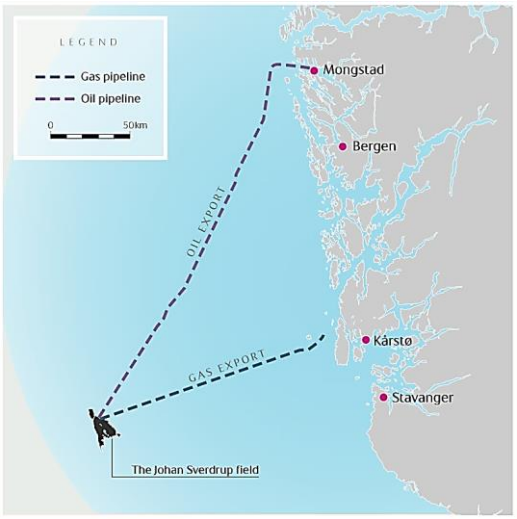


Figure 4.1: Johan Sverdrup field map [5].

This field was discovered in 2010 and production from the first phase of that was started with about 350000 bbl/d from October 2019. It is expected that the plateau production from this field reaches 440000 bbl/d in 2020. The second phase of the Johan Sverdrup field is developing and the production from this phase will start in 2022. After completion of the second phase, it is predicted that the field will produce 660000 bbl/d in total. Table 4.1 represents the current resource estimations for this filed in mill. $Sm^3$ estimated by Norwegian Petroleum Directorate (NPD). Currently, Equinor is the operator of this field and also the largest ownership interest of this field belongs to this company. The other partners are Ludin Petroleum, Total E&P Norge, Petoro, and Aker BP [61, 63].

Table 4.1: NPD's current resource estimations for the Johan Sverdrup oil field [61].

| | Oil | Gas | NGL | Condensate | Sum |
|---|---|---|---|---|---|
| Recoverable reserves originally | 406.6 | 10.2 | 8.6 | 0.0 | 425.4 |
| Remaining reserves | 402.9 | 10.1 | 8.5 | 0.0 | 421.4 |

## 4.1 Well 16/2-D-12

Since there is a plan for developing the Johan Sverdrup field (JSF) in the near future, and a few studies have been done on this field so far, further studies are needed to promote technologies and obtain more cost-effective oil recovery in this field. Therefore, the thesis focuses on making a model for near well simulation of oil production from one of the production wells in this oil field. According to NPD's fact pages [64], several production wells have been drilled in the JSF but since there is more information available about the characteristics of the reservoir near the well 16/2-D-12, this well has been chosen for the study, modeling, and simulation in the thesis. The drilling information and the location of well 16/2-D-12 are shown in Figure 4.2. This well has the total length or measured depth (MD) of 3875 m and the final vertical depth (TVD) of this well is 1876 m. The general information of the well 16/2-D-12 has been presented in Appendix B.

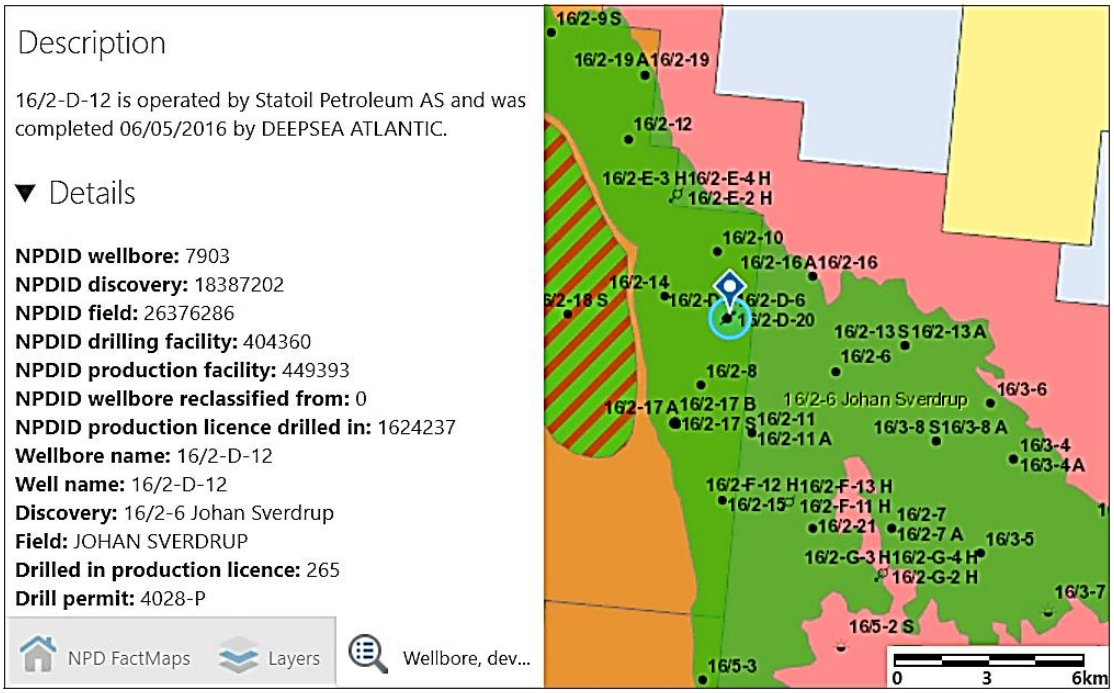


Figure 4.2: Drilling information and the location of the well 16/2-D-12 in the Johan Sverdrup oil field [64].

## 4.2 Characteristics of the reservoir near the well 16/2-D-12

To prepare a realistic model for simulation of oil production from the well 16/2-D-12 in OLGA/ROCX it is necessary to know the realistic characteristics of the reservoir near the drainage area of this well. According to NPD's fact pages [64], in order to evaluate the hydrocarbon resources and investigate the characteristics of the Johan Sverdrup field, several appraisal wells have been drilled. The well 16/2-8 is one of these appraisal wells which is the nearest well to the production well 16/2-D-12. As a result, the characteristics of the reservoir near the drainage area of the well 16/2-D-12 can be approximated by the obtained information from the well 16/2-8. The general information of the well 16/2-8 has been presented in Appendix C.

In the following subchapters, the most important reservoir rock and fluid properties near the well 16/2-D-12 used in the modeling and simulation are investigated.

### 4.2.1 Reservoir pressure and temperature

Based on the well test data, the bottom hole temperature of the well 16/2-8 is 81 ˚C. Moreover, by using the reported formation pressure data, the formation pressure near this well can be approximated to be about 240 bar. The formation pressure data for the well 16/2-8 and the approximation of the pressure have been given in Appendix D [64].

### 4.2.2 Reservoir fluid properties

According to the Equinor's crude summary report and the well test data provided by NPD for the well 16/2-8, the given information in Table 4.2 for the crude oil properties near the well 16/2-8 has been collected [61, 65]. The NPD's well test data and the Equinor's crude summary report have been presented in Appendix C and Appendix E respectively.

Table 4.2: Crude oil properties in the JSF.

| **Parameter** | **Temperature** | **Value** |
|---|---|---|
| Density | 15 ˚C | 0.887 kg/$m^3$ |
| Density | Reservoir conditions | 0.820 kg/$m^3$ |
| API gravity | Standard conditions | 28.0 |
| Viscosity | 20 ˚C | 23.15 cP |
| Viscosity | 40 ˚C | 10.64 cP |
| Viscosity | 50 ˚C | 7.76 cP |
| Viscosity* | Reservoir conditions | 3 cP |
| GOR | Reservoir conditions | 44 $Sm^3/Sm^3$ |

* Since there is no information for the value of crude oil viscosity at the reservoir conditions, the value of that has been obtained by doing curve-fitting on the existing data explained in the method and calculation chapter, subchapter 5.1. Based on the information of Table 4.2 and comparing them with the criteria for the classification of reservoir fluids given in Table 3.2, the reservoir fluids near the well 16/2-8 is classified as the black oil type.

### 4.2.3 Reservoir rock properties

The following subchapters cover the most important properties of the reservoir rock near the drainage area of the simulated well.

#### 4.2.3.1 Reservoir thickness and fluid saturations

Based on the petrophysical analysis, the JSF consists of continuous reservoirs created by sandstones deposited in the Late Triassic and Middle to Upper Jurassic ages. The main part of the resources is located in the Intra Draupne sandstone formation. The sandstones from the Statfjord Group, the Vestland Group, and some in the Zechstein contain the rest of oil resources. Figure 4.3 shows the cross-section of the JSF from west to east. In the east, the reservoir has the minimum thickness and situated directly on the basement. In the western part of the reservoir, the thickness of the oil column is maximum and the production wells in the first phase of the JSF are located in this part near the well 16/2-8 [64, 66].

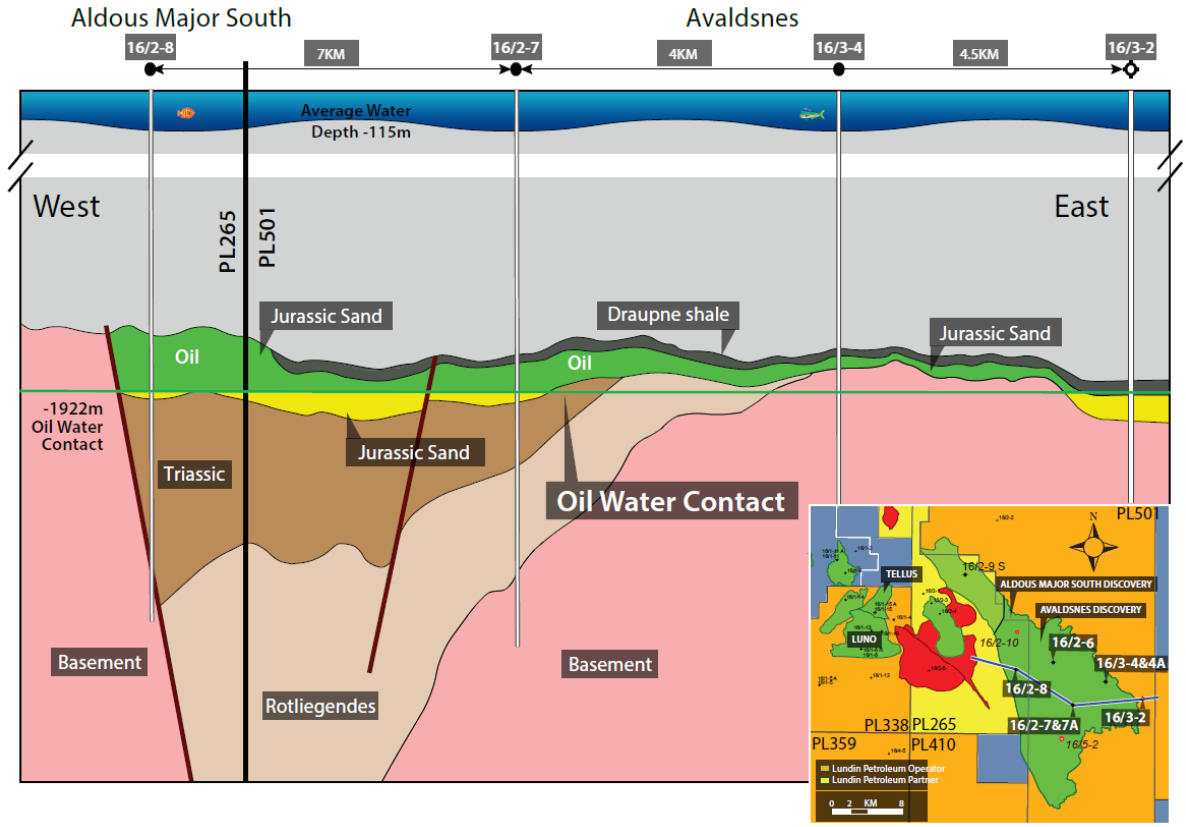


Figure 4.3: West to east cross-section of the JSF [67].

Based on the NPD's well test data obtained from the well 16/2-8 [64], the main reservoir has an oil column of 67.5 m started from the depth of 1877 m and ended to the depth of 1944.5 m. Moreover, the reservoir is located in two zones with different types of sandstone. from the depth of 1877 m to 1911 m, the reservoir is located in the Intra Draupne sandstone formation, and between the depth of 1911 m and 1944.5 m, it is mostly located in the Vestland Group sandstones (a small part of this zone is located in Hugin sandstone formation). Figure 4.4

represents the composite well log displays from the well 16/2-8. As can be seen in the figure, the red color illustrates the hydrocarbon saturation. In the first zone (Intra Draupne sandstone formation) the reservoir is highly saturated with oil, and oil saturation has small variations along the depth direction. However, in the second zone (Vestland Group sandstone) the reservoir has lower oil saturation with higher variations along the depth direction [64, 66]. Moreover, a small part of the reservoir located in Hugin sandstone formation has a very low oil saturation.

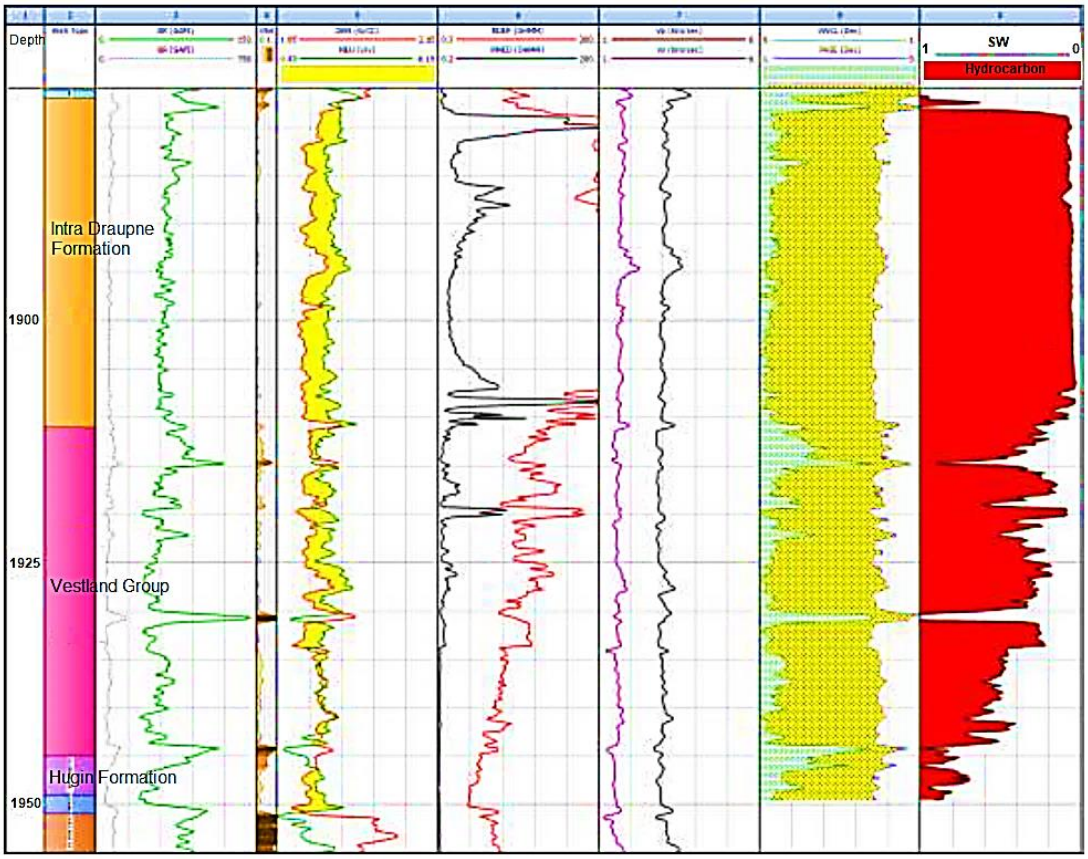


Figure 4.4: Composite well log displays from well 16/2-8 [66].

Based on the obtained information from the analysis of the well log data of the well 16/2-8, the thickness of the net pay zone, the shale volume, and water saturation of the reservoir near this well have been calculated and they are summarized in Table 4.3.

Table 4.3: Thickness of the net pay zone, average water saturation, and shale volume for the well 16/2-8 [66].

| **Zone** | **Res. Depth** | **Gross Res. Thick.** | **Net Pay Thick.** | **Average $S_w$** | **Average $V_{sh}$** |
|---|---|---|---|---|---|
| Zone 1 | 1877-1911 MD | 33.83 m | 32.46 m | 0.062 | 0.09 |
| Zone 2 | 1911-1945 MD | 33.99 m | 22.86 m | 0.322 | 0.122 |

#### 4.2.3.2 Porosity

There are several well logs including the Density Log, Nuclear Magnetic Resonance Log (NMR), Sonic Log, and the Neutron Log that can be used for estimating the porosity of a reservoir. Based on the analysis of well logs of the well 16/2-8, by using different methods, the porosity of the reservoir near this well has been calculated and illustrated in Figure 4.5. In the figure, PHIE indicates the effective porosity, PHIDen is the porosity calculated from the density log, PHIT is the total porosity and PHISon is the porosity calculated from the sonic log. It also must be mentioned that the range of variation of the reservoir rock porosity is between 0 and 0.5. Based on the calculation, the average effective porosity for both zones of the reservoir near the well 16/2-8 is 0.27 or 27% [66].

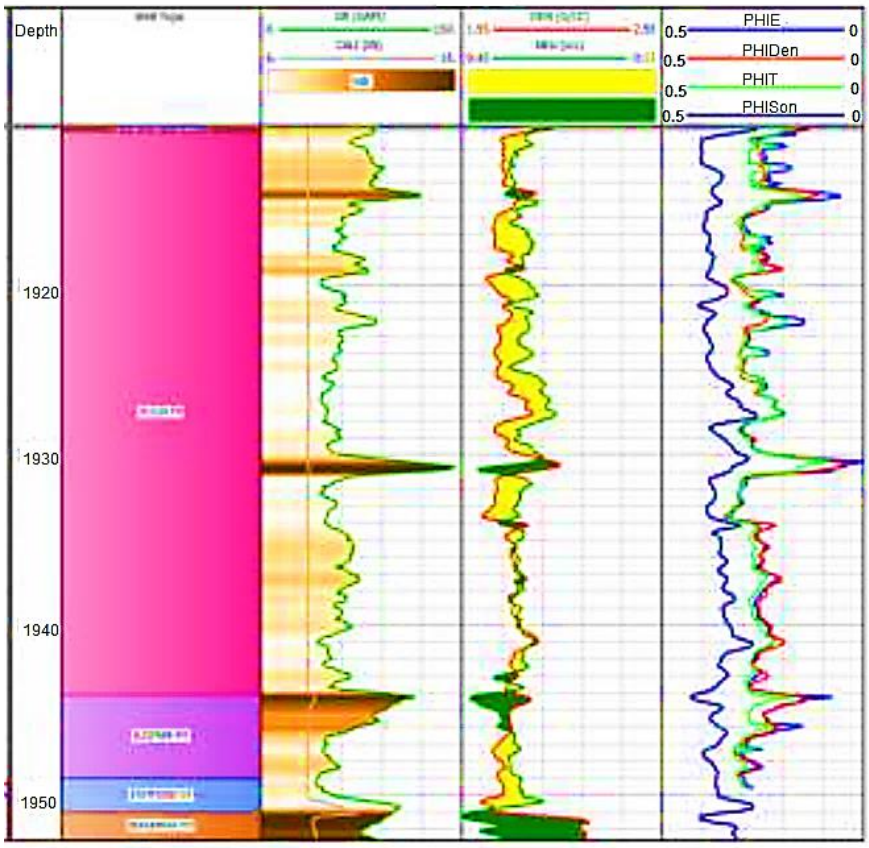


Figure 4.5: Calculated porosity of the well 16/2-8 by using different methods [66].

#### 4.2.3.3 Absolute permeability

Due to ideal deposition conditions, the main reservoir of the JSF has an exceptionally high permeability. By analysis of more than 1500 core samples, it can be concluded that the median permeability for the main reservoir is 19 D. However, the reservoir is highly heterogeneous and the permeability varies significantly across the field which is between 0.5 to 40 D near different appraisal wells. Figure 4.6 shows the median permeability for different appraisal wells in the JSF. As can be seen in the figure, the reservoir near the well 16/2-8 has a median permeability of 14.7 D [68].

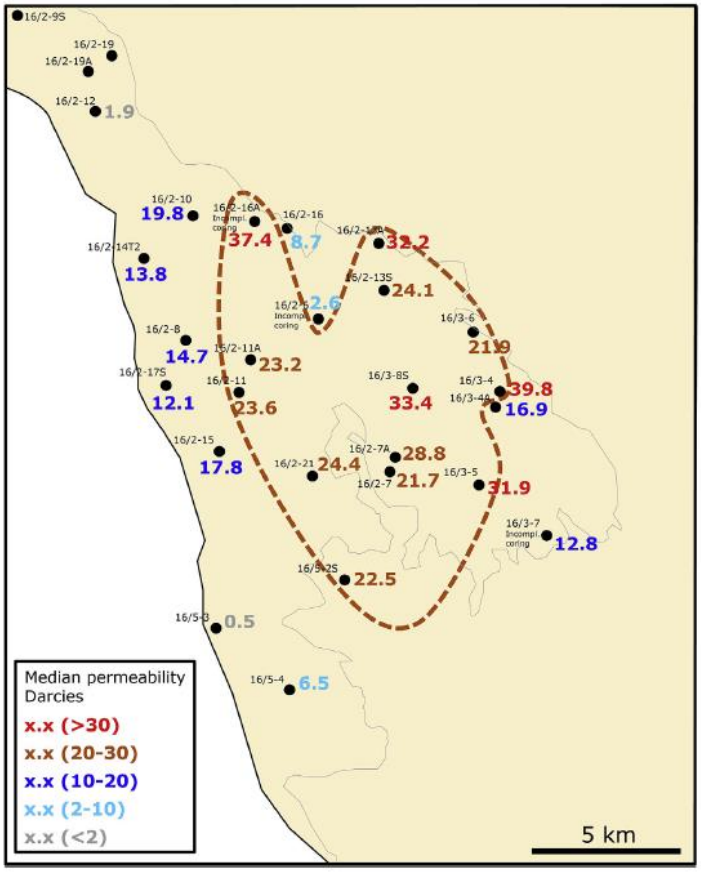


Figure 4.6: Median permeability for individual wells in the JSF [68].

#### 4.2.3.4 Wettability

The wettability in a reservoir depends on several factors like polar components in oil, formation water composition and salinity as well as rock composition. Since all clean sedimentary rocks are strongly water-wet, it can be believed that almost all reservoirs were water-wet initially in several million years ago. However, when oil invades into the rock over a long period of time because of the adsorption of polar components on the rock surface, the wettability of the reservoir rock can be altered. Besides, reservoir pressure and temperature affect the initial wettability. In order to change the initial wettability, the crude oil must have polar components that can be absorbed on the clay surface. Due to the temperature below 100˚C and shallow burial, this can happen easily in the Johan Sverdrup reservoir. In addition to that, since the adsorption of polar components requires the negatively charged clay surface, the reservoir must contain clay and this criterion also is met in the Johan Sverdrup reservoir. Another parameter that can affect the initial wetting is the pH of the formation water, which depends on the salinity of formation water. By considering all these parameters and criteria it can be believed that the Johan Sverdrup reservoir has a mixed-wet wettability state [69].

#### 4.2.3.5 Relative Permeability

Since there is no information about the relative permeability of the Johan Sverdrup reservoir in the literature, this parameter must be estimated base on the available information about the relative permeability of the other sandstone reservoirs in the North Sea with almost the same

characteristics. The Frøy field is located in the central part of the North Sea and it was shut down in 2001 due to the technical problems as well as the oil price. This field contains a sandstone reservoir and it is located in the middle Jurassic sandstones at a depth of 3200 to 3300 m. The Frøy filed is highly heterogeneous but it has high porosity and high absolute permeability in most places. Based on the analysis of several core plugs collected from Frøy reservoir, this reservoir has the porosity ranging from 12.1% to 25.3% and absolute permeability between 11 mD and 4800 mD. The physical properties of the core plugs collected from the Frøy field is attached in Appendix F. Moreover, the analysis of different samples from this reservoir indicates that the wettability of the Frøy reservoir varies between neutral, mixed-wet, and strongly oil-wet with Amott-Harvey indices ranging from 0 to -0.73. Therefore, the Frøy reservoir is a sandstone reservoir with high porosity and absolute permeability almost like the Johan Sverdrup reservoir, and also it has some mixed-wet zones like the Johan Sverdrup reservoir. As a result, the values of relative permeability of the Johan Sverdrup reservoir can be considered almost the same as that of the Frøy reservoir in the mixed-wet zones [70, 71].

Based on the obtained information from testing different core samples collecting from the Frøy reservoir, six sets of values for relative permeability endpoints and Corey parameters have been considered in this Master's thesis [70] for the calculation of relative permeability in the Frøy reservoir. Three of them are based on the SINTEF RESLab recommendations used in the Det norske's reservoir simulation model of the Frøy reservoir (Det norske have been the operator of the Frøy oil field). The rest has been proposed based on the recommended Corey parameters for different wetting characteristics. Table 4.4 represents these six sets of values for the different wettability states in the Frøy reservoir. In this table, ResLab's Low Case set of values is used for the most oil-wet state in the Frøy reservoir and the Water zone set of values is considered for the most water-wet state in this reservoir [70].

Table 4.4: End points and Corey parameters for calculation of relative permeability in the Frøy field [70].

| | $n_o$ | $n_w$ | $S_{wi}$ | $S_{or}$ | $k_{ro}(S_{wi})$ | $k_{rw}(S_{or})$ |
|---|---|---|---|---|---|---|
| ResLab's Low Case | 6 | 1 | 0.12 | 0.12 | 1 | 1 |
| ResLab's Base Case | 5.5 | 1.3 | 0.12 | 0.08 | 1 | 0.8 |
| ResLab's High Case | 5 | 1.8 | 0.12 | 0.05 | 1 | 0.6 |
| Mixed-wet | 4 | 2 | 0.12 | 0.05 | 1 | 0.4 |
| Slightly water-wet | 3 | 4 | 0.12 | 0.05 | 1 | 0.35 |
| Water zone | 2 | 7 | 0.12 | 0 | 1 | 0.25 |

As explained in the subchapter 4.2.3.4, the Johan Sverdrup reservoir is a mixed-wet reservoir. As a result, it can be considered that the relative permeability in the Johan Sverdrup reservoir is the same as that of the Frøy reservoir for the mixed-wet zones. Therefore, the Mixed-wet set of values for the endpoints and Corey parameters given in Table 4.4 can be used for calculating the relative permeability in the Johan Sverdrup reservoir as well. Figure 4.7 shows the relative permeability curves for the Johan Sverdrup reservoir calculated by recommended values given in Table 4.4 and using Equation 3.22 and 3.23, and considering an oil-water system.

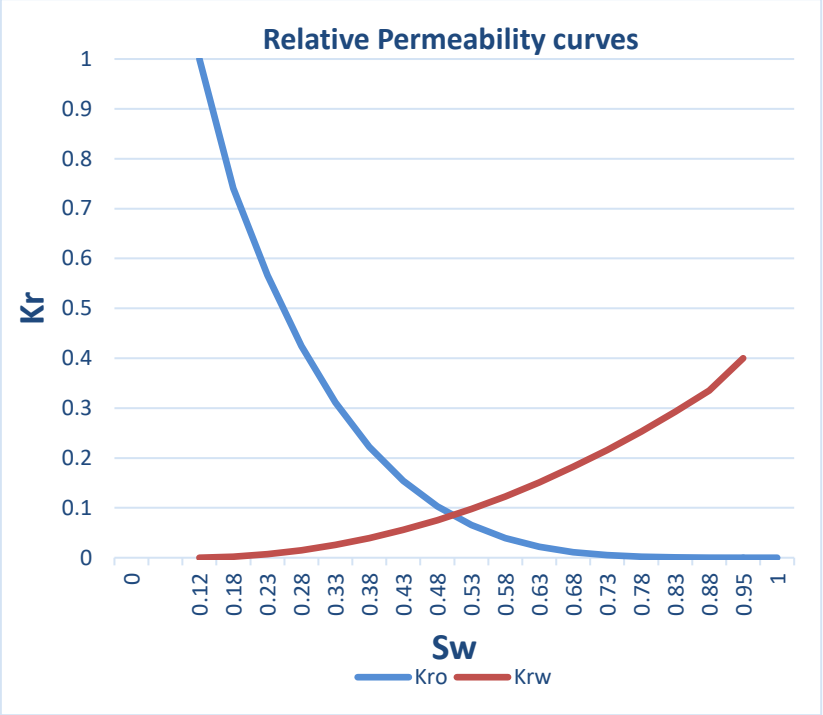


Figure 4.7: Relative permeability curves for the Johan Sverdrup reservoir.

# 5 Methods and calculations

This chapter contains the description of the methods used for the calculation of all unknown parameters needed for developing the OLGA/ROCX model and conducting the simulations.

## 5.1 Calculation of crude oil viscosity at the reservoir conditions

As mentioned in subchapter 4.2.2, there is no information about the viscosity of crude oil of the JSF at the reservoir conditions in the literature. However, its value is known in temperatures 20˚C, 40˚C, and 50˚C and they are given in Table 4.2. Therefore, based on the available values, the value of crude oil viscosity at the reservoir conditions (the pressure of 240 bar and the temperature of 81˚C) should be extrapolated. The method that is used for extrapolation is based on the linear regression method described in subchapter 3.6. To use this method, at first, a mathematical model between temperature and viscosity must be defined (the effect of pressure on viscosity can be neglected). Several empirical models have been proposed for describing the relation between viscosity and temperature. Equation 5.1 is a commonly used empirical equation for viscosity [72].

$$\mu = Ae^{B/T} \tag{5.1}$$

where *A* and *B* are unknown constant parameters that must be defined empirically. By taking logarithm form both side of Equation 5.1 it can be written as:

$$\ln \mu = \ln A + B/T \tag{5.2}$$

and as a result, it can be written as a matrix form as:

$$\ln \mu = \begin{bmatrix} 1 & 1/T \end{bmatrix} \begin{bmatrix} \ln A \\ B \end{bmatrix} \tag{5.3}$$

Equation 5.3 can be written as:

$$y = \varphi^T(x)\theta \tag{5.4}$$

if it is considered that $y = \ln \mu$, $\varphi^T = \begin{bmatrix} 1 & 1/T \end{bmatrix}$ and $\theta = \begin{bmatrix} \ln A \\ B \end{bmatrix}$.

Moreover, the matrices of $\phi$ and *Y* can be created by using the existing values of viscosity in different temperatures given in Table 4.2. By considering Equation 5.4, Equation 3.52 can be used for calculating the parameters *A* and *B*. Therefore, a curve can be fitted on the existing values given in Table 4.2 in order to extrapolate the crude oil viscosity for the temperature of 354 K (81˚C, the reservoir temperature). For solving these equations, a MATLAB code has been written and the result of running this MATLAB code shows that the crude oil viscosity of JSF at the reservoir condition is 2.9976 cP ~ 3 cP. Figure 5.1 illustrates the fitted curve on the known values of viscosity in temperatures of 20˚C, 40˚C, and 50˚C (293 K, 313 K, and 323 K). As can be seen, the curve perfectly fitted on the known values. The curve is fitted by using

the linear regression method and the extrapolated value of crude oil of JSF at the reservoir condition (354 K) by using this method is shown in the figure. The MATLAB code written for using this method is presented in Appendix G.

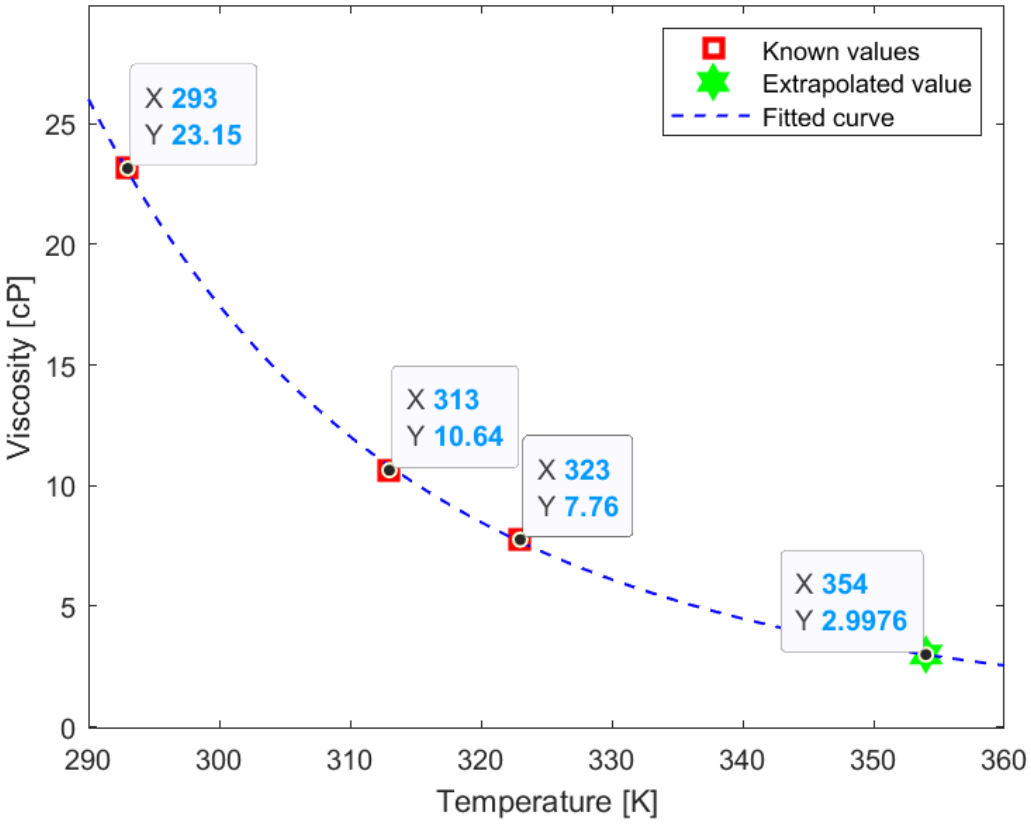


Figure 5.1: Estimation of crude oil viscosity of JSF at the reservoir temperature.

## 5.2 Calculation of the permeability anisotropy

As shown in Figure 4.4 and Table 4.3, the reservoir near the well 16/2-D-12 consists of two different zones. As a result, the average shale volume for the reservoir, $V_{sh,average}$, can be calculated as:

$$V_{sh,average} = \frac{h_{zone1} \cdot V_{sh\_zone1} + h_{zone2} \cdot V_{sh\_zone2}}{h_{zone1} + h_{zone2}} \qquad 5.5$$

where $h_{zone1}$ and $h_{zone2}$ are the net pay thicknesses of the first and second zones. Also, $V_{sh,zone1}$ and $V_{sh,zone2}$ are the shale volume of the first and second zones respectively.

By using Equations 3.7, 3.8, and 3.9, the values of permeability in the *x*, *y* and *z* directions, $k_x$, $k_y$, and $k_z$ respectively, as well as permeability anisotropy, $a = k_v / k_H$, can be calculated. The calculation procedure is presented in Appendix H, and Table 5.1 shows the results.

Table 5.1: Results from the permeability anisotropy calculation.

| **Parameter** | $V_{sh,average}$ | $k_x$ | $k_y$ | $k_z$ | $a$ |
|---|---|---|---|---|---|
| **Value** | 0.103 m | 22.2 D | 22.2 D | 6.4 D | 0.3 |

## 5.3 Calculation of the horizontal length and production of the well 16/2-D-12

In the following subchapters, based on the available information from NPD, the length of the horizontal part of the well 16/2-D-12 and its production are estimated.

### 5.3.1 Calculation of the length of the horizontal section

As Figure 5.2 is showing, the total length of the wellbore path of a well is called *measured depth*, *MD*, and in the deviated or horizontal wells, the measured depth is bigger than *true vertical depth*, *TVD.*

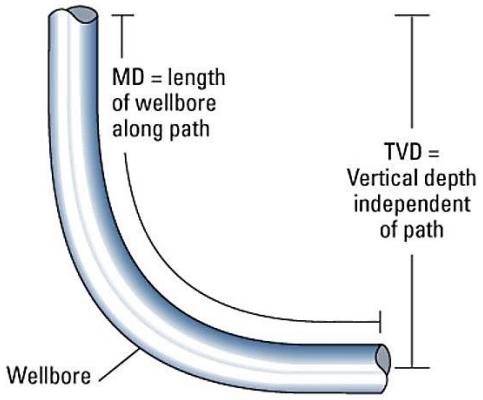


Figure 5.2: Schematic figure of measured depth and total depth [73].

The length of the horizontal section of each well, $L_{horizontal}$ , can be calculated as:

$$L_{MD} = L_{TVD} + L_{kickoff} + L_{horizontal} \qquad 5.6$$

The procedure for the calculation of the length of the horizontal section in the well 16/2-D-12 is presented in Appendix H, and based on that:

$L_{horizontal} = 1612$ m

### 5.3.2 Estimation of the oil production

Based on Equinor's prediction [63], the plateau production from the first phase of the JSF will be 440,000 bbl/day in 2020. Based on the available information in the NPD's fact pages [64], given in Appendix I, oil is produced through 22 production wells in this filed, although there is no detailed information about the value of production from each well. If it is assumed that the production of all these wells are equal and the total estimated production is divided by 22 wells, the production of 20000 bbl/day form each well can be expected. In other words:

$\dot{Q}_{oil,estimation} = 20000 \text{ bbl/d} = 3200 \text{ m}^3/\text{d}$

## 5.4 Calculation of the frictional pressure drop

As explained in subchapter 3.4, the frictional pressure drop in a horizontal pipe can be calculated by using the Darcy-Weisbach equation, Equation 3.36, and the Colebrook-White equation, Equation 3.38. Since the Colebrook-White equation is implicit, using this equation needs doing several trial and error. Therefore, to calculate the pressure drop by using this equation a MATLAB code has been written and used. This code is presented in Appendix J.

For the well 16/2-D-12, it is considered that the diameter of the production tubing is 5.5 inch, which means $d_{pipe} = 5.5 \text{ inch} = 0.1397 \text{ m}$. Moreover, practically, the production tubing is made of stainless steel with a surface roughness of $\varepsilon = 15 \text{ μm}$ [74]. Besides, it is assumed that oil enters the tubing from 13 zones which have equal production. As a result, the flow rate of oil in the production tubing increases gradually and in the last section of the tubing, it reaches $\dot{Q}_{oil,estimation} = 20000 \text{ bbl/d}$ calculated in subchapter 5.3.2. In addition to that, $\mu_{oil} = 3 \text{ cP}$ and $\rho_{oil} = 820 \text{ kg/m}^3$. By running the MATLAB code based on these parameters, the pressure drop for the horizontal section of the well 16/2-D-12 is calculated and it is equal to 2.1 bar or:

$\Delta P_{pipe,friction} = 2.1 \text{ bar}$.

## 5.5 Calculation of the productivity index for the well 16/2-D-12

As discussed in subchapter 3.3, the productivity index, *J*, for horizontal wells can be calculated by using the Babu and Odeh model. Based on the reservoir rock and fluid properties, and comparing the Odeh's model parameters shown in Figure 3.10 with the geometry of the reservoir considered for developing the model in this thesis shown in Figure 6.2, the calculation of the productivity index by using the Odeh's model is conducted. The calculation procedure is given in Appendix H and based on that:

$J = 19885 \text{ stb/d/psi} = 46133 \text{ m}^3/\text{d/bar}$.

## 5.6 Developing a mathematical model for RCP valves

One of the commonly used types of RCP valves is the TR7 RCP valve. This type of RCPs is small enough and can be mounted on standard passive ICD housings [57]. Therefore, it is

assumed that the wells in the Johan Sverdrup field have been completed with the TR7 RCP valve. In the following subchapters, based on the available experimental data, a mathematical model for the TR7 RCP valve is developed.

### 5.6.1 Extracting experimental data for the performance of the TR7 RCP valve

In order to investigate the performance of the TR7 RCP valve, several laboratory tests under different conditions have been done in Equinor's multiphase flow laboratory in Porsgrunn. In literature, there are some experimental data for the performance of the TR7 RCP valve under the single-phase flow of oil, water and gas at the Troll filed conditions shown in Figure 5.3.

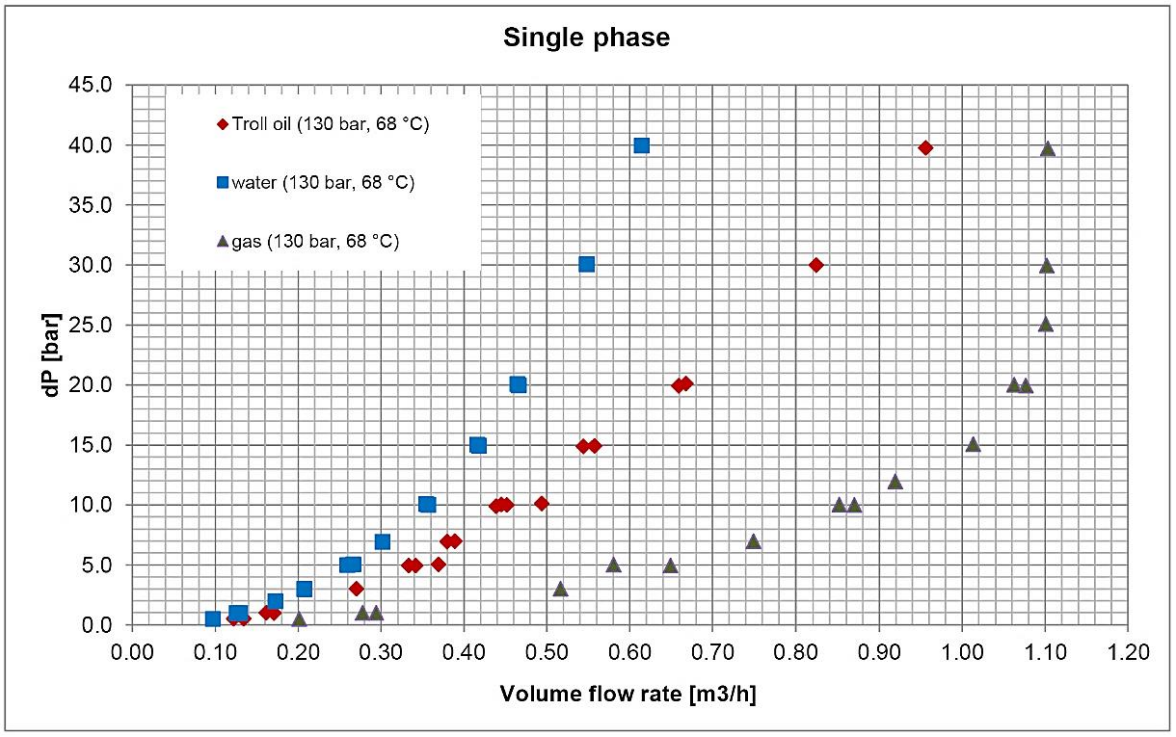


Figure 5.3: Experimental results for the performance of the TR7 RCP valve under single-phase fluid flow[57].

These experimental results have been obtained based on the testing of the TR7 RCP valve performance for single-phase flow of oil with a viscosity of 2.7 cP and a density of 890 kg/m$^3$, saltwater with a viscosity of 0.45 cP and a density of 1100 kg/m$^3$ as well as gas with a viscosity of 0.02 cP and a density of 1.5 kg/m$^3$ [57]. Since these experimental results are based on oil with a viscosity of 2.7 cP, and the viscosity of oil in the Johan Sverdrup field is 3 cP, these experimental results can be used for developing a mathematical model for implementing the behavior of TR7 RCP valve in the JSF conditions.

For extracting the exact values of the experimental results from Figure 5.3, a graph analysis software called "GetData Graph Digitizer" is used. The experimental values of the pressure difference versus the volume flow rate for oil and water extracted from Figure 5.3 by using this

software are presented in Table 5.2. The application of this software for extracting the data for oil is presented in Appendix K and for extracting the data for water it is similar.

Table 5.2: Extracted experimental results for the performance of the TR7 RCP valve from Figure 5.3

| **Experimental results for oil flow** | | **Experimental results for water flow** | |
|---|---|---|---|
| **Q** [m3/h] | **dP** [bar] | **Q** [m3/h] | **dP** [bar] |
| 0.12 | 0.48 | 0.10 | 0.48 |
| 0.13 | 0.56 | 0.13 | 0.88 |
| 0.16 | 1.04 | 0.17 | 2.01 |
| 0.17 | 1.04 | 0.21 | 2.97 |
| 0.27 | 3.05 | 0.26 | 5.06 |
| 0.33 | 4.98 | 0.30 | 6.99 |
| 0.34 | 4.98 | 0.36 | 10.04 |
| 0.37 | 5.06 | 0.42 | 15.03 |
| 0.38 | 6.99 | 0.47 | 20.09 |
| 0.39 | 6.99 | 0.55 | 30.13 |
| 0.44 | 9.88 | 0.61 | 40.02 |
| 0.45 | 9.96 | - | - |
| 0.49 | 10.13 | - | - |
| 0.54 | 14.87 | - | - |
| 0.56 | 14.95 | - | - |
| 0.66 | 19.93 | - | - |
| 0.67 | 20.17 | - | - |
| 0.82 | 30.05 | - | - |
| 0.96 | 39.78 | - | - |

### 5.6.2 Driving the mathematical equation for the TR7 RCP valve based on the experimental data

As explained in subchapter 3.5.2.2, the pressure drop across an RCP valve can be calculated by equation 5.7 as:

$$\Delta P = a_{AICD} \cdot \left( \frac{\rho^2{}_{mix}}{\rho_{cal}} \right) \cdot \left( \frac{\mu_{cal}}{\mu_{mix}} \right)^{y} \cdot \dot{Q}^{x} \qquad 5.7$$

where:

$$\rho_{mix} = \alpha_{oil}\rho_{oil} + \alpha_{water}\rho_{water} + \alpha_{gas}\rho_{gas}$$
$$\mu_{mix} = \alpha_{oil}\mu_{oil} + \alpha_{water}\mu_{water} + \alpha_{gas}\mu_{gas} \quad 5.8$$

Therefore, to find an equation for modeling the behavior of the TR7 RCP valve the values of $a_{AICD}$, $y$, $x$, $\rho_{cal}$ and $\mu_{oil}$ called *RCP coefficients* must be determined based on the experimental data given in Table 5.2. The determination of these values is challenging and needs curve fitting by MATLAB. For reaching this purpose, several methods of curve fitting based on linear or nonlinear regression can be used. In this thesis, the linear regression base on the least square method describing in subchapter 3.6 is used to develop a MATLAB code for finding the RCP coefficients based on Equations 5.7, 5.8, and extracted experimental data given in Table 5.2.

By taking logarithm from both sides of Equation 5.7, it can be written as:

$$\log \Delta P = \log\left[ a_{AICD} \cdot \left( \frac{\rho^2{}_{mix}}{\rho_{cal}} \right) \cdot \left( \frac{\mu_{cal}}{\mu_{mix}} \right)^{y} \cdot \dot{Q}^{x} \right] \quad 5.9$$

and by rearranging Equation 5.9, it can be written as:

$$\log\left[ \frac{\Delta P \cdot \rho_{cal}}{\rho^2{}_{mix}} \right] = \log a_{AICD} + y \log\left( \frac{\mu_{cal}}{\mu_{mix}} \right) + x \log \dot{Q} \quad 5.10$$

as a result, Equation 5.10 is rewritten as:

$$\log\left[ \frac{\Delta P \cdot \rho_{cal}}{\rho^2{}_{mix}} \right] = \begin{bmatrix} 1 & \log\left( \frac{\mu_{cal}}{\mu_{mix}} \right) & \log \dot{Q} \end{bmatrix} \begin{bmatrix} \log a_{AICD} \\ y \\ x \end{bmatrix} \quad 5.11$$

therefore, Equation 5.11 can be presented in the form of $y = \varphi^T(x) \cdot \theta$ where:

$$y = \log\left[ \frac{\Delta P \cdot \rho_{cal}}{\rho^2{}_{mix}} \right],\ \varphi^T = \begin{bmatrix} 1 & \log\left( \frac{\mu_{cal}}{\mu_{mix}} \right) & \log \dot{Q} \end{bmatrix},\ \theta = \begin{bmatrix} \log a_{AICD} \\ y \\ x \end{bmatrix} \quad 5.12$$

Moreover, based on experimental data given in Table 5.2 describing the performance of the TR7 RCP valve, the $\phi$ and $Y$ matrices, can be formed. Therefore, based on equation 3.52, a MATLAB code has been developed in order to find $\rho_{cal}$, $\mu_{cal}$, $a_{AICD}$, $y$ and $x$. By running this MATLAB program, the RCP coefficients are calculated and the values of them are given in Table 5.3 as:

Table 5.3: Calculated values of RCP coefficients for the mathematical model of RCP valves.

| **Coefficient** | $a_{AICD}$ | $y$ | $x$ | $\rho_{cal}$ | $\mu_{cal}$ |
|---|---|---|---|---|---|
| **Value** | 0.7624 | 0.1097 | 2.1554 | 10000 | 1 |

Moreover, the comparison between the mathematical model based on these RCP coefficients, and experimental data is shown in Figure 5.4. As can be seen in the figure, the mathematical model fits very well the experimental data both for oil and water, especially for the pressure difference below that 20 bar. As a result, by using the calculated RCP coefficient, a very good mathematical model for describing the performance of the TR7 RCP can be achieved which can be confidently used for implementing the behavior of this type of valve in the OLGA/ROCX model of oil production from the Johan Sverdrup field.

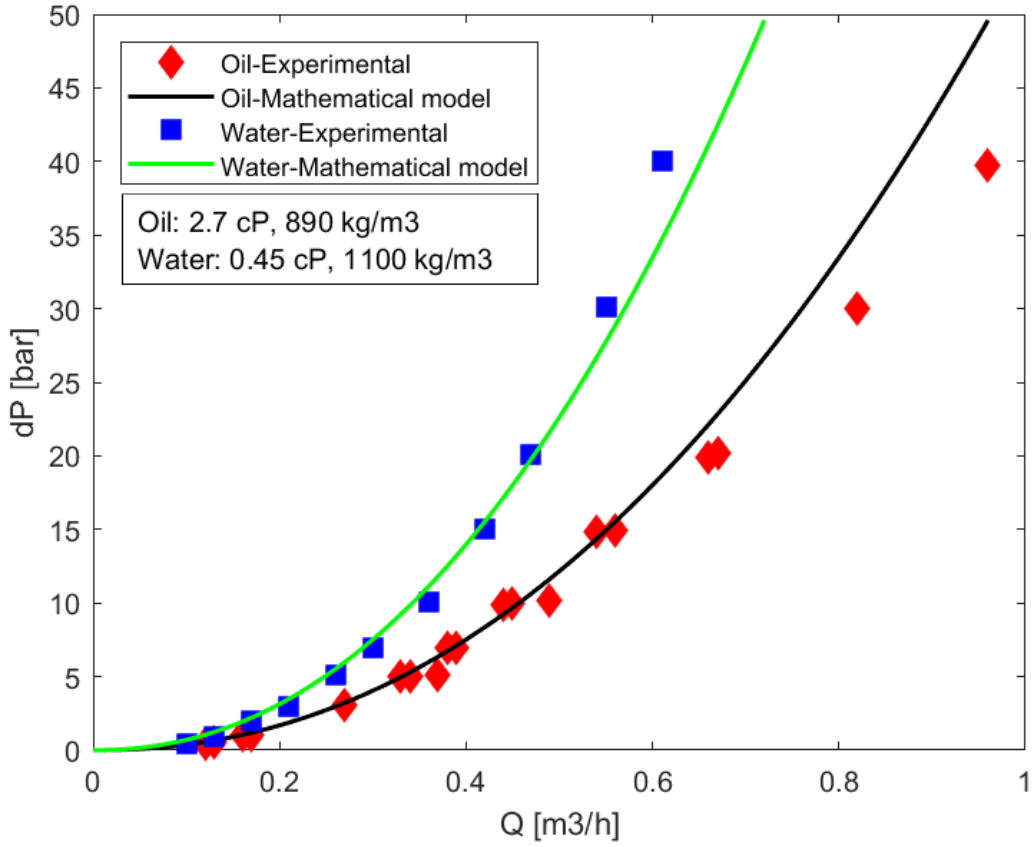


Figure 5.4: Mathematical model of the TR7 RCP valve compare to the experimental values.

Based on the calculated RCP coefficients and Equation 5.7, the mathematical model governing the TR7 RCP valve is developed as:

$$\Delta P_{RCP} = 0.7624 \cdot \left( \frac{\rho^2{}_{mix}}{10000} \right) \cdot \left( \frac{1}{\mu_{mix}} \right)^{0.1097} \cdot \dot{Q}_{RCP}^{2.1554} \qquad 5.13$$

where the $\Delta P_{RCP}$ is in bar, and $\dot{Q}_{RCP}$ in $m^3/h$.

Equation 5.13 provides a flexible model for predicting the performance of the TR7 RCP valve for different ranges of fluid properties and reservoir conditions. The MATLAB code used for developing this model is presented in Appendix L.

## 5.7 Calculation of the average pressure drop across the TR7 RCP valve and the number of them for the well 16/2-D-12

In subchapter 5.3.2 the production of the well 16/2-D-12 is estimated to be 20000 bbl/d =3200 $m^3$/day. Moreover, the length of the well is 1612 m and it is considered that it consists of 130 joints, each 12.4 m long. If only one TR7 RCP valve is considered to be installed on each joint, based on Equation 5.13, this leads to occurring a relatively high pressure drop across the valve. Therefore, two TR7 RCP valves are considered to be installed on each joint, and based on that the required number of the TR7 RCP valves, $N_{RCP}$, for the well 16/2-D-12 can be calculated. In this case, the pressure drop across each TR7 RCP valve, $\Delta P_{RCP,estimation}$, can be estimated by using Equation 5.13. The calculation procedure is presented in Appendix H and the obtained results are given in Table 5.4.

Table 5.4: The number of required TR7 RCP valves and the pressure drop across each valve.

| **Parameter** | $N_{RCP}$ | $\Delta P_{RCP,estimation}$ |
|---|---|---|
| **Value** | 260 | 10.78 bar |

## 5.8 Developing a control function for implementing RCP behavior in OLGA

OLGA does not have any options that can be used for implementing the behavior of the RCP valves in modeling and simulation of oil production. Therefore, for developing an OLGA model based on the RCP valves, the behavior of the RCP valves must be implemented by estimating the diameter of the equivalent orifice valve and using a controller for regulating the orifice valve opening based on the mathematical model of the RCP valves.

In subchapter 5.6.2, based on existing experimental data and by using a MATLAB code the mathematical model of the TR7 RCP valve was developed and presented by Equation 5.13. Equation 5.13 can be combined with the mathematical model of the simple orifice valve which is presented by Equation 3.43 described in subchapter 3.5.1.

By combining the mathematical model of the TR7 RCP valve (describing by Equation 5.13) and the mathematical model of orifice valve (describing by Equation 3.43) it can be concluded that:

$$aA_2 = \frac{\left[\frac{\Delta P_{RCP}}{10^5 \times 0.7624 \cdot (\rho_{mix}^2 / 10000) \cdot (1/\mu_{mix})^{0.1097}}\right]^{\frac{1}{2.1554}}}{3600 \times C_D \cdot \sqrt{\frac{2\Delta P_{RCP}}{\rho_{mix}}}} \qquad 5.14$$

As calculated in subchapter 5.7, $\Delta P_{RCP,estimation} = 10.78 \times 10^5$ Pa, based on considering 2 TR7 RCP valves for each joint with a length of 12.4 m in the well 16/2-D-16. For having a simpler model in OLGA, only one equivalent orifice valve is considered for every10 joints, meaning one equivalent orifice valve for every 20 TR7 RCP valves in a segment with a length of 124 m ($10 \times 12.4$ m). Therefore, by using Equation 5.14 the cross-sectional area and diameter of the equivalent orifice hole, $A_{orifice}$ and $d_{orifice}$ respectively, can be calculated as shown in Appendix H. The calculation results are given in Table 5.5 as:

Table 5.5: Cross-sectional area and diameter of the equivalent orifice hole for each joint in the well 16/2-D-12.

| **Parameter** | $A_{orifice}$ | $d_{orifice}$ |
|---|---|---|
| **Values** | $9.1 \times 10^{-5}$ m$^2$ | 10.8 mm |

By using the calculated value for $A_{orifice}$ from Table 5.5 and Equation 5.14, the value of valve opening, $a$, can be calculated by equation 5.15 as:

$$a = \frac{\left[\frac{10.78 \times 10^5}{10^5 \times 0.7624 \cdot (\rho_{mix}^2 / 10000) \cdot (1/\mu_{mix})^{0.1097}}\right]^{\frac{1}{2.1554}}}{9.1 \times 10^{-5} \times 3600 \times 0.61 \cdot \sqrt{\frac{2 \times 10.78 \times 10^5}{\rho_{mix}}}} \qquad 5.15$$

Equation 5.15 describes the value of valve opening based on $\rho_{mix}$ and $\mu_{mix}$ which can be calculated by Equation 5.16 as:

$$\begin{aligned} \rho_{mix} &= \alpha_{oil}\rho_{oil} + \alpha_{water}\rho_{water} \\ \mu_{mix} &= \alpha_{oil}\mu_{oil} + \alpha_{water}\mu_{water} \end{aligned} \qquad 5.16$$

Based on equations 5.15 and 5.16, the value of valve opening changes with water cut and it can be calculated based on that. When only oil passing through the orifice valve, $a = 1$ and the valve is fully open. By increasing the water cut, the value of valve opening decreases and the valve

is closed partially. In order to calculate the value of valve opening, *a*, based on the water cut, *WC*, used for implementing the behavior of the TR7 RCP valve in OLGA, a MATLAB code has been written and presented in Appendix M. Figure 5.5 shows the diagram of the valve opening versus water cut for the TR7 RCP valve based on the mixture of oil and water in the JSF conditions. ( $\mu_{oil} = 3$ cP, $\rho_{oil} = 820$ kg/m$^3$, $\mu_{water} = 0.45$ cP, $\rho_{water} = 1100$ kg/m$^3$ ) . As can be seen in the figure, since there is no big difference between the viscosity of oil and water, when the water cut reaches its maximum (WC=1), the valve opening reaches 0.835 meaning the valve is closed by 16.5 %.

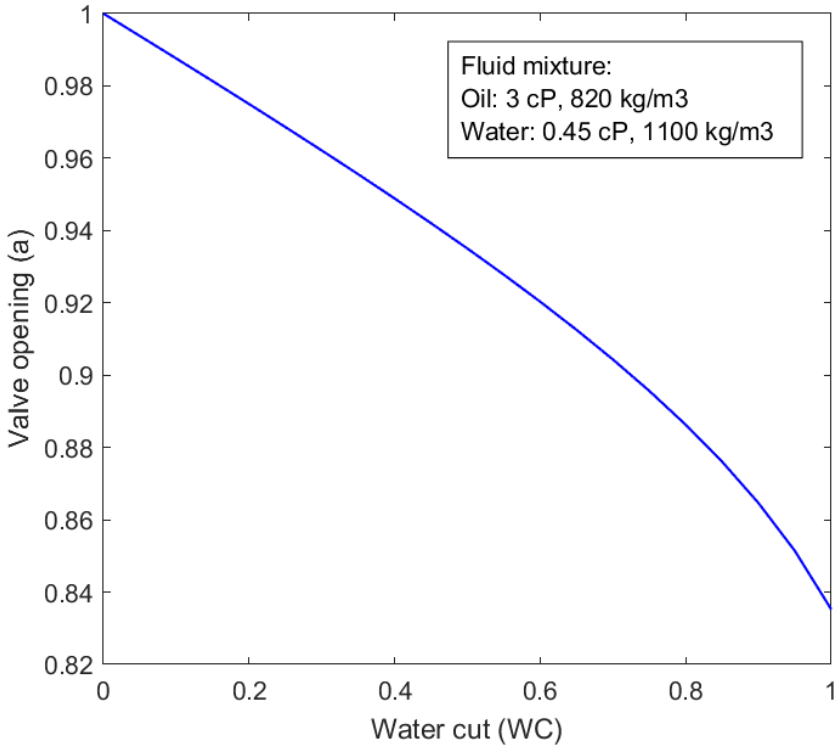


Figure 5.5: Valve opening versus water cut for the TR7 RCP valve under JSF conditions.

In order to implement the behavior of the TR7 RCP valve in the OLGA/ROCX model, a controller must be considered to control the valve opening based on the mathematical model of valve opening described by Equation 5.15 and Equation 5.16.

In all previous works, a PID controller has been used for controlling the valve based on a fixed set point. However, PID controllers can not be used for controlling the valve opening when the valve opening changes autonomously by fluid water cut variations (There is no only one specific setpoint). For solving this problem, a new method of controlling in OLGA called *Table Control* can be used. In this method, at first, the control signals for controlling the valve are calculated based on the mathematical model of the valve opening. Then, the signal values are introduced as tabulated data to a Table Control in OLGA. The control signal table for the TR7 RCP valve for the mixture of oil and water in the JSF conditions has been calculated by a MATLAB code based on Equation 5.15 and Equation 5.16 and presented in Appendix M. This control signal table is represented as:

Table 5.6: Control signal table for controlling the TR7 RCP valve in the JSF conditions.

| |
|---|
| 0.00,1.0000, 0.05,0.9938, 0.10,0.9876, 0.15,0.9813, 0.20,0.9750, 0.25,0.9686, 0.30,0.9621, 0.35,0.9556, 0.40,0.9489, 0.45,0.9420, 0.50,0.9350, 0.55,0.9278, 0.60,0.9203, 0.65,0.9125, 0.70,0.9043, 0.75,0.8956, 0.80,0.8863, 0.85,0.8761, 0.90,0.8646, 0.95,0.8514, 1.00,0.8352 |

Each pair of numbers in the control signal list describe the value of the valve opening based on the value of the water cut. This list is prepared by considering 20 control signals but OLGA automatically interpolates the values that do not exist in the list. By using this method, the autonomous behavior of the TR7 RCP valve can be completely implemented in the OLGA/ROCX model. Therefore, by using this new method, the OLGA/ROCX model of oil production from horizontal wells with RCP valves or other kinds of autonomous valves can be developed accurately. Figure 5.6 shows the implementation of the autonomous behavior of the TR7 RCP valve based on this new method.

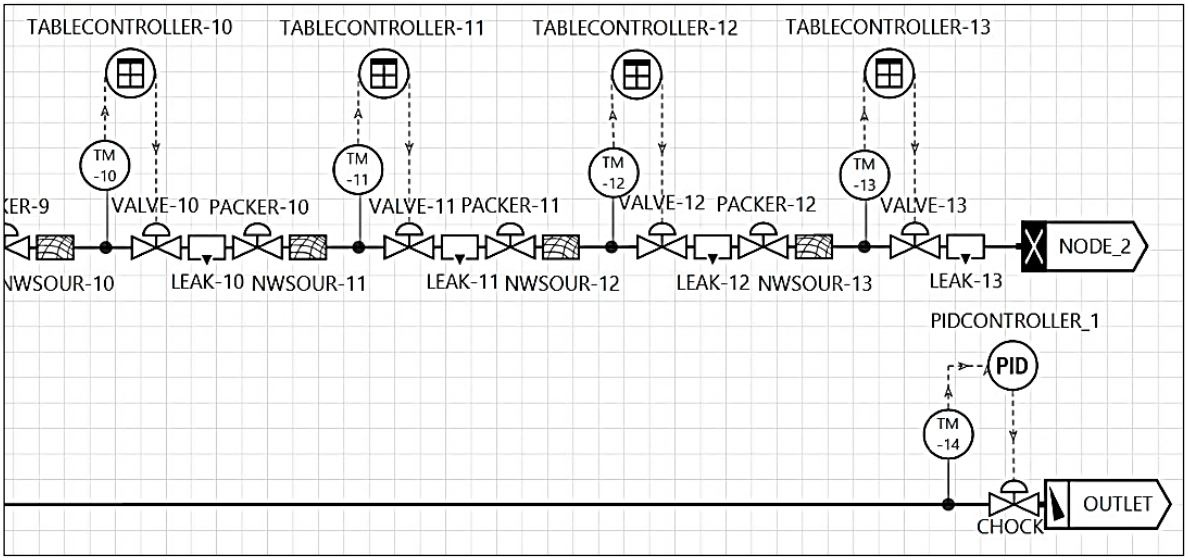


Figure 5.6: Implementation of autonomous behavior of the TR7 RCP valve by using the Table Controller.

## 5.9 Estimation of the pressure drawdown for the well 16/2-D12

The difference between the reservoir pressure and the tubing pressure is called pressure drawdown. Pressure drawdown drives fluid from the reservoir into the tubing and the production rate of a well has a direct relation with this parameter [75]. As a result, estimating a realistic value for the pressure drawdown has a direct impact on the accuracy of the simulation results. The pressure difference between the reservoir and tubing pressure simply can be calculated by adding the pressure drop across the formation and pressure drop across RCP valves. Figure 5.7 is made to illustrate the nomenclature that is used for estimating the pressure drawdown for the well 16/2-D-12.

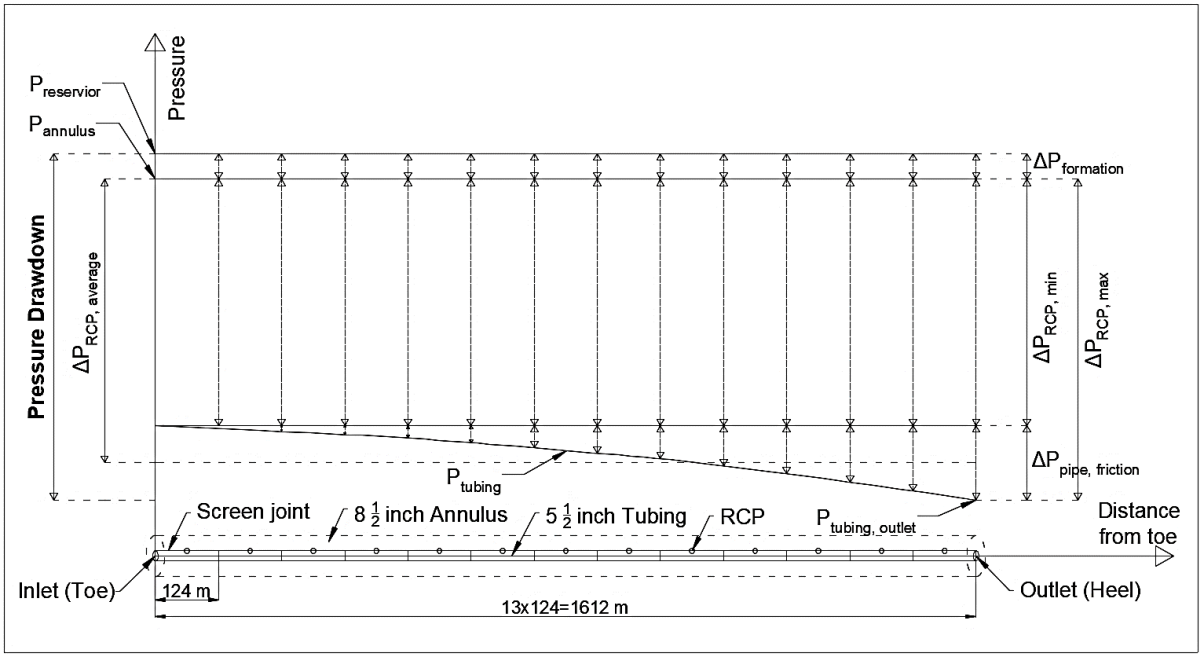


Figure 5.7: Schematic of the pressure variation in for the well 16/2-D-12.

According to Figure 5.7, it can be written that:

$$\Delta P_{RCP,\max} = P_{reservior} - P_{tubing,outlet} - \Delta P_{formation} \qquad 5.17$$

Moreover, it can be considered that:

$$\Delta P_{RCP,\max} = \Delta P_{RCP,\min} + \Delta P_{pipe,friction} \qquad 5.18$$

The average pressure difference across the RCP valve can be defined as:

$$\Delta P_{RCP,average} = \frac{\Delta P_{RCP,\max} + \Delta P_{RCP,\min}}{2} \qquad 5.19$$

By manipulating Equations 3.39, 5.18 and 5.19, the pressure drawdown can be concluded as:

$$\Delta P_{drawdown} = P_{reservior} - P_{tubing,outlet} = \Delta P_{RCP,average} + \frac{\Delta P_{pipe,friction}}{2} + \Delta P_{formation} \qquad 5.20$$

Based on the definition of the productivity index, *J*, it can be written that:

$$\Delta P_{formation} = \frac{\dot{Q}_{oil}}{J} \qquad 5.21$$

Therefore, by using equation 5.20 the pressure drawdown can be calculated by equation 5.22 as:

$$\Delta P_{drawdown} = \Delta P_{RCP,average} + \frac{\Delta P_{pipe,friction}}{2} + \frac{\dot{Q}_{oil}}{J} \qquad 5.22$$

In order to calculate the pressure drawdown for the well 16/2-D-12, $\dot{Q}_{oil}$, $\Delta P_{pipe,friction}$, $J$ and $\Delta P_{RCP,average}$ were calculated in subchapters 5.3.2, 5.4, 5.5 and 5.7 respectively. Therefore, the pressure drawdown for the well 16/2-D-12 in JSF based on estimated oil production of 20000 bbl/d = 3200 $m^3$/d and considering 260 TR7 RCP valves for this well, can be calculated by using Equation 5.22. Moreover, the outlet pressure of the tubing for the well 16/2-D-12 used for developing the OLGA/ROCX model can be calculated by Equation 5.23 as:

$$P_{tubing,outlet} = P_{reservior} - \Delta P_{drawdown} \qquad 5.23$$

The procedure for calculating the pressure drawdown, $\Delta P_{drawdown}$, and outlet pressure of the tubing, $P_{tubing,outlet}$, are presented in Appendix H. The calculated values of them are given in Table 5.7 as:

Table 5.7: Pressure drawdown and outlet pressure of the tubing for the well 16/2-D-12.

| **Parameter** | $\Delta P_{drawdown}$ | $P_{tubing,outlet}$ |
|---|---|---|
| **Value** | 12 bar | 228 bar |

# 6 Development of the OLGA/ROCX model

Enhancing oil recovery requires a detailed understanding of multiphase flow behavior from the reservoir pore to the production tubing. The combination of OLGA and ROCX provides a robust tool for achieving this purpose. In this study, near-well oil production from the well 16/2-D-12 in JSF with considering ICD and RCP completion is modeled by using OLGA in combination with ROCX. The procedure of developing this model is described step by step in this chapter.

## 6.1 Development of the reservoir model in ROCX

In this subchapter, the main settings for developing the model of the reservoir near the well 16/2-D-12 in ROCX are described.

### 6.1.1 Determining the dimensions of the reservoir drainage area

In order to create a near-wellbore model of oil production, the first step is to determine the dimensions of the drainage area near the well. As discussed in subchapter 3.1.2.2, in reality, the drainage area of a horizontal well has an ellipsoidal shape. However, due to the ROCX limitation for creating an ellipsoidal geometry, a rectangular drainage area is considered for developing the model. As mentioned in Table 4.3 the total thickness of the net pay reservoir near the well 16/2-D-12 is 55.5 m (32.46 + 22.86 = 55.32 ~ 55.5 m). Therefore, the height of the drainage area is considered to be equal to 55.5 m. The length of the well is 1612 m and the length of the drainage area is considered the same as that of the well. To determine the width of the drainage area, oil production from five test cases with similar heigh and length but different width of the drainage area is simulated in OLGA. The drainage area dimensions of these cases are presented in Table 6.1. The simulations are conducted for a horizontal well with a length of 124 m and one ICD valve in a reservoir with the same rock and fluid properties as the JSF.

Table 6.1: Drainage area dimensions of the test cases for the determination of the width of reservoir.

| Case | Width | Height | Length |
|---|---|---|---|
| Case 1 | 60 m | 55.5 m | 124 m |
| Case 2 | 80 m | 55.5 m | 124 m |
| Case 3 | 100 m | 55.5 m | 124 m |
| Case 4 | 120 m | 55.5 m | 124 m |
| Case 5 | 140 m | 55.5 m | 124 m |

Figure 6.1 shows the accumulated oil production during 120 days of simulation for the given cases. As can be seen in the figure, by increasing the width of the drainage area, the time of water breakthrough and accumulated oil production increases but it is converging in such a way that there is no big difference between accumulated oil production in cases 4 and 5. As a result, it can be concluded that considering the width of the drainage area for the main model as case 4 and equal to 120 m can be a good estimation. Of course, considering the width of the drainage area equal to 140 m leads to more accurate results, however, it also increases the time of the simulation. Therefore, for developing the main model the width of the drainage area is considered to be equal to 120 m.

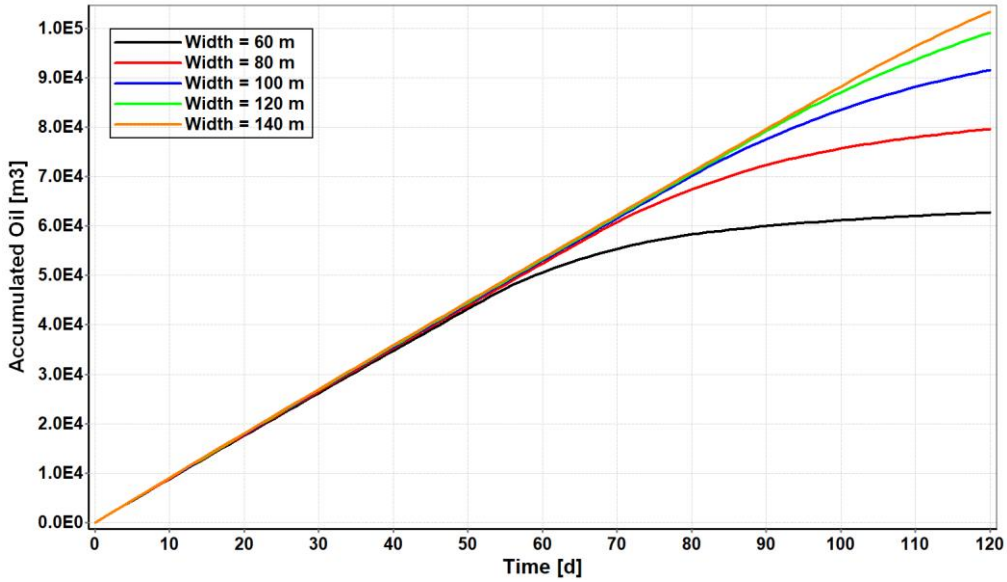


Figure 6.1: Analysis of oil production from a well with different width of the drainage area.

Since in the JSF oil is produced by water drive, for delaying water breakthrough the well must be positioned as near as possible to the top of the drainage area. Therefore, for developing the model, it is assumed that the well is located 5.5 m below the top of the drainage area. The geometry of the drainage area and the position of the well, considered for developing the model of oil production from the well 16/2-D-12 in the JSF is schematically depicted in Figure 6.2.

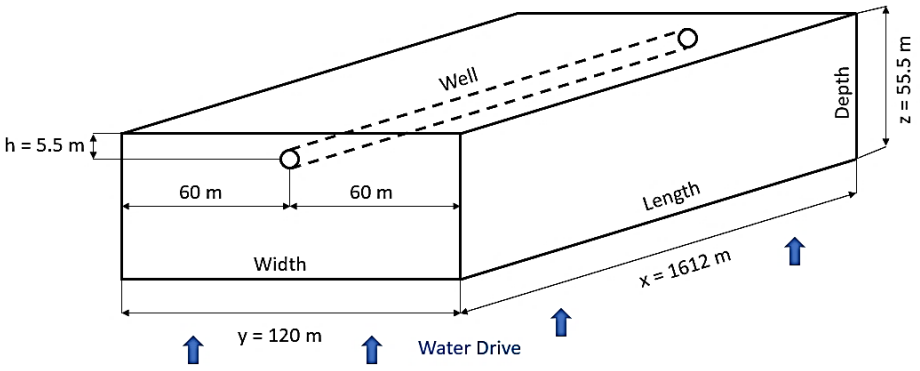


Figure 6.2: Schematic geometry of the drainage area.

### 6.1.2 Grid setting and mesh sensitivity analysis

The reservoir geometry can be defined either in the Cartesian coordinate system or in the cylindrical coordinates system. However, for horizontal wells, it is more straightforward to use Cartesian coordinates where *x* , *y*, and *z* specify the direction of the well, the reservoir width, and reservoir depth respectively. After the determination of the dimensions of the reservoir near the well, the number of grids in (*x*,*y*,*z*) coordinates must be determined for discretizing the reservoir in ROCX. The more the number of grids, the more accurate results. However, there is a trade-off between grid resolution and time of calculation. Therefore, choosing a suitable grid resolution is of key importance to develop an appropriate OLGA/ROCX model. In general, a suitable grid setting can be achieved by using finer mesh in the places with high variation in the fluid properties and coarser mesh in the other places. Figure 6.3 shows the fluid pressure variations near an open hole production oil well. As can be seen, the variation of the fluid pressure close to the well is significantly higher than the other places. As a result, the mesh must be refined as much as possible close to the well.

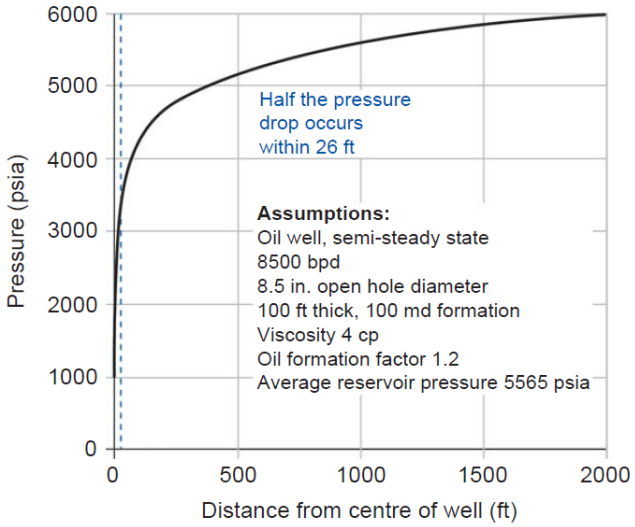


Figure 6.3: Pressure drop near an open hole oil production well [45].

Since the cross-section of the reservoir is located in the Y-Z plane, the fluid pressure in the Y-Z plane around the well drops significantly. Therefore, to achieve more accurate results, finer mesh in the *y* and *z* directions close to the well must be defined in the grid setup. The length of the well is in the *x*-direction. As a result, the fluid pressure has small variations in the *x*-direction, and considering uniform mesh in the *x*-direction can maintain enough accuracy.

In reality, as can be seen in Figure 2.14, each production tubing joint consisting of the sand screen and inflow control valves has a length of 12.4 m. However, in order to develop the model, it is assumed that the well 16/2-D-12 contains 13 joints, each 124 m long and consisting of one equivalent valve. As a result, 13 uniform cells are considered for the reservoir in the *x*-direction. In the *y* and *z* directions, the meshes are not uniform, and finer meshes are used close to the well. The suitable number of cells in the *y* and *z* directions must be defined based on the analysis of the mesh sensitivity. By doing this analysis, the grid resolution can be reduced as

much as it can maintain enough accuracy. For testing the sensitivity of the results to the number of meshes in the *y* and *z* directions, the production from some test cases with different grid resolutions in these directions is tracked. These test cases include a well with a length of 124 m consisting of only one ICD valve in a reservoir with the same characteristics as the JSF and with only one cell in the *x*-direction. For the mesh sensitivity analysis in the *z*-direction the grid resolution in the *y*-direction remains constant and the number of cells in the *z*-direction, *nz*, increases. Similar to that, for testing the impact of the grid resolution in the *y*-direction, the number of cells in the *z*-direction is considered constant and the number of meshes in the *y*-direction, *ny*, is increased. Figure 6.4 shows the grid setup of test cases for mesh sensitivity analysis in the *z*-direction (left) and *y*-direction (right).

(a) Mesh refinement in the *z*-direction

(b) Mesh refinement in the *y*-direction

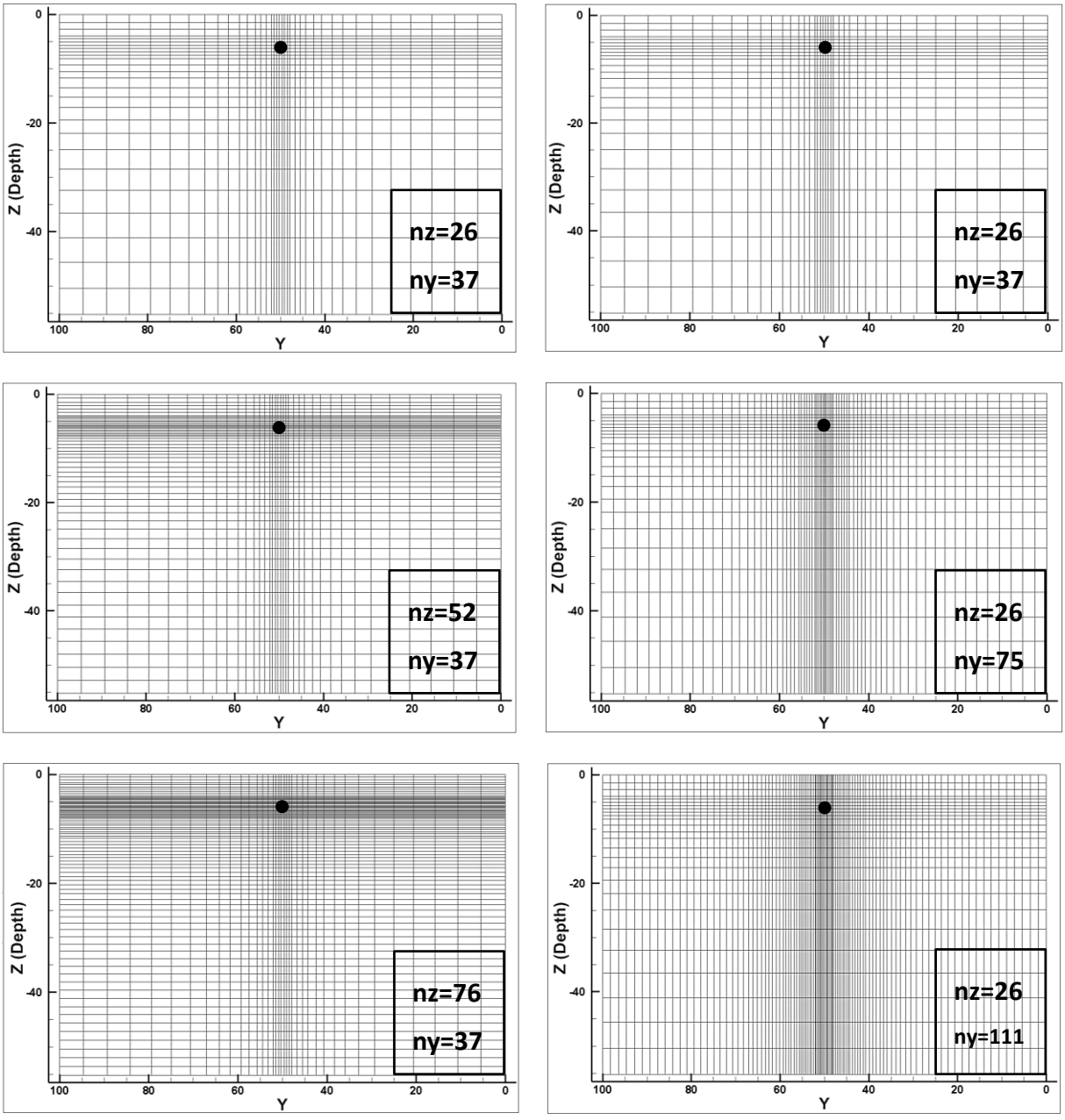


Figure 6.4: Grid setup for mesh sensitivity analysis in the (a) *z*-direction and (b) *y*-direction.

### 6.1.2.1 Mesh sensitivity analysis in the *z*-direction

Figure 6.5 shows the accumulated oil and water as well as the volume flow rate of oil and water diagrams for the three same cases but with 26, 52, and 78 cells in the *z*-direction during 120 days. As can be seen in the figures, the accumulated and flow rate of oil and water for the cases with 52 and 78 cells have a very slight difference but the results for the case with 26 cells are relatively different from those two. The plots clearly show that the results are sensitive to decrease the number of cells in the *z*-direction. However, the obtained results from the case with 26 cells, especially for the accumulated oil and water, are close enough to the obtained results from the cases with 52 and 78 cells. As a result, using 26 cells or even less in the *z*-direction can maintain enough accuracy for developing the main model.

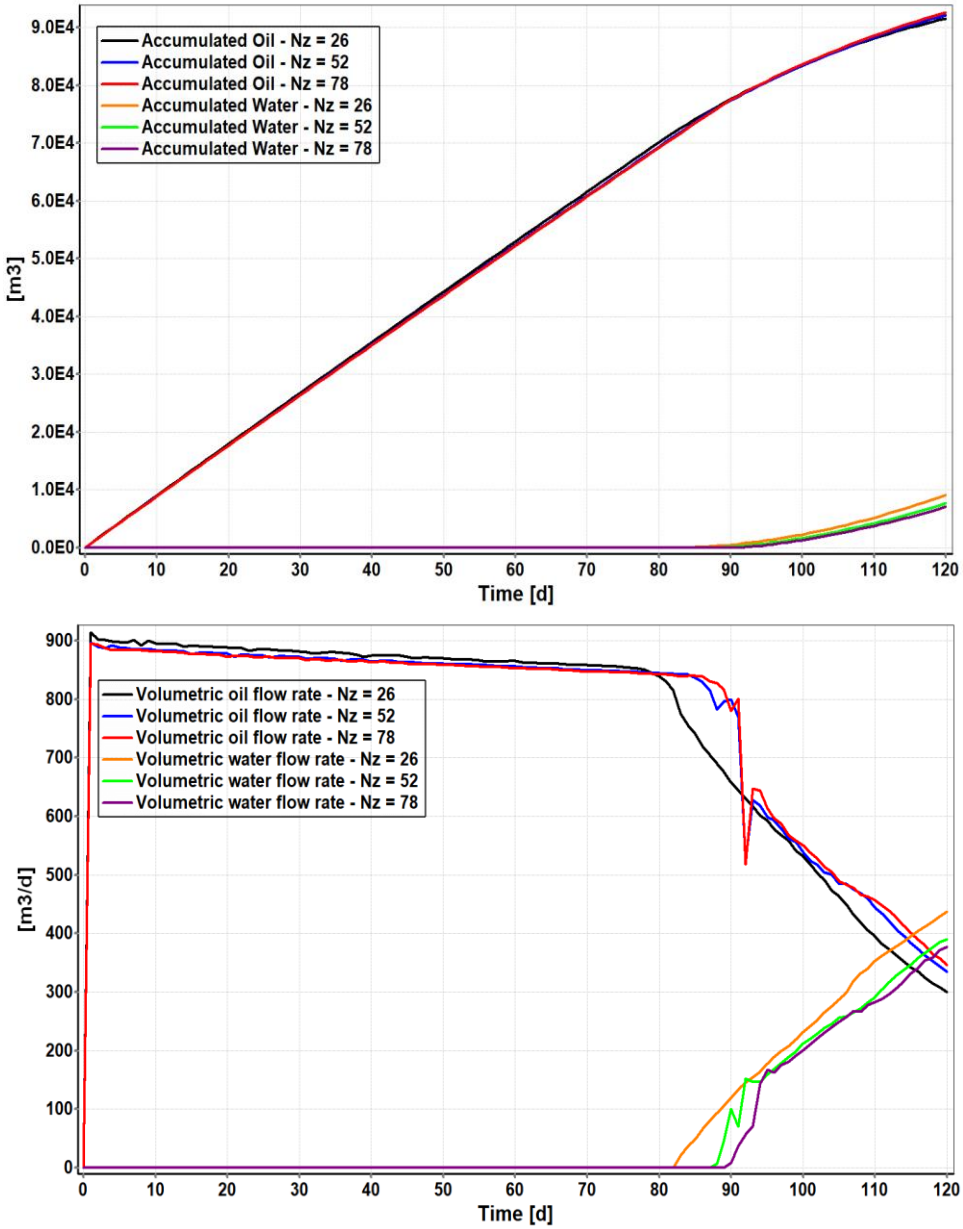


Figure 6.5: Sensitivity of oil and water production to the number of grids in the *z*-direction.

### 6.1.2.2 Mesh sensitivity analysis in the *y*-direction

The diagrams of accumulated oil and water as well as the volume flow rate of oil and water obtained from three same cases but with 37, 75, and 111 cells in the *y*-direction during 120 days is shown in Figure 6.6. As the figures are showing, the accumulated and flow rate of oil and water for the cases with 75 and 111 cells have no difference but the results for the case with 37 cells are slightly different from those two. As a result, it can be concluded that the results do not have a considerable sensitivity to decrease the number of cells in the *y*-direction. Therefore, the main case confidently can be modeled by using even less than 37 cells in the *y*-direction.

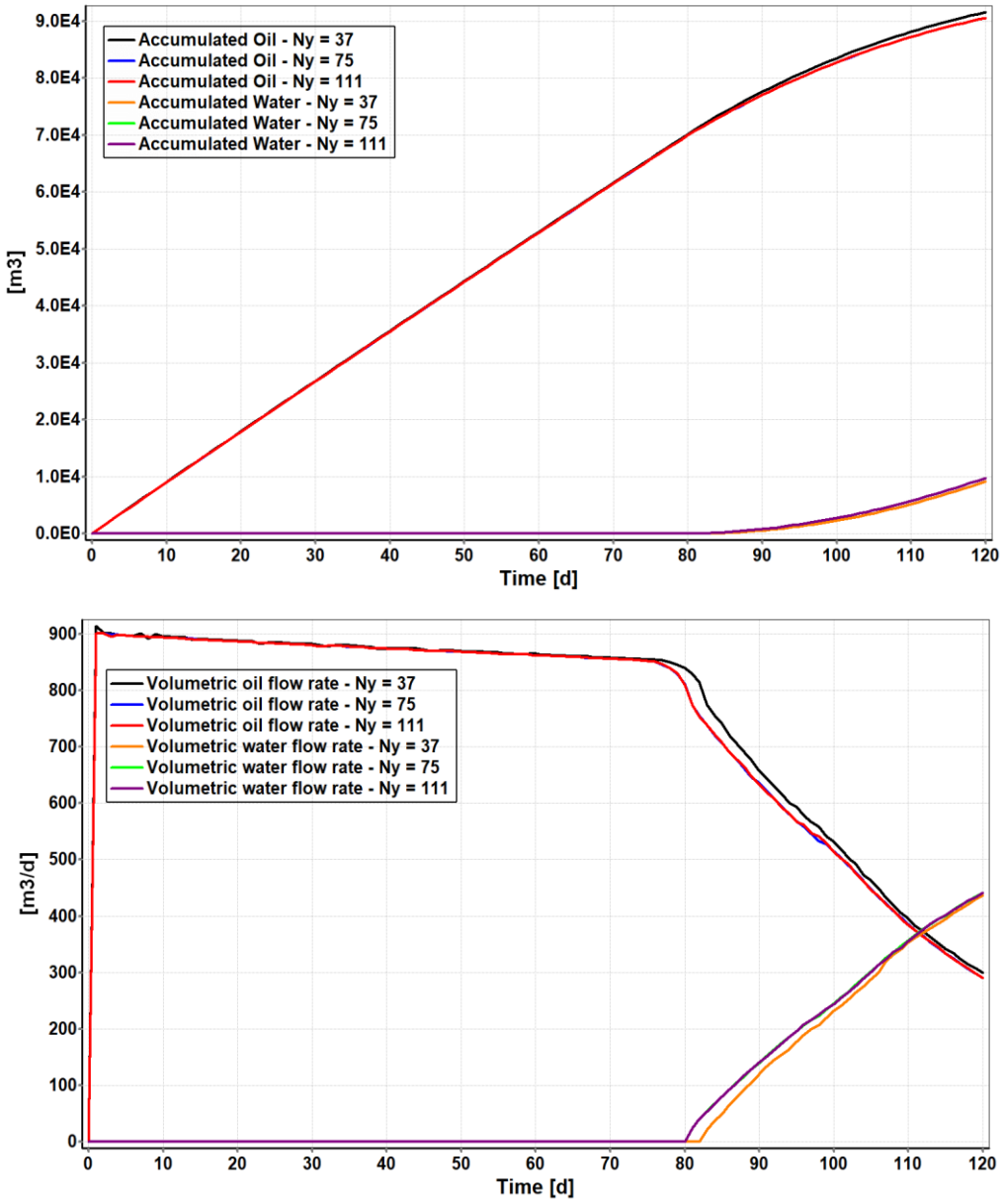


Figure 6.6: Sensitivity of oil and water production to the number of grids in the *y*-direction.

#### 6.1.2.3 Grid setting for developing the main model

Based on discussions in subchapter 6.1.2 and grid sensitivity analysis in subchapters 6.1.2.1 and 6.1.2.2, and also considering the time of simulation, the number of cells in the *x*, *y* and *z* directions for the near-well reservoir are set to 13, 25 and 15 respectively for developing the model of oil production from the well 16/2-D-12. In the *x*-direction, uniform meshes are used but in the *y* and *z* directions, the meshes are refined close to the well. The grid setting in ROCX including the number of cells and their sizes are given in Table 6.2.

Table 6.2: Number of cells and their sizes for the grid setting in ROCX.

| Direction | Number of cells | Size of the cells (m) |
|---|---|---|
| x | nx = 13 | 124 (constant) |
| y | ny = 25 | 6.5,5,5,5,4,4,4,4,3,3,3,2.5,2.5,2.5,2,2,1.5,1,1.5,2,2,2.5,2.5, 2.5,3,3,3,4,4,4,4,5,5,5,6.5 |
| z | nz = 15 | 2,2,1.5,1,1.5,2,2,2.5,2.5,2.5,3,3,3,4,4,4,5,5,5 |

Figure 6.7 shows the grid resolution in different views for the near-well reservoir and the position of the well in the Y-Z plane. It should be mentioned that the 3D view of the grid resolution is not on the real scale.

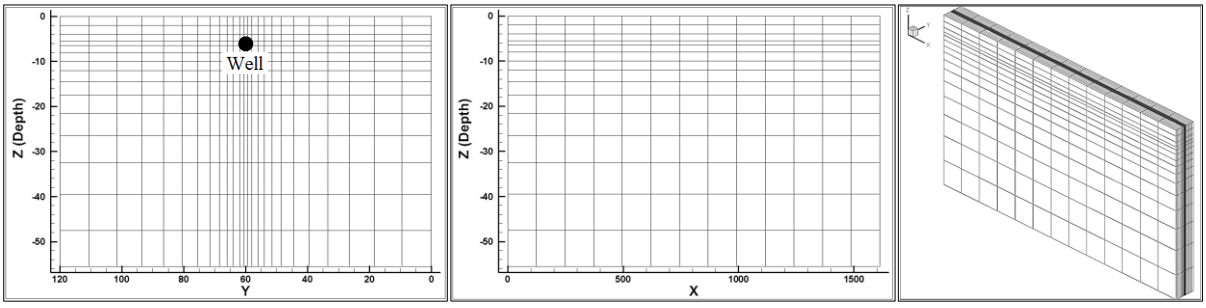


Figure 6.7: Y-Z, X-Z and 3D view of the grid resolution and the well position in the Y-Z plane.

## 6.1.3 Fluid property settings

The reservoir fluid properties can be introduced to ROCX either by using the black oil option or PVT table option. As discussed in subchapter 3.2.3, in order to create a PVT table, the phase behavior of the reservoir fluids over a wide range of pressure and temperature must be determined. This can be done by doing laboratory tests or using commercial software (like PVTsim or Multiflash). However, doing laboratory tests for determining the PVT data is difficult and access to commercial soft is not easy. As a result, the PVT table option can not be used for developing the model in this thesis.

Based on the characteristics of five types of reservoir fluids given in Table 3.2, the reservoir fluid can be classified as black oil when the API gravity is between 15 and 40, the viscosity is more than 2, the GOR is less than 1750 and mol % of $C_{7+}$ is more than 20. By comparing these criteria with the crude oil properties in the JSF given in Table 4.2, it can be concluded that the reservoir fluid in the JSF can be classified as the black oil type and the black oil option in ROCX can be used. Under the black oil option, several empirical correlations developed based on laboratory test results, are available to choose from. Knowing the reservoir fluid composition is not required for using these empirical models due to the fact that in these models the reservoir fluids are considered as black oils. The Lasater model is a commonly used black oil model and it is chosen for developing the OLGA/ROCX model in this thesis. By comparing the reservoir fluid properties of the JSF given in Table 4.2 with the required conditions for using the Lasater correlations presented in Table 3.3, it can be concluded that the Lasater correlations are valid for the JSF conditions. Table 6.3 represents the oil properties used for developing the model of oil production from the well 16/2-D-12 by using the black oil option in ROCX.

Table 6.3: Reservior oil properties used in developing the OLGA/ROCX model.

| **Parameter** | **Value** |
|---|---|
| Oil specific gravity | 0.82 |
| Gas specific gravity | 0.64 |
| Viscosity | 3 cP |
| GOR | 44 $Sm^3/Sm^3$ |
| Pressure | 240 bar |
| Temperature | 81 ˚C |

Since in the JSF, oil is produced with water drive, the components of the water feed and oil feed must be defined in ROCX. Table 6.4 presents oil and water feed components.

Table 6.4: Oil and water feed components.

| **Feed** | **Gas fraction** | **Water cut** |
|---|---|---|
| Oil | 44 (GOR) | 0.0001 |
| Water | 0.0001 (GLR) | 0.99 |

### 6.1.4 Reservoir property settings

Based on the reservoir rock properties in the JSF given in Table 4.3, the average effective porosity in this reservoir near the well 16/2-D-12 is 0.27 and for developing the model, the porosity is considered constant throughout the reservoir and equal to 0.27.

Since the Johan Sverdrup reservoir is heterogeneous with respect to permeability, for the investigation of the oil production from the well 16/2-D-12, the OLGA/ROCX model is developed for both homogeneous and heterogeneous reservoirs based on permeability. For the homogeneous case, by considering the permeability anisotropy calculated in subchapter 5.2, permeability in the *x* and *y* directions are constant and equal to 22.2 D, and permeability in the *z*-direction is constant and equal to 6.4 D throughout the reservoir.

As explained in subchapter 4.2.3.3, the permeability in the JSF varies between 0.5 to 40 D while the average permeability in the reservoir near the well 16/2-D-12 is 14.7 D. As a result, there are some places in the reservoir where the permeability is more than 2.5 (40/14.7 ~ 2.7) times higher than the average permeability. Moreover, heterogeneity may exist in the horizontal, vertical, or angled direction. Therefore, for creating a heterogeneous case, the permeability in some random zones in the horizontal, vertical, and angled directions is considered 1.5, 2, and 2.5 times higher than the average permeability in the near-well reservoir.

The permeability distribution in the homogeneous and heterogeneous reservoir used for developing the OLGA/ROCX model is shown in Figure 6.8.

(a) Homogeneous reservoir (b) Heterogenous reservoir

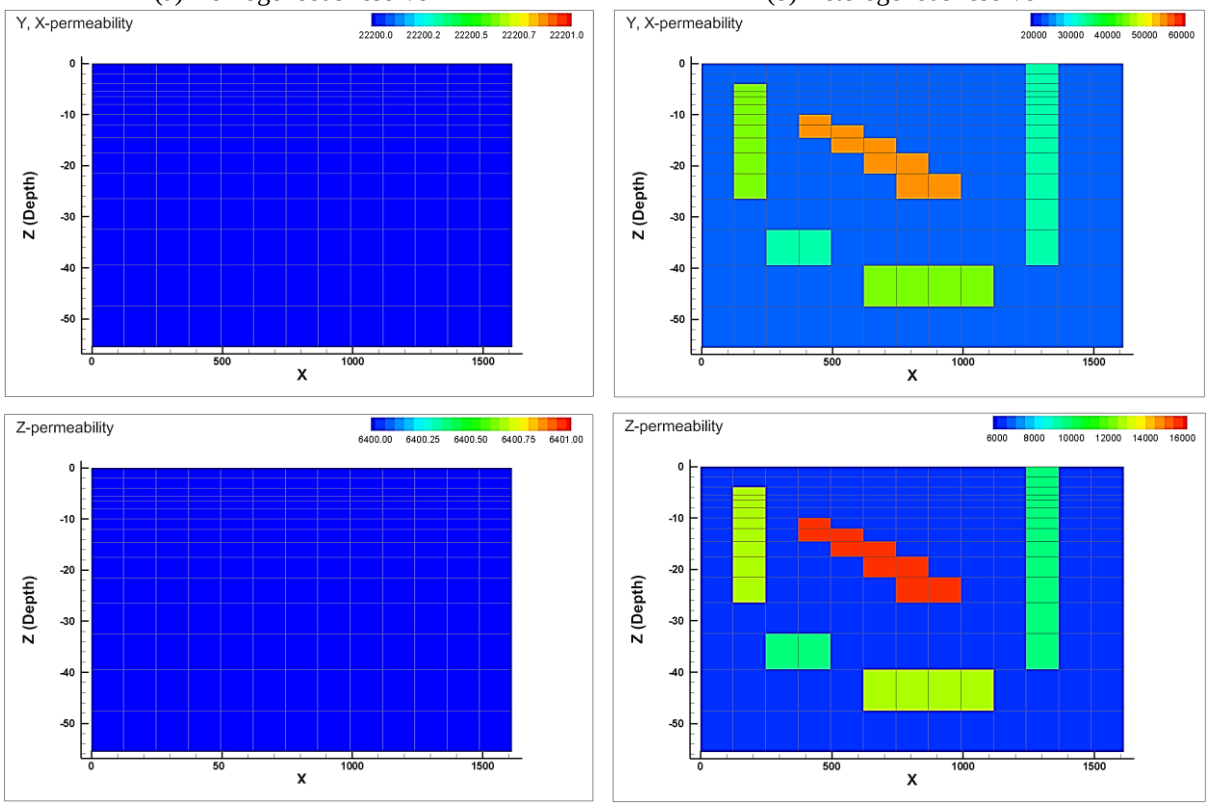


Figure 6.8: Permeability distribution in (a) homogeneous reservoir (b) heterogeneous reservoir.

Implementation of heterogeneity in different directions in ROCX is challenging and in this case, the permeability in the *x*, *y*, and *z* directions must be defined for each cell separately through using the ijk option in ROCX. Based on the subchapter 6.1.2.3 the reservoir is discretized to 4875 cells ( $nx \cdot ny \cdot nz = 4875$ ). As a result, for defining some high permeability zones in different directions, the permeability in the *x*, *y*, and *z* directions must be defined for 4875 cells one by one. For solving this problem, MATLAB can be used for generating the required values of permeability for all 4875 cells as a text file that can be imported to ROCX. The MATLAB code written for this purpose is presented in Appendix N.

### 6.1.5 Relative permeability setting

Based on the discussions in subchapters 4.2.3.4 and 4.2.3.5, the Corey and Stone II model with given values in Table 6.5 is used for defining the relative permeability of the reservoir in the OLGA/ROCX model.

Table 6.5: Values for the parameters of the Corey and Stone II model.

| | | |
|---|---|---|
| **Residual Saturations** | Swc = 0.12 | Sor = 0.05 |
| **Corey Model** | Krwoc = 0.4 | nw = 2 |
| **Stone II Model** | Krowc =1 | now = 4 |

### 6.1.6 Initial condition settings

Based on the given information in Table 4.3, the reservoir near the well 16/2-D-12 consists of two zones with different types of sandstone. The first zone has a water saturation of 0.062 and the second zone has a water saturation of 0.322. Therefore, for developing the model it is assumed that initially the reservoir in both zones filled with oil but with a water saturation of 0.062 and 0.322 in the first and second zone respectively. Besides, the initial pressure and temperature are 240 bar and 81˚C respectively. Figure 6.9 represents the initial water saturation in the reservoir.

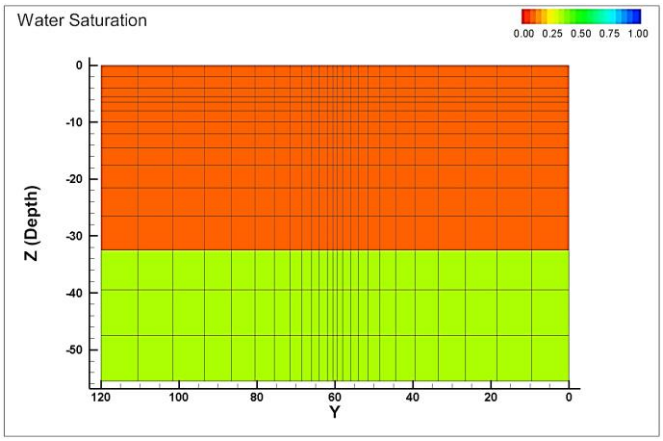


Figure 6.9: Initial water saturation in the reservoir.

### 6.1.7 Boundary condition settings

As shown in Figure 6.2, for developing the OLGA/ROCX model, it is assumed that the well is positioned parallel to the *x*-direction, in the middle of the reservoir in the *y*-direction, and 5.5 m below the top of the reservoir. Moreover, 13 joints have been considered for the well, and based on that the reservoir in the *x*-direction has been discretized to 13 cells. Therefore, based on the grid setup given in Table 6.2, under the well pressure tab, the location of well is defined by setting *x*-coordinate from 1 to 13, *y*-coordinate equals to 13, and *z*-coordinate equals to 4 in the (*i*,*j*,*k*) coordinate systems. Moreover, the diameter of the wellbore is set to 0.2159 m and the direction of flow is defined parallel to the *x*-axis. Also, the temperature and pressure of the well are 81˚C and 240 bar respectively. Since there is a large aquifer at the bottom of the reservoir, under the reservoir pressure tab, a water feed with a pressure of 240 bar and temperature of 81˚C from the bottom plane of the reservoir with the *z*-coordinate of 15 is defined in ROCX.

### 6.1.8 Simulation settings

In order to run the model, the minimum time step is considered equal to 0.1 s and the maximum time step is set to 20 s.

## 6.2 Development of the well model in OLGA

This subchapter includes the main steps for developing the model of well 16/2-D-12 in OLGA and combining it whit the reservoir model created in ROCX.

### 6.2.1 Case definition settings

In order to investigate oil production from the well 16/2-D-12 in the JSF, the model is run for 750 days. The minimum and maximum time steps are set to 0.1 s and 20 s respectively. A three-phase system with the black oil model is considered for developing the model and a first-order discretization scheme is chosen for solving the mass equations.

### 6.2.2 Compositional settings

In the compositional tab, three black oil components which are gas, oil, and water, as well as water and oil feeds, are defined in the same way that they are defined in ROCX.

### 6.2.3 Flow component settings

For developing the well model in OLGA, one pipe with a length of 1612 m, a diameter of 0.1397 m (5.5 inch), and roughness of 15 μm is considered for representing the production tubing. Another pipe with the same length but a diameter of 0.2159 m (8.5 inch) is considered for representing the wellbore. It is assumed that oil is produced from 13 zones in the well and each zone contains two hypothetical sections. Therefore, the production tubing and wellbore are discretized to 26 hypothetical sections, each 62 m long. The simplified model of oil production from each zone is represented in Figure 6.10.

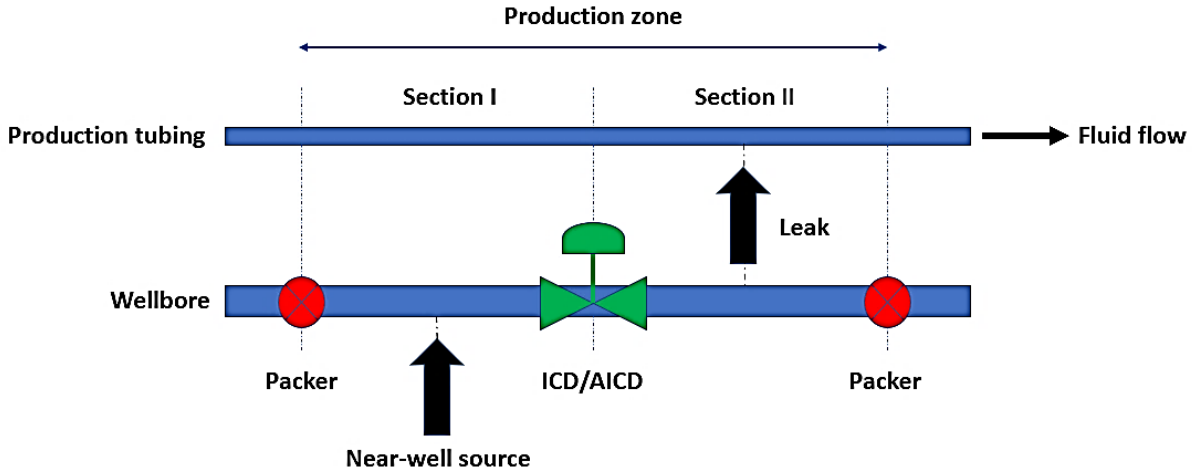


Figure 6.10: Simplified representation of a single production zone.

As can be seen in the figure, in order to stop flowing the reservoir fluids between different zones in the annulus, each production zone in the wellbore is separated by two packers. Moreover, by using a near-well source connected to the ROCX model, the reservoir fluids enter the wellbore after passing an inflow control device located in the first section of the wellbore. The reservoir fluids that pass through the inflow control device enter the production tubing via a leak connected to the second section of the production tubing and move towards the heel of the well. This setup has been proposed and used in [4]. The specifications of all components of this zonal production setup, including the near-well source, packer, ICD/AICD, and leak used for developing the OLGA/ROCX model are given in Table 6.6.

Table 6.6: Specifications of the components used in the zonal production setup in OLGA.

| Component | OLGA Module | Description |
|---|---|---|
| Near-well source | Near-well | Coupled with the correspond ROCX model file |
| Leak | Leak | Diameter = 0.12 m, CD = 1, Connected to the production tubing. |
| ICD/AICD | Valve/Table Controller | Diameter = 0.0108 m, CD = 0.61, Connected to the wellbore, AICD is controlled by a Table Control. |
| Packer | Valve (closed) | Diameter = 0.12 m, Opening = 0 (fully closed), Connected to the wellbore. |

For developing the OLGA/ROCX model, in addition to implementing the zonal production setup in OLGA, the boundary conditions for the production tubing and wellbore must be defined as well. As calculated in subchapter 5.9, the outlet pressure of production tubing is 228 bar. The other boundary condition is given in Table 6.7.

Table 6.7: Flow path boundary conditions.

| Flow Path | Boundary Name | Boundary Type |
|---|---|---|
| Production tubing | Inlet | Closed node |
| | Outlet | Closed node |
| Wellbore | Inlet | Closed node |
| | Outlet | Pressure node, Pressure =228 bar, Temp. = 81˚C |

In order to implement the autonomous behavior of the AICD in OLGA, a controller must be used for chocking the AICD based on the characteristics of the AICD and reservoir fluid mixtures. For developing the model of oil production from the well 16/2-D-12 with RCP valve completion, the Table Control module in OLGA is used for controlling the valve. In this model, at first, by using the Transmitter module in OLGA, the water cut of the fluid mixture is measured. Then the Table Control, based on the measured water cut of the fluid mixture and some tabulated data (which is calculated based on the mathematical model and control function of the RCP valve), provides a corresponding control signal for partially chocking the RCP valve. The mathematical model and control function of the TR7 RCP has been developed in subchapters 5.6, 5.6.2, and 5.8, and the control signal table used by the Table Control in the OLGA/ROCX model has been presented in Table 5.6. The implementation of the table controller for an RCP valve in the OLGA/ROCX model is illustrated in Figure 6.11.

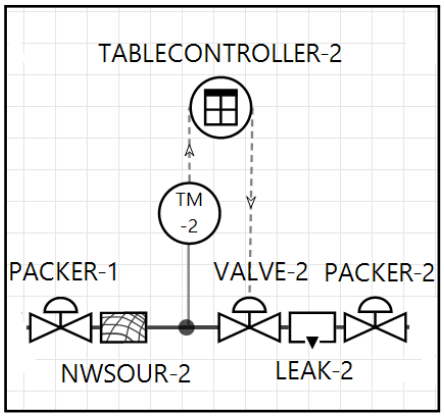


Figure 6.11: Representation of the RCP valve control setup in OLGA.

## 6.3 Simulated cases

In this thesis, for investigation of the oil production from the well number 16/2-D-12 in the JSF and comparing the functionality of ICD and RCP valves in both homogeneous and heterogeneous reservoirs, the simulations are conducted for 750 days based on four different cases in parallel. The description of the simulation cases is given in Table 6.8.

Table 6.8: Description of the main simulated cases.

| Case | Description |
|---|---|
| Case 1 | The well 16/2-D-12 in the JSF with considering ICD completion and homogeneous reservoir – ICD valve diameter = 0.0108 m, Equivalent ICD numbers =13, Pressure drawdown = 12 bar |
| Case 2 | The well 16/2-D-12 in the JSF with considering TR7 RCP completion and homogeneous reservoir, Controlling by the Table Controller based on the mathematical model and control function of the TR7 RCP valve – RCP valve diameter in the fully open mode = 0.0108 m, Equivalent RCP numbers =13, Pressure drawdown = 12 bar |
| Case 3 | The well 16/2-D-12 in the JSF with considering ICD completion and heterogeneous reservoir with some high permeable zones in different directions – ICD valve diameter = 0.0108 m, Equivalent ICD numbers =13, Pressure drawdown = 12 bar |
| Case 4 | The well 16/2-D-12 in the JSF with considering TR7 RCP completion and heterogeneous reservoir with some high permeable zones in different directions, Controlling by the Table Controller based on the mathematical model and control function of the TR7 RCP valve – RCP valve diameter in the fully open mode = 0.0108 m, Equivalent RCP numbers =c13, Pressure drawdown = 12 bar |

As a sample, the summary report for the ROCX and OLGA model for Case 2 is presented in Appendices O and P respectively.

# 7 Results and discussion

In this chapter, to investigate oil production from the well 16/2-D-12 under different conditions, the obtained simulation results from the OLGA/ROCX model developed in the previous chapters are presented and discussed. Besides, the functionality of ICD and RCP valves in enhancing oil recovery from this well is evaluated. The simulations have been conducted for four main cases described in Table 6.8.

## 7.1 Fluid flow distribution and time of water breakthrough

Water coning can significantly reduce the well productivity, and delaying water is one of the main measures that must be taken to maximize the field's ultimate oil recovery. The fluid flow distribution around the well is affected by three main forces, which are capillary forces, gravity forces, and viscous forces. At any given time, the balance between these forces determines the distribution of fluid flow around the well. When there is a large enough pressure gradient between the well and reservoir, enough viscous forces for overcoming gravity and capillary forces are created. As a result, water tends to move towards the well. However, until the water saturation near the well exceeds the irreducible water saturation ($S_{wc}$ is considered to be equal to 0.12 in the JSF), water does not enter the wellbore. Oil production can be continued until the oil saturation falls below the residual oil saturation ($S_{or}$ is considered to be 0.05 in the JSF). Because of the frictional pressure drop along the horizontal well, the pressure drawdown reaches its maximum value at the heel of the well. Consequently, the water cone will grow much faster and breaks into the well much sooner at the heel compared to the toe of the well. In the heterogeneous reservoirs, the permeability varies along the well, which brings about an uneven inflow profile along the well. Based on Darcy's law, due to the lower flow resistance in the high permeable zones, the water cone grows faster in these zones. Consequently, the early water breakthrough starts from the high permeable zones.

Figure 7.1 illustrates the outlet water cut from the well 16/2-D-12 without considering any inflow control devices (open-hole well) for both homogeneous and heterogeneous reservoirs. It can clearly be seen from the figure that the water breakthrough in the homogeneous reservoir occurs after 9 days whereas it takes place on the 3$^{rd}$ day for the heterogeneous reservoir. The water breakthrough in the heterogeneous reservoir takes place sooner because, as explained in the subchapter 6.1.4, the heterogeneous reservoir consists of some zones with higher permeability than average permeability in the homogeneous reservoir. Moreover, based on Darcy's law, when there are no inflow control devices, the inflow to the well in the high permeable zones is higher than the other zones. As a result, as can be seen in Figure 7.1, the water cut experiences much faster growth in the heterogeneous reservoir compared to the homogeneous reservoir.

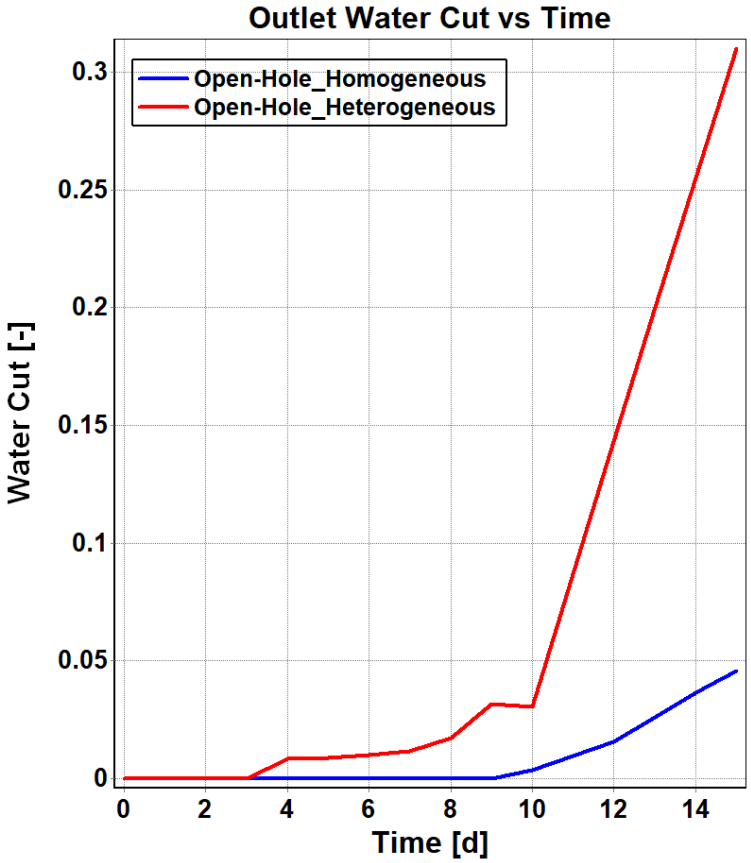


Figure 7.1: Outlet water cut from the well 16/2-D-12 for the open-hole conditions.

Figure 7.2 shows the oil saturation contours for the homogeneous and heterogeneous reservoir near the open-hole well after 10 days of production (right after the water breakthrough in the homogeneous case). These contours have been obtained from Tecplot RS which is a software for visualizing the reservoir simulation results. The well consists of 13 zones and the 3D contour illustrates the oil saturation distribution from all the 13 zones. For the homogeneous reservoir, the Y-Z plane contour represents the oil saturation in the 13$^{th}$ zone located at the heel of the well. For the heterogeneous reservoir, the Y-Z plane contour shows the oil saturation in the 11$^{th}$ zone, which has the highest permeability. As shown in the contours, once the water breakthrough takes place, the water saturation profile has a conical shape. Besides, it can be clearly seen that the water cone grows faster and breaks into the well sooner at the heel compared to the toe of the well. Moreover, based on the contours, it is obvious that the early water breakthrough in the heterogeneous reservoir occurs in the high permeable zones ( 2$^{nd}$ an 11$^{th}$ zones) and the water cone develops much faster in these zones. Therefore, it can be said that physically, the simulation results for the open-hole well comply with what is expected from the theory.

(a) Open-Hole well / Homogeneous reservoir (b) Open-Hole well / Heterogeneous reservoir

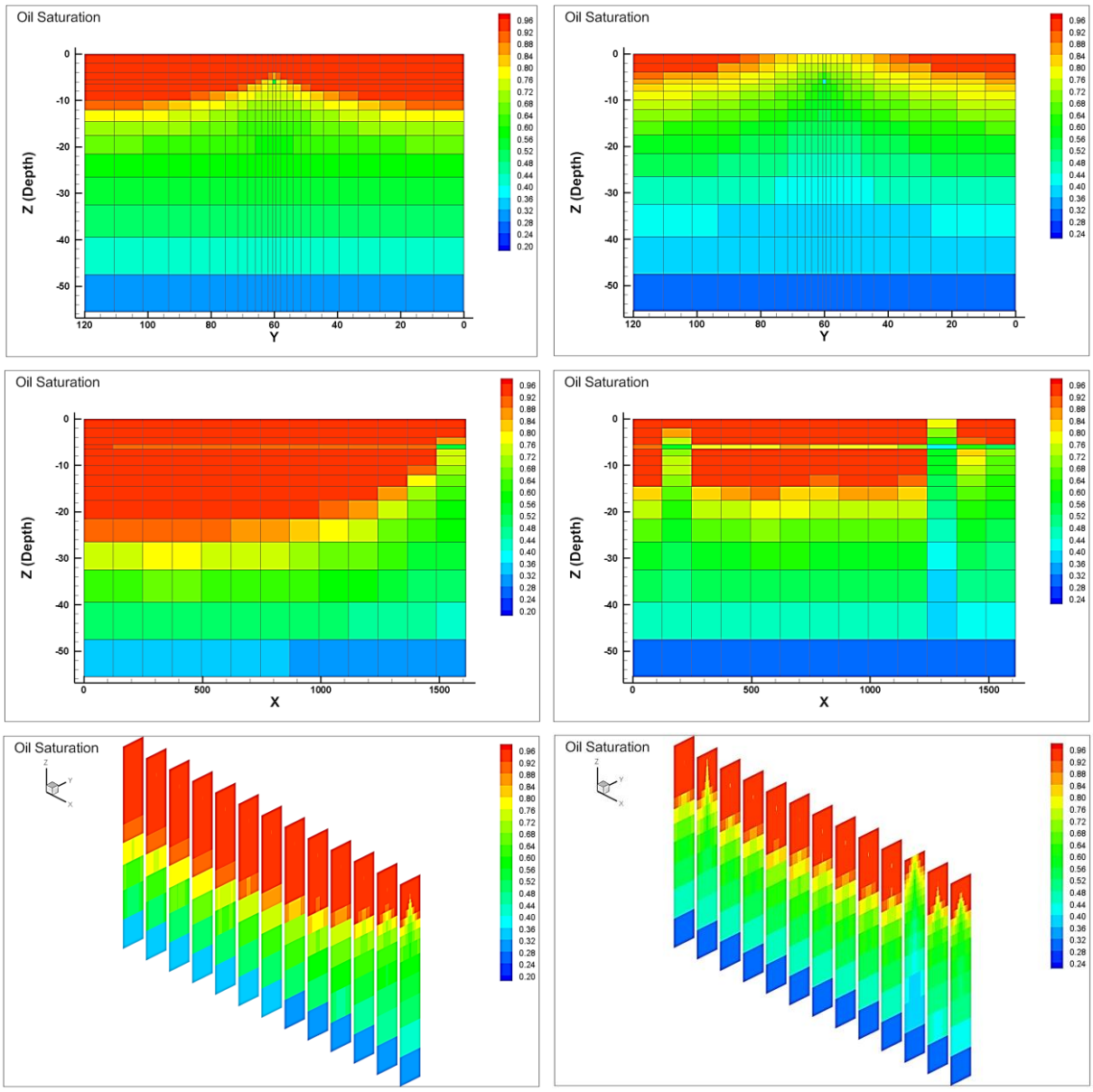


Figure 7.2: Oil saturation distribution after 10 days for open-hole well in (a) Homogeneous reservoir (b) Heterogeneous reservoir.

ICDs are used for balancing the inflow along the well and thereby delay the early water breakthrough in horizontal wells. ICDs have no ability to choke the water back after breakthrough. However, RCP valves have a moveable disk and can be partially closed for low viscous fluids like water. As a result, in addition to delaying the water breakthrough, RCP valves can reduce the production of water after breakthrough autonomously.

The outlet water cut from the well 16/2-D-12 by considering ICD and RCP completion versus time under different conditions is shown in Figure 7.3. Based on the figure, the water breakthrough for both types of well completion (with ICD or RCP) in the homogeneous reservoir takes place after 262 days. However, water enters the well for both cases in the

heterogeneous reservoir 4 days sooner on the 258th day of production. This can be expected because, before the water breakthrough, RCP valves remain fully open, and consequently they perform the same as ICDs. Therefore, there should not be any difference between the time of water breakthrough for well completion with ICD and RCP. In the heterogeneous reservoir, there are some zones with higher permeability than the average permeability in the homogeneous reservoir. As a result, the water breakthrough in the heterogeneous reservoir occurs sooner compared to the homogenous reservoir.

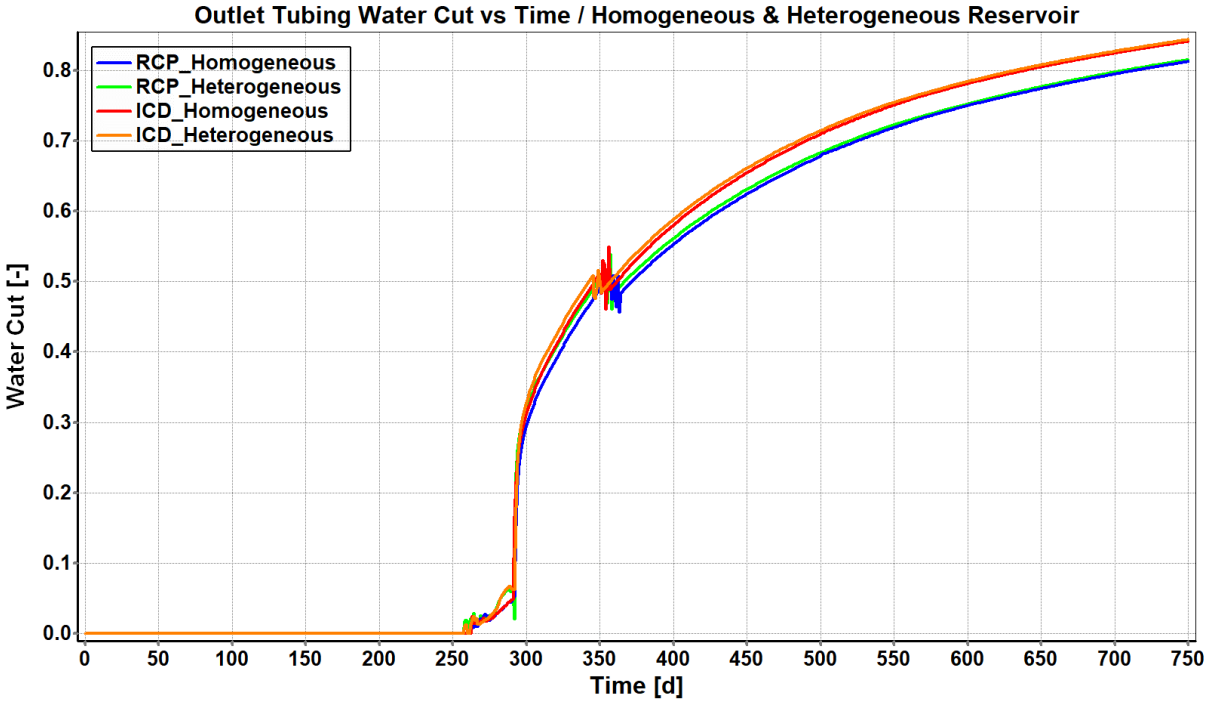


Figure 7.3: Outlet water cut from the well 16/2-D-12 for the simulation cases.

Another observation from Figure 7.3 is that after the initial water breakthrough, the water cut experiences a slight increase until the 291st day of production. This is due to the fact that the water starts to enter the well from the heel side of the well in the homogeneous reservoir and from the high permeable zones in the heterogeneous reservoir. However, by increasing the water saturation around the well and entering the water to the well from all over the reservoir, more water tends to be produced and after the 291st day of production, the water cut increases dramatically.

The obtained data from Figure 7.1 and Figure 7.3, related to the water breakthrough time for open-hole well and well with inflow control devices are presented in Table 7.1. Based on the table, it can be concluded that by completion of the well 16/2-D-12 with ICD or RCP valves the water breakthrough can be delayed by 253 days in the homogenous reservoir and 255 days in the heterogeneous reservoir compared to the open-hole well. As a result, using inflow control devices can significantly enhance oil recovery from this well by delaying early water breakthrough. In addition to that, it can be argued that using inflow control devices is more effective in heterogeneous reservoirs.

Table 7.1: Water breakthrough time for the open-hole well and well with inflow control devices.

| Item | Breakthrough Time Open-hole well | Breakthrough Time Well with ICD or RCP |
|---|---|---|
| **Homogeneous res.** | 9 days | 262 days |
| **Heterogeneous res.** | 3 days | 258 days |

Figure 7.4 shows the water cut along the well 16/2-D-12 for the homogeneous and heterogeneous reservoirs on the 265$^{th}$ day of production, which is 3 days after the time that water breakthrough occurs in the homogeneous reservoir. As can be seen in this figure, water breakthrough occurs sooner in the heterogeneous reservoir from its high permeable zones. Moreover, the figure shows that the initial water breakthrough in the homogeneous reservoir takes place from the heel side of the well.

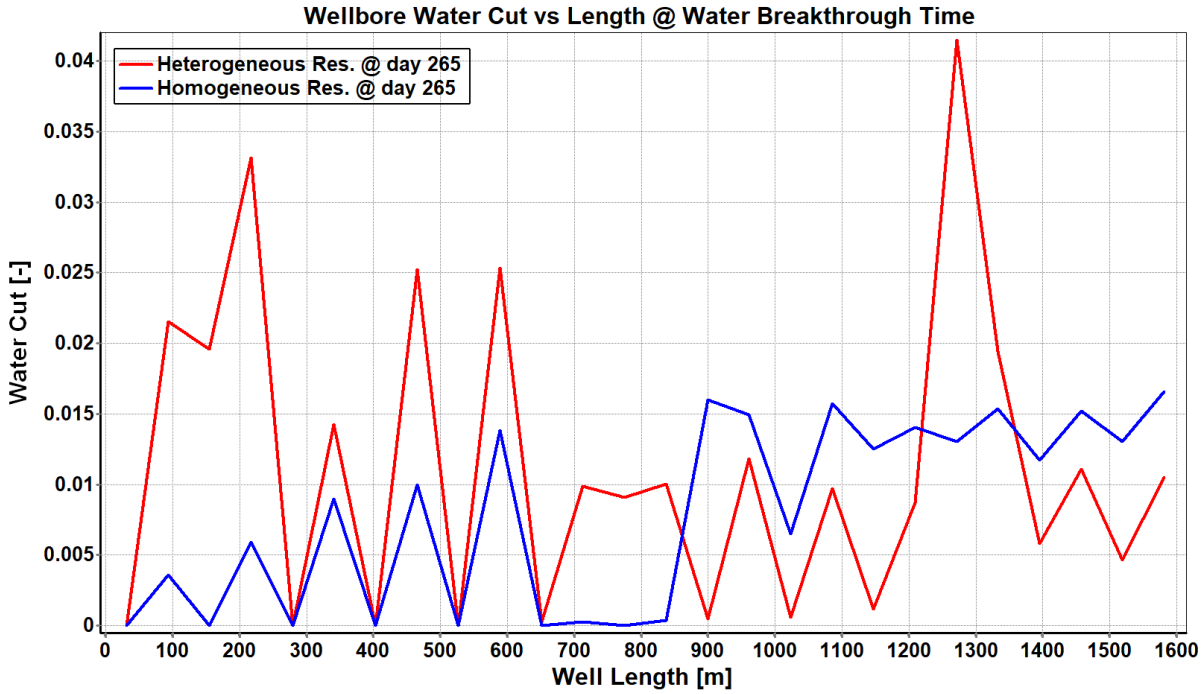


Figure 7.4: Wellbore water cut along the well 16/2-D-12 at the 265$^{th}$ day of production for the homogeneous and heterogeneous reservoir.

The oil saturation contours for both the homogeneous and heterogeneous reservoirs near the well 16/2-D-12 with considering inflow control devices are illustrated in Figure 7.5. For both cases, the contours show the oil saturation distribution right after the water breakthrough in the homogeneous reservoir. The well consists of 13 zones and the 3D contour illustrates the oil saturation distribution from all the 13 zones. For the homogenous reservoir, the Y-Z plane contour represents the oil saturation in the 13$^{th}$ zone located at the heel of the well. For the

heterogeneous reservoir, the Y-Z plane contour shows the oil saturation in the 11$^{th}$ zone which has the highest permeability.

(a) Homogeneous reservoir (b) Heterogeneous reservoir

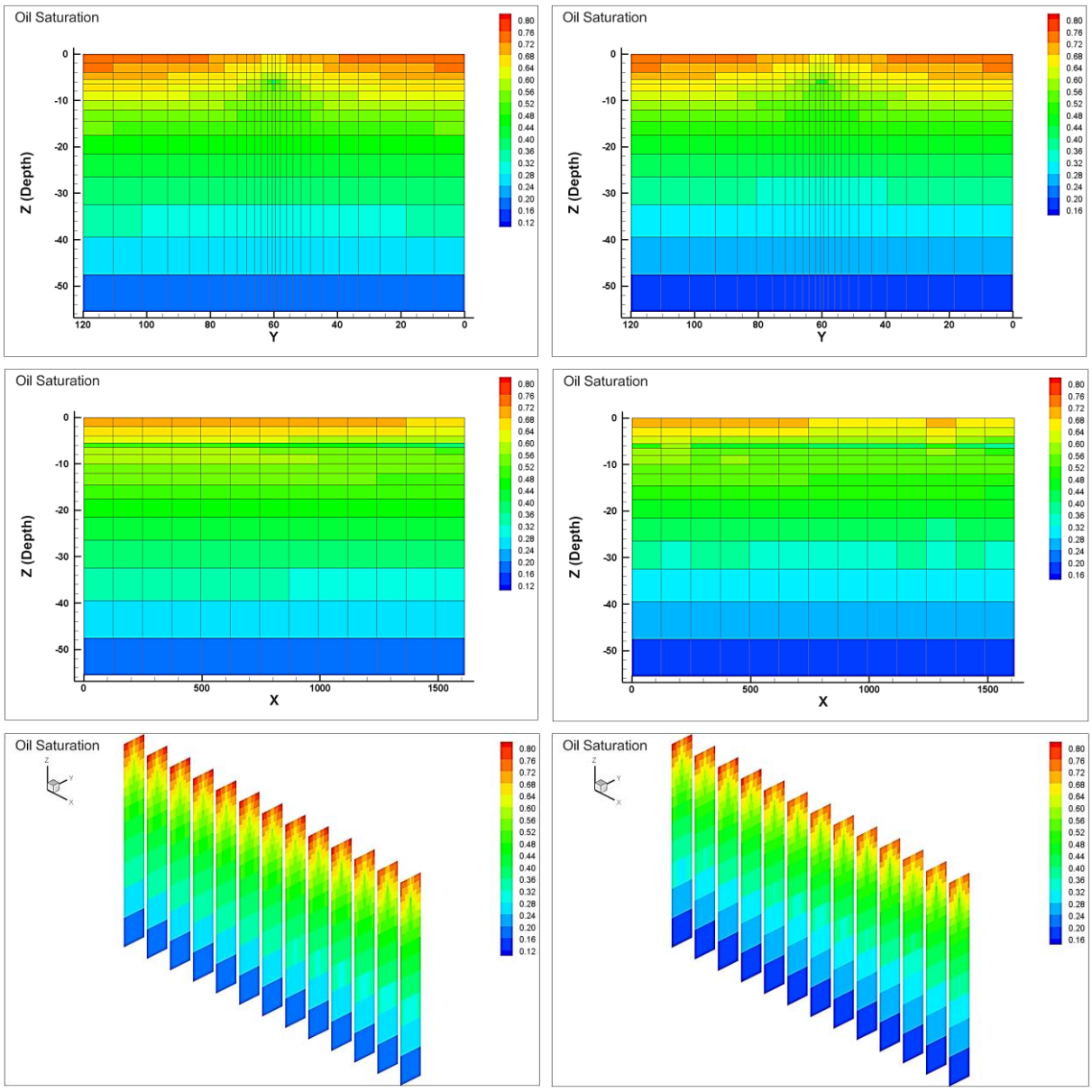


Figure 7.5: Oil saturation distribution for (a) Homogeneous reservoir and (b) Heterogeneous reservoir, right after water breakthrough in the homogeneous reservoir.

As shown in the contours, once the water breakthrough takes place, the water saturation profile has a conical shape. Besides, it can be clearly seen that the water cone grows faster at the heel side compared to the toe side of the well in the homogeneous reservoir. Moreover, based on the contours, it is obvious that the water saturation profile develops faster at the high permeable zones in the heterogeneous reservoir. By comparing Figure 7.2 and Figure 7.5, it can be

concluded that the inflow along the well completed with inflow control devices is much more balanced compare to the open-hole well. Therefore, by using the inflow control devices the flow influx along a horizontal well can be effectively evened out.

## 7.2 Performance of the implemented RCP valve in OLGA for choking the water

OLGA does not have any options that can be used for implementing the autonomous behavior of the RCP valves in modeling and simulation of oil production. Therefore, in subchapters 5.6 and 5.8, based on experimental data, a mathematical model as well as a control function for implementing the autonomous behavior of this valve in OLGA, was developed. Figure 7.6 and Figure 7.7 illustrate the performance of the implemented RCP valve in partially chocking the water back under different conditions during oil production from the well 16/2-D-12. The figures show the variations of the RCP valve opening based on the variations of the water cut. The well consists of 13 joints and one RCP valve has been considered for each joint. However, to have a good illustration, only the performance of the RCP valve in the toe and heel sides of the well in the homogeneous reservoir is shown in Figure 7.6. In addition, the performance of the RCP valve in low permeable and high permeable zones in the heterogeneous reservoir is shown in Figure 7.7.

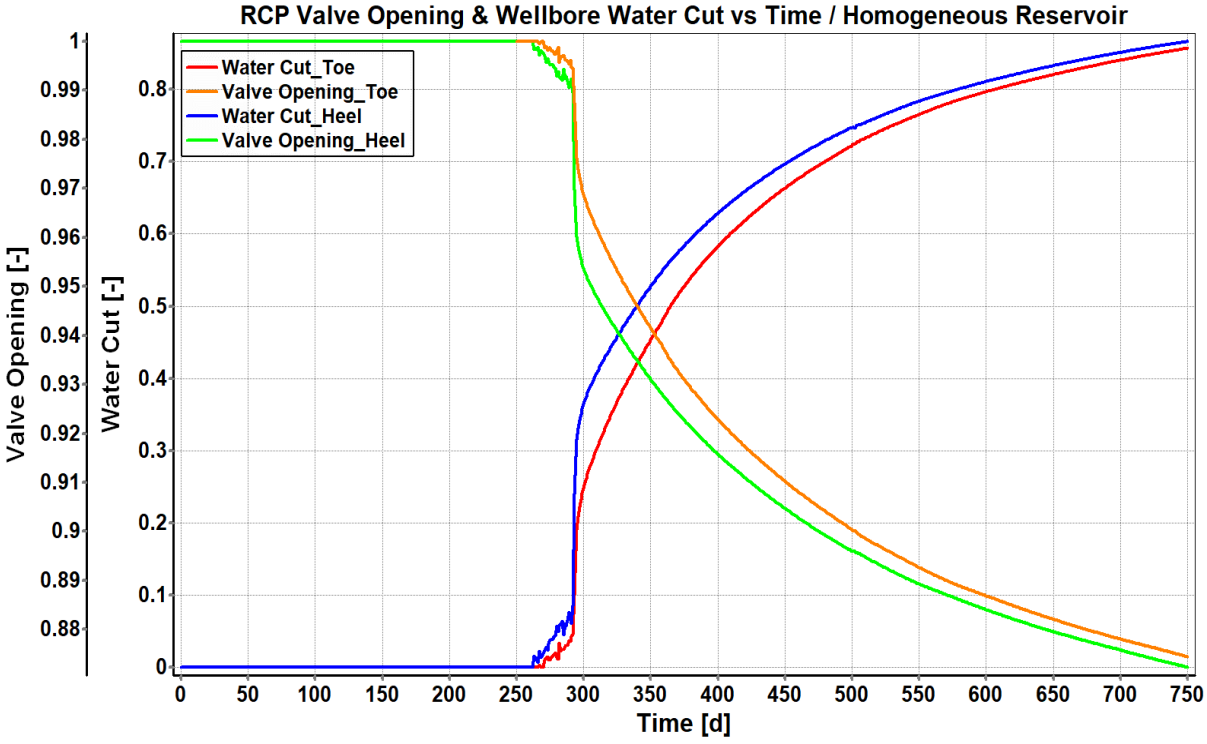


Figure 7.6: Performance of the RCP valve located in the toe and heel sides of the well in the homogeneous reservoir.

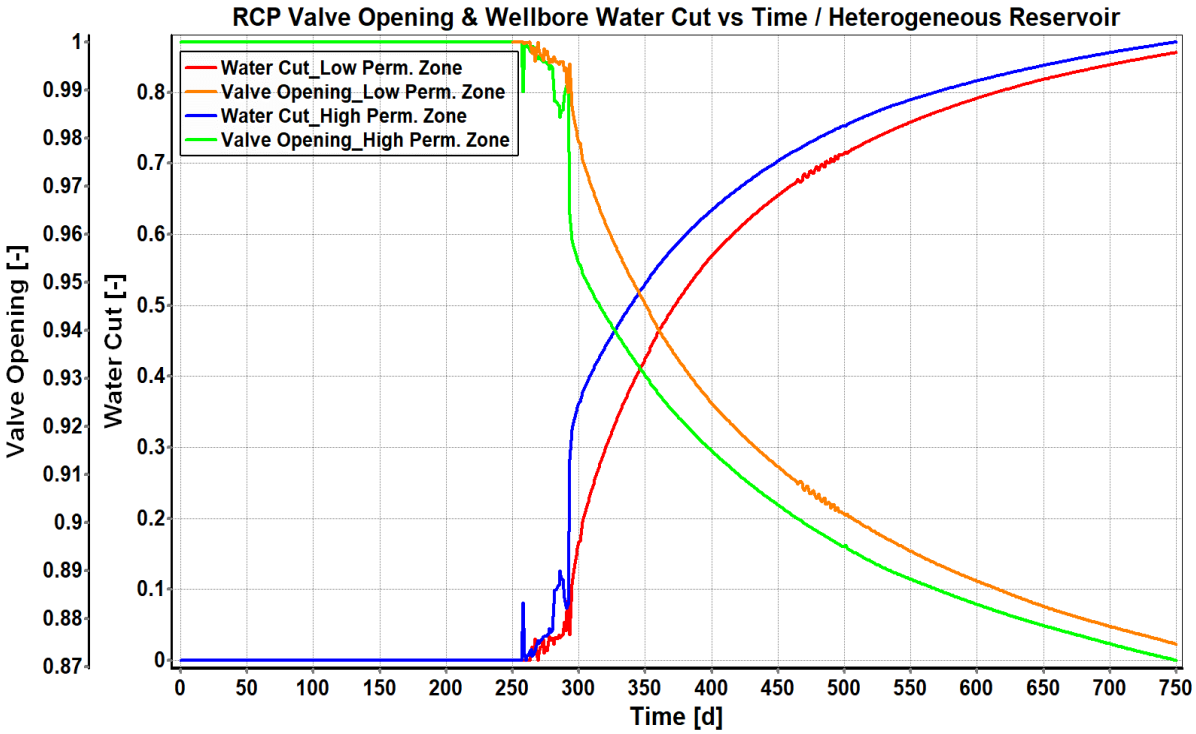


Figure 7.7: Performance of the RCP valve located in the low permeable and high permeable zones in the heterogeneous reservoir.

As can be seen in the figures, for all cases, the RCP valve opening and the water cut have opposite trends in such a way that by increasing the water cut, the valve opening decreases. Moreover, it can be clearly seen that the implemented RCP valve is even sensitive to very small variations in the water cut and the RCP valve opening varies exactly based on the water cut variations. On the toe side of the well the water cut is lower compared to the heel side, and therefore the RCP valve opening experiences a lower decrease. The performance of the RCP valve in the low permeable zone compared to the high permeable zone in the heterogeneous reservoir is in the same way. According to Figure 7.6 and Figure 7.7, it can be argued that the implemented RCP valve in OLGA based on the developed mathematical model and the control function can appropriately simulate the autonomous behavior of this valve for partially choking the water back during oil production.

The values of the RCP valve opening and water cut in different locations of the well 16/2-D-12 after 750 days of production for both homogeneous and heterogeneous reservoirs obtained from Figure 7.6 and Figure 7.7 are presented in Table 7.2. According to the table, after 750 days of production, the wellbore water cut peaks at 0.871 (87.1%) in the high permeable zone of the heterogeneous reservoir. In this condition, the RCP valve experience a maximum closure of 12.9%. As explained in subchapter 5.8, since there is no considerable difference between the viscosity of oil in the JSF (3 cP) and water (0.45 cP), when the water cut reaches its maximum at 1, the valve opening reaches its minimum at 0.835. This means that the RCP valve can not be closed more than 16.5% for the JSF conditions. Therefore, if the production continues after 750 days and the water cut increases more, the RCP valve can be partially closed up to 16.5% in the JSF conditions.

Table 7.2: Performance of the RCP valve under different conditions after 750 days of production.

| Item | Toe side/ Homogeneous reservoir | Heel side/ Homogeneous reservoir | Low perm. zone/ Heterogeneous reservoir | High perm. zone/ Heterogeneous reservoir |
|---|---|---|---|---|
| Wellbore water cut | 0.857 | 0.867 | 0.856 | 0.871 |
| RCP valve opening | 0.874 | 0.872 | 0.875 | 0.871 |
| % of valve closing | 12.6% | 12.8% | 12.5% | 12.9% |

## 7.3 Comparing the functionality of the ICDs and RCP valves in the homogenous reservoir

In this subchapter, the simulation results for oil production from the well 16/2-D-12 by considering ICD and RCP completion in the homogeneous reservoir for 750 days of production are presented and described.

### 7.3.1 Accumulated oil and water production

In order to investigate oil production and comparing the performances of different inflow control devices, accumulated oil and water are the two most important parameters that must be taken into account. Figure 7.8 illustrates the accumulated oil and water produced from the well 16/2-D-12 by considering ICD and RCP completion in the homogeneous reservoir. As can be seen in the figure, after 750 days of production, there is a very small difference between accumulated oil in the ICD and RCP cases. However, due to the choking effect of the RCP valve for low viscous fluids like water, the amount of accumulated water considerably drops when the well is completed by RCP valves.

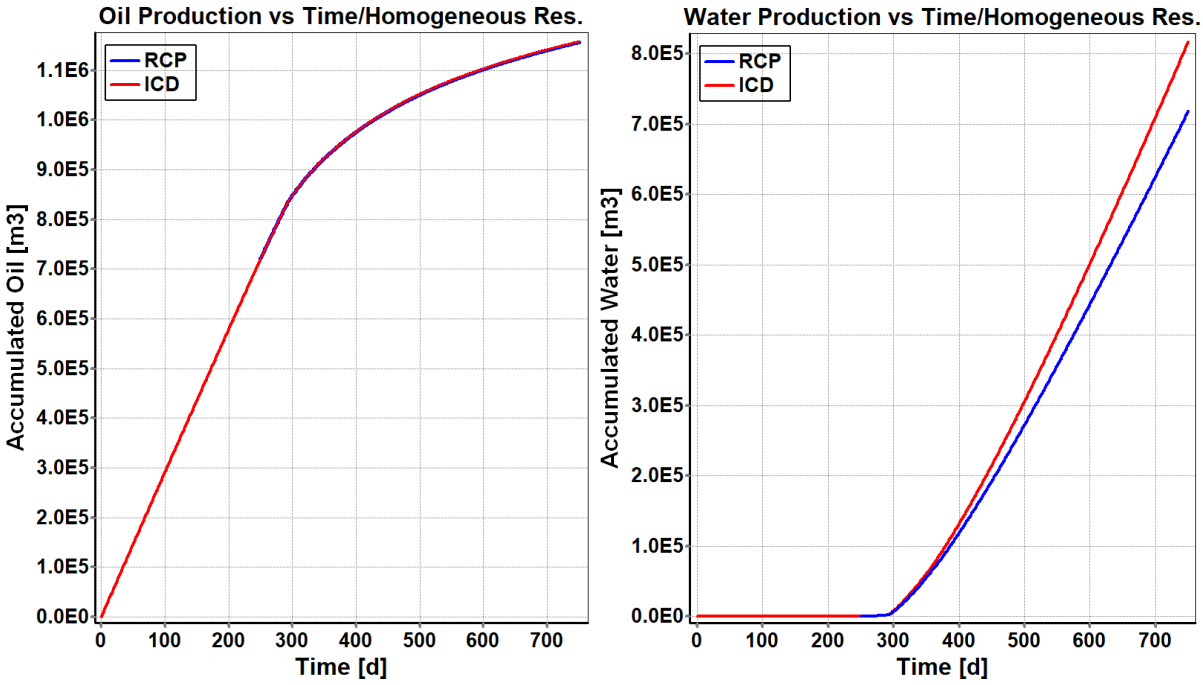


Figure 7.8: Accumulated oil and water from the well 16/2-D-12 with ICD and RCP completion in the homogeneous reservoir.

The values of accumulated oil and water for the ICD and RCP cases obtained from Figure 7.8 are presented in Table 7.3. According to the table, by completion of the well 16/2-D-12 with RCP valves, after 750 days the accumulated oil drops by only 0.1% while the accumulated water is considerably reduced by 12.1%. As a result, by considering a homogeneous reservoir near the well 16/2-D-12, using the RCP valves in addition to producing approximately the same amount of oil, can prevent the production of a large volume of unwanted fluids.

Table 7.3: Values of accumulated oil and water in the homogeneous reservoir after 750 days.

| Item | Accumulated oil | Accumulated water |
|---|---|---|
| **Well with ICD completion** | 1158407 $m^3$ | 817117 $m^3$ |
| **Well with RCP completion** | 1156998 $m^3$ | 718242 $m^3$ |
| **% of change (RCP to ICD)** | - 0.1% | - 12.1% |

### 7.3.2 Oil and water flow rate

The other important parameters that must be considered for comparing the functionality of the RCP and ICD valves are the flowrate of oil and water. Figure 7.9 illustrates the volumetric flow rate of oil and water production from the well 16/2-D-12 in the homogeneous reservoir near

this well for a period of 750 days. The figure includes the oil and water flow rate for this well by considering ICD and RCP completion.

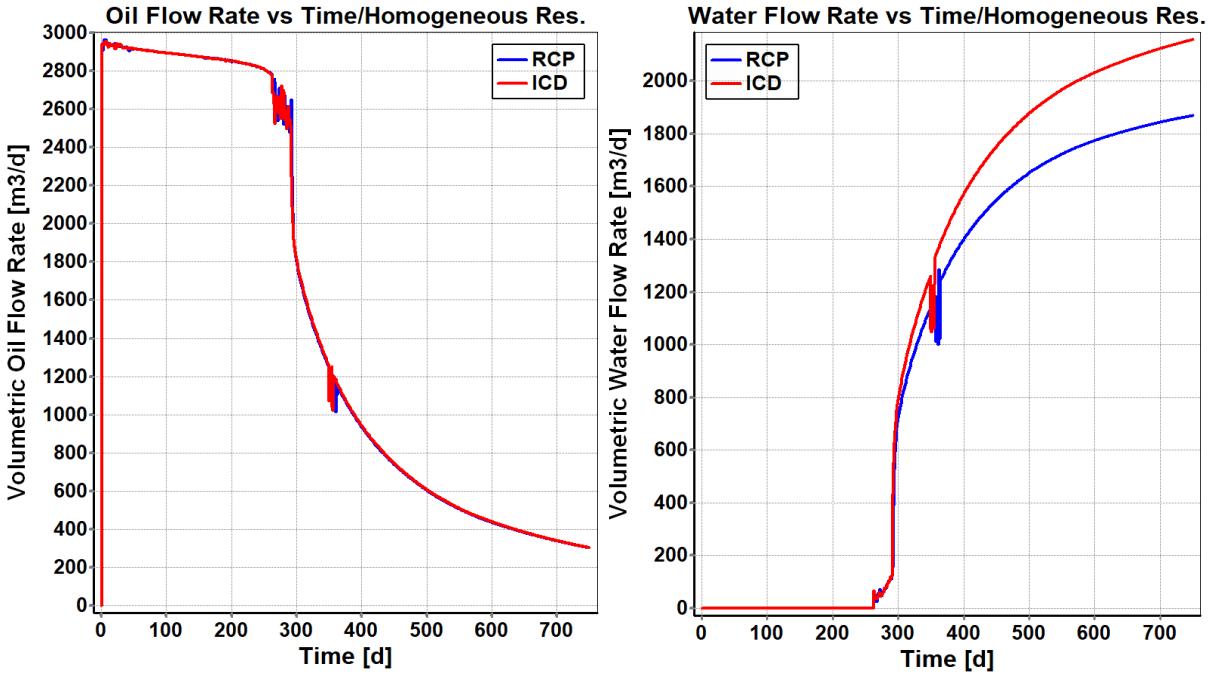


Figure 7.9: Flow rate of oil and water for the well 16/2-D-12 with ICD and RCP completion in the homogeneous reservoir.

As can be seen in the figure, over the whole period of production for both cases, the oil flow rate is nearly the same. As a result, it can be concluded that practically there is no difference between using ICD and RCP with respect to the oil flow rate over the first 750 days of production. However, since after water breakthrough the RCP valves begin to gradually close, the diagram of the water flow rate for the ICD and RCP cases, start to deviate from each other after the water breakthrough. As the RCP valves close more, more water is choked back, resulting in a further deviation of the water flow rate diagrams of these two cases. It can be clearly seen from Figure 7.9 that the well completed by RCP valves considerably declines the rate of water production after water breakthrough compared to the well with ICDs.

The obtained values from Figure 7.9 related to oil and water flow rate for the simulated cases are summarized in Table 7.4. According to the table, at the end of the production period (750 days), the oil flow rate in the RCP case is only 0.3% lower than that of the ICD case whereas the water flow rate experience a considerable decline in the RCP case by -13.3%. Moreover, the maximum flow rate of oil production form both cases is almost equal and peaks at approximately 2960 $m^3$/d. In order to develop the OLGA/ROCX model, the oil production has been estimated as 3200 $m^3$/d in subchapter 5.3.2. Therefore, by comparing the simulation results for the rate of oil production and the estimated value, it can be argued that the simulation result and the estimated value for the rate of oil production have a good consistency with only a 7.5% difference.

Table 7.4: Values of volumetric flow rates of oil and water in the homogeneous reservoir after 750 days.

| Item | Volumetric oil flow rate | | Volumetric water flow rate |
|---|---|---|---|
| | Maximum | Minimum | |
| **Well with ICD completion** | 2956 $m^3/d$ | 303 $m^3/d$ | 2157 $m^3/d$ |
| **Well with RCP completion** | 2966 $m^3/d$ | 302 $m^3/d$ | 1870 $m^3/d$ |
| **% of change (RCP to ICD)** | 0.3% | - 0.3% | - 13.3% |

### 7.3.3 Outlet water cut

On average in the world, an oil well produces about 3 barrels of water per barrel of oil. However, a significantly higher amount of water production from some wells may still be profitable. As an example, there are some wells in the North Sea Shell Expro Brent fields and in the BP-Amoco Forties fields which have more than 85% water cut but still produce enough hydrocarbons to be economical [76]. Lifting, handling, and then disposing of water, costs a lot of money. Therefore, controlling the water cut is one of the most important measures that must be taken to achieve cost-effective oil production.

Figure 7.10 illustrates the outlet water cut from the well 16/2-D-12 with the completion of ICD and RCP valves by considering a homogeneous reservoir near this well. Besides, the variation of water cut along the production tubing after 750 days of production is shown in the figure.

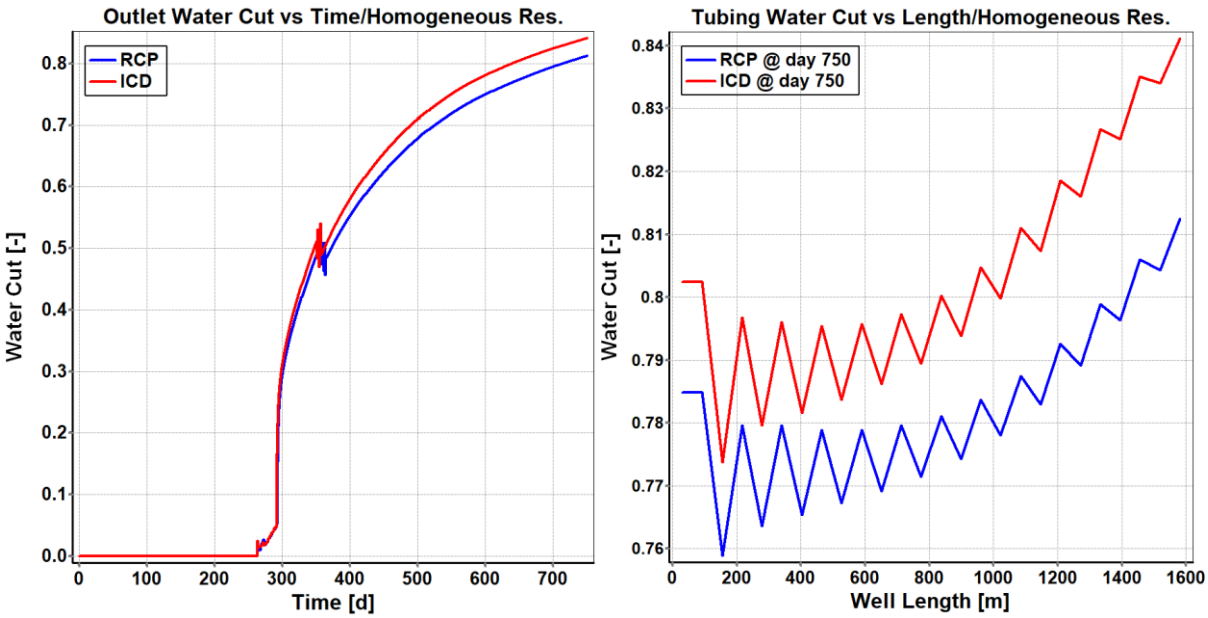


Figure 7.10: Outlet water cut as well as water cut along the production tubing after 750 days for the well 16/2-D-12 in the homogeneous reservoir.

For comparing the functionality of the RCP valves and the ICDs in achieving cost-effective oil production, the outlet water cut from the well 16/2-D-12 by using these technologies must be evaluated. To reach this purpose, since oil production with a water cut of 85% may still be profitable, the simulations have been conducted for 750 days in order to let the water cut reaches about 85% for the worst scenario (well completion with ICD in the heterogeneous reservoir).

As shown in Figure 7.10, because of the gradual closure of the RCP valves after water breakthrough, the diagrams of the water cut for ICD and RCP cases start to deviate from each other after water breakthrough. After 750 days of production, the difference between the water cut for these cases reaches its maximum. It can be clearly seen that by using RCP valves, oil can be produced with a relatively lower water cut.

The values of outlet water cut for the ICD and RCP cases after 750 days of production obtained from Figure 7.10 are presented in Table 7.5. Based on the table, by completion of the well 16/2-D-12 with ICDs in the homogeneous reservoir, the proportion of the water cut peaks at 84.1 % after 750 days of production. However, by using RCP valves the water cut can be reduced to 81.2 %. As a result, oil production from the well 16/2-D-12 can be more cost-effective if this well is completed with RCP valves.

Table 7.5: Outlet water cut from the well 16/2-D-12 in the homogeneous reservoir after 750 days.

| Item | Outlet water cut |
|---|---|
| **Well with ICD completion** | 84.1% |
| **Well with RCP completion** | 81.2% |
| **Change (RCP to ICD)** | - 2.9% |

## 7.4 Comparing the functionality of the ICDs and RCP valves in the heterogeneous reservoir

In this subchapter, based on the simulation results for oil production from the well 16/2-D-12 by considering ICD and RCP completion in the heterogeneous reservoir for 750 days, the functionality of ICDs and RCP valves in enhancing oil recovery in the heterogeneous reservoir is investigated.

### 7.4.1 Accumulated oil and water production

The accumulated oil and water produced from the well 16/2-D-12 by considering ICD and RCP completion in the heterogeneous reservoir are shown in Figure 7.11. It can be clearly seen from the figure that there is a negligible deviation between the diagrams of accumulated oil in the ICD and RCP cases. However, since the RCP valve is able to autonomously choke the water back, the diagram of accumulated water in the RCP case considerably falls below that of the ICD case after the water breakthrough.

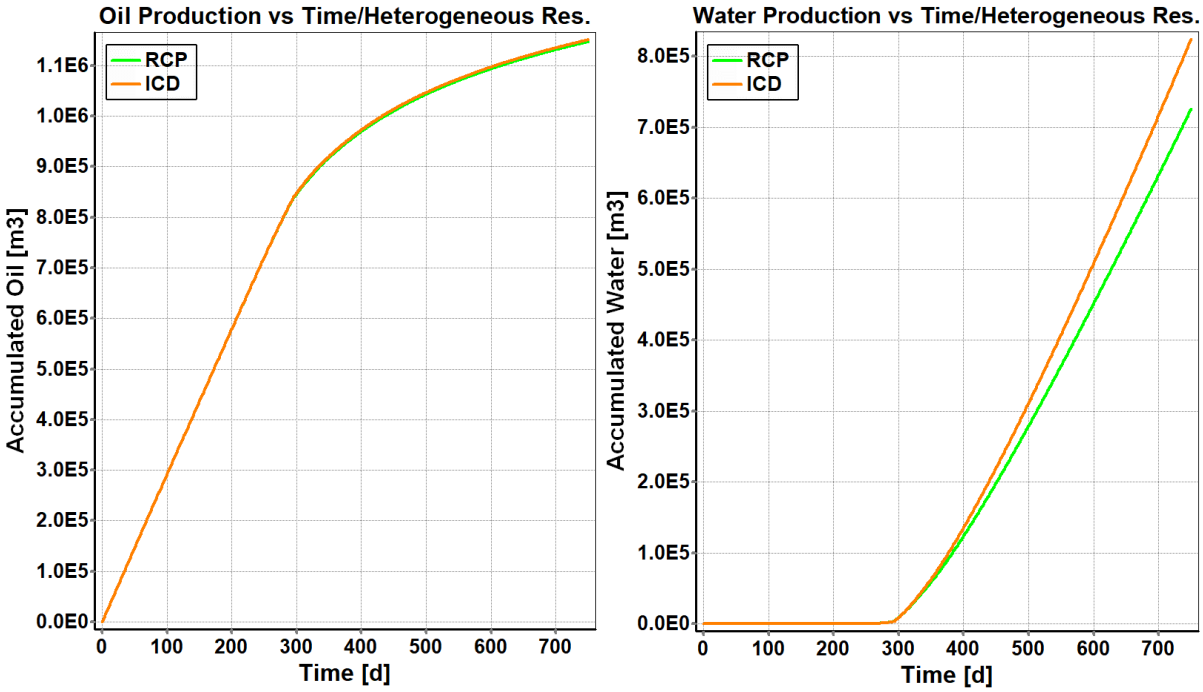


Figure 7.11: Accumulated oil and water from the well 16/2-D.12 with ICD and RCP completion in the heterogeneous reservoir.

The data given in Table 7.6 represents the values of accumulated oil and water for the ICD and RCP cases obtained from Figure 7.11. Based on these data, it can be concluded that by completion of the well 16/2-D-12 with the RCP valves in the heterogeneous reservoir, the accumulated water production can be considerably reduced by 11.9 % compared to the well completion with ICDs after 750 days. However, the use of RCPs has a negligible impact on the accumulated oil production. As a result, by considering a heterogenous reservoir near the well 16/2-D-12, using the RCP valves in addition to producing approximately the same amount of oil, can prevent the production of a large volume of unwanted fluids.

Table 7.6: Values of accumulated oil and water in the heterogeneous reservoir after 750 days.

| Item | Accumulated oil | Accumulated water |
|---|---|---|
| **Well with ICD completion** | 1151085 $m^3$ | 824324 $m^3$ |
| **Well with RCP completion** | 1147105 $m^3$ | 725989 $m^3$ |
| **% of change (RCP to ICD)** | - 0.3% | - 11.9% |

### 7.4.2 Oil and water flow rate

The volumetric flow rate of oil and water production from the well 16/2-D-12 with ICD and RCP completion in the heterogeneous reservoir for a period of 750 days are shown in Figure 7.12.

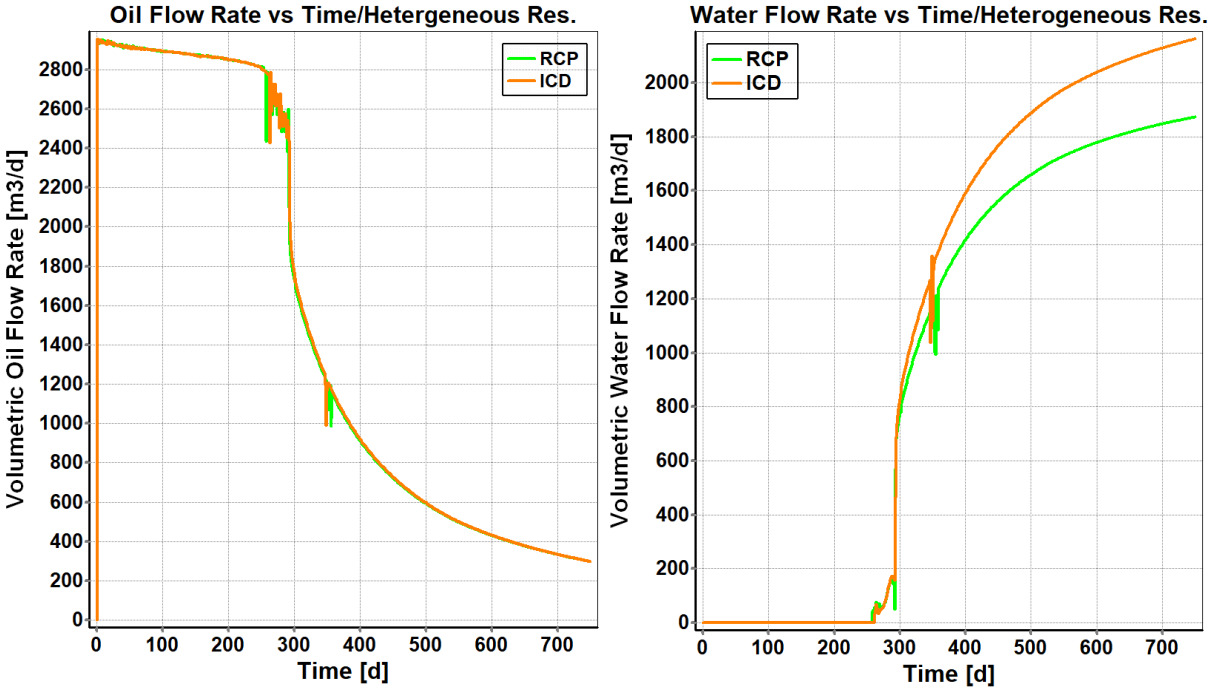


Figure 7.12: Flow rate of oil and water for the well 16/2-D-12 with ICD and RCP completion in the heterogeneous reservoir.

As shown in the figure, just after starting the production, the oil flow rate in the RCP and ICD cases reaches its peak. By increasing the water saturation around the wellbore in the subsequent days, the rate of oil production experiences a slight decrease until the time of water breakthrough. At the time of water breakthrough, the water saturation near the wellbore exceeds the irreducible water saturation ($S_{wc}$ is considered to be equal to 0.12 in the JSF), and as a result, water enters the well. Once water begins to enter the well, the reservoir tends to produce more water than oil. Consequently, after the water breakthrough, the rate of oil production drops substantially. The oil production can be continued until the oil saturation falls below the residual oil saturation ($S_{or}$ is considered to be 0.05 in the JSF). Therefore, after 750 days some amount of oil is produced.

According to Figure 7.12, over the whole period of production (750 days), oil production in both the ICD and RCP cases is almost similar. As a result, it can be concluded that practically there is no difference between using ICD and RCP with respect to oil flow rate over the first 750 days of production in the heterogeneous reservoir. However, after water breakthrough, due to the capability of the RCP valve for choking the water back, the diagram of the water flow rate in the RCP case, considerably falls below that of the ICD case. Therefore, the well completed by RCP valves can significantly reduce the rate of water production after water breakthrough compared to using ICDs. Table 7.7 contains the obtained values of oil and water flow rate for the simulated cases from Figure 7.12. According to the table, the values of

maximum and minimum oil flow rate for the ICD and RCP cases (with a very small difference in maximum values) are the same. However, there is a noticeable difference between the values of the water flow rate in these cases in such a way that after 750 days of production, the water flow rate in the RCP case is -13.4 % lower compared to that of the ICD case. Therefore, it can be concluded that for the well 16/2-D-12 in the heterogeneous reservoir, the RCP valves have very good functionality in attenuating the water production without affecting the oil production.

Table 7.7: Values of volumetric flow rates of oil and water in the heterogeneous reservoir after 750 days.

| Item | Volumetric oil flow rate | | Volumetric water flow rate |
|---|---|---|---|
| | Maximum | Minimum | |
| **Well with ICD completion** | 2956 $m^3/d$ | 297.5 $m^3/d$ | 2163 $m^3/d$ |
| **Well with RCP completion** | 2957 $m^3/d$ | 297 $m^3/d$ | 1873 $m^3/d$ |
| **% of change (RCP to ICD)** | 0.03% | - 0.2% | - 13.4% |

## 7.4.3 Outlet water cut

Figure 7.13 shows the outlet water cut from the well 16/2-D-12 with the completion of ICD and RCP valves by considering the heterogeneous reservoir near this well. In addition to that, the variations of the water cut along the production tubing after 750 days of production are illustrated in the figure.

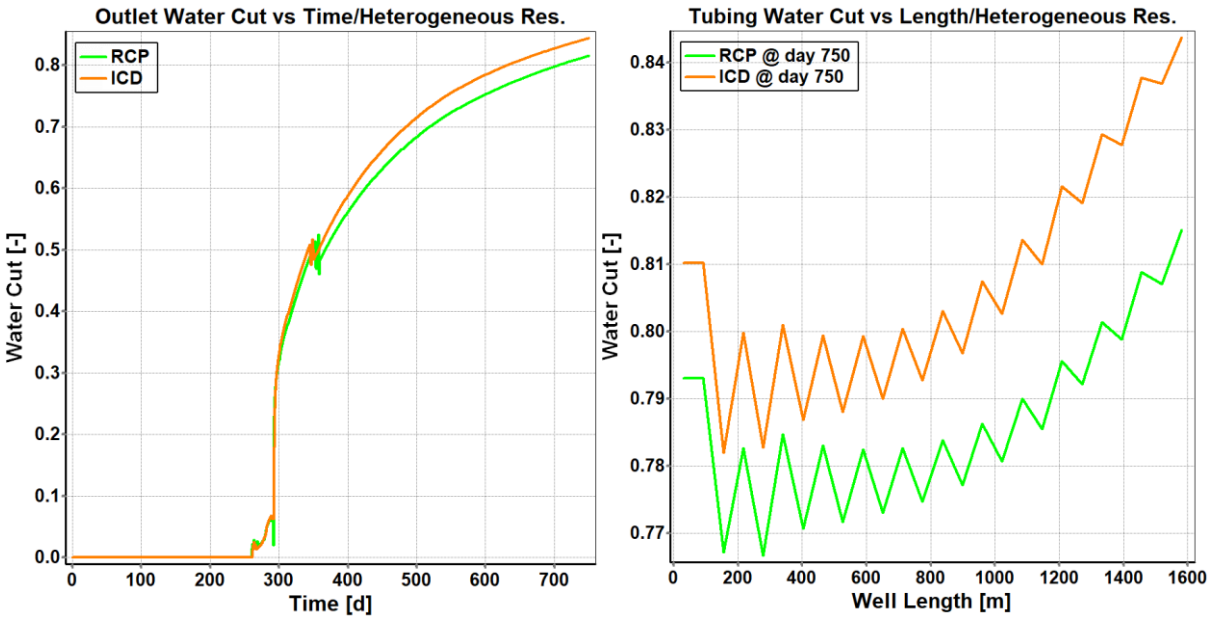


Figure 7.13: Outlet water cut as well as the water cut along the production tubing after 750 days for the well 16/2-D-12 in the heterogeneous reservoir.

Owing to the gradual closure of the RCP valves after water breakthrough, the plots of the water cut for the ICD and RCP cases start to deviate from each other. After 750 days of production, the difference between the water cut for these cases reaches its maximum. Based on the figure, it can be concluded that by using RCP valves, less water is produced per barrel of oil production from the well in the heterogeneous reservoir.

Table 7.8 contains the simulation results for the outlet water cut in the ICD and RCP cases after 750 days of production obtained from Figure 7.13. According to the given values in the table, after 750 days of production from the well 16/2-D-12 with ICD completion in the heterogeneous reservoir, the proportion of the water cut is 84.4%. However, the outlet water cut can be dropped to 81.5 % by using RCP valves. It means that by the completion of the well 16/2-D-12 with the RCP valve, less water is produced per barrel of oil resulting in increasing the efficiency and decreasing the cost of oil production from this well.

Table 7.8: Outlet water cut from the well 16/2-D-12 in the heterogeneous reservoir after 750 days.

| Item | Outlet water cut |
|---|---|
| **Well with ICD completion** | 84.4 % |
| **Well with RCP completion** | 81.5 % |
| **Change (RCP to ICD)** | - 2.9 % |

## 7.5 Discussion

Under the following subchapters, the key findings obtained from the simulation results are discussed.

### 7.5.1 Effect of the grid resolution on the simulation results

The sensitivity of the simulation results to the grid resolution for a simplified OLGA/ROCX model based on the characteristics of the JSF is analyzed in subchapter 6.1.2. For conducting the grid sensitivity analysis, the length of the horizontal well is considered to be in the *x*-direction. According to this analysis, the simulation results are noticeably sensitive to decrease the number of grids in the *z*-direction (depth of the near-well reservoir). However, the results do not have a considerable sensitivity to decrease the number of grids in the *y*-direction (width of the reservoir). The reason for that is the existence of the pressure boundary condition at the bottom of the near-well reservoir resulting in an upward fluid flow in the *z*-direction. Therefore, it can be argued that for developing an OLGA/ROCX model of oil production with water drive, the mesh resolution in the *z*-direction (depth direction) is more important than that of the *y*-direction (width direction). As a result, to achieve an optimum grid setup, in addition to using non-uniform mesh (finer mesh near the wellbore and coarser mesh far from the wellbore), finer mesh in the *z*-direction compared to *y*-direction must be used in the grid setup.

### 7.5.2 Effect of the width of the drainage area on the simulation results

The effect of the width of the near-well reservoir is investigated in subchapter 6.1.1. According to that, by increasing the width of the near-well reservoir, the time of water breakthrough, and the accumulated oil production increases. However, the results have a converging pattern with respect to increasing the near-well reservoir width. Therefore, in order to achieve a true picture of oil production from a well, determining the optimum width of the drainage area near the well is highly important.

### 7.5.3 Impact of heel-toe effect on oil production

As shown by the simulation results presented in subchapter 7.1, water begins to enter the well from the heel side of the well. Due to the frictional pressure drop along the horizontal well, the maximum pressure drawdown exists at the heel side of the horizontal well. Higher pressure drawdown leads to faster growth of the water cone towards the well. Consequently, water breakthrough to the well initially occurs from the heel side of the well. As the simulation results show, early water breakthrough due to the heel-toe effect leads to a significant drop in oil production, and to achieve cost-effective oil production, water breakthrough must be delayed. According to the obtained results, both ICDs and RCPs can effectively even out the flow influx along the horizontal well and consequently delay the water breakthrough significantly. Since RCP valves remain fully open before the water breakthrough, they act exactly the same as ICDs before the breakthrough time. Therefore, there is no difference between the functionality of these types of inflow control devices in delaying the time of water breakthrough.

### 7.5.4 Impact of heterogeneity on oil production

According to the simulation results presented in subchapter 7.1, the water breakthrough in the heterogeneous reservoir takes place faster compared to the homogeneous reservoir due to the existence of some high permeable zones in the heterogeneous reservoir. Besides, due to lower flow resistance in the high permeable zones, the water cone grows faster in these zones. Consequently, the early water breakthrough starts from the high permeable zones in the heterogeneous reservoir. Based on the simulation results, both ICDs and RCP valves through restricting the flow by adding extra pressure drop, are able to significantly delay the early water breakthrough in the heterogeneous reservoir. Moreover, comparing the simulation results for the performance of the inflow control devices in the homogeneous and heterogeneous reservoirs shows that the use of these inflow control devices in the heterogeneous reservoir is more effective.

### 7.5.5 Performance of the implemented RCP valve in OLGA

Since there is no option in OLGA for implementation of the autonomous behavior of the RCP valves directly, the performance of these valves must be implemented in OLGA by using other methods. In the previous works, this has been done by using a PID controller. However, since a PID controller acts based on a specific setpoint, it can not appropriately implement the partial closure of the RCP valve over the range of water cut variations. Besides, the PID controller must be appropriately tuned and this is challenging. Wrong tuning of the PID controller may cause a slow response or too many fluctuations, resulting in some errors in the final results.

Therefore, in this thesis by using a new method based on developing a mathematical model and a control function for the RCP valves, the autonomous behavior of these valves was implemented in OLGA. According to the simulation results presented in subchapter 7.2, the new method of implementing the RCP valves in OLGA works very well and can appropriately simulate the autonomous behavior of the RCP valves in choking the water back over the range of water cut variations.

### 7.5.6 Accuracy of the calculated pressure drawdown used in developing the OLGA/ROCX model

In order to develop a model of oil production in OLGA/ROCX, it is necessary to know the value of the pressure drawdown. In this study, the pressure drawdown for the well 16/2-D-12 was calculated in subchapter 5.9 based on the estimation of oil production from this well. According to the simulation results given in Table 7.3 and Table 7.6, the value of oil production from the well 16/2-D-12 obtained from the simulations has a very good consistency with the initial estimated oil production from this well. Therefore, it can be argued that the calculated pressure drawdown used for developing the OLGA/ROCX model for this well was close to the target.

### 7.5.7 Functionality of ICDs and RCPs in enhancing oil recovery from the well 16/2-D-12

ICD valves are used for delaying early water breakthrough by adding extra pressure drop and thereby even out the flow influx along a horizontal well. The pressure drop across an ICD is a function of flow rate, the geometry of ICD, and the fluid density, but it does not depend on the fluid viscosity. One of the main drawbacks of passive ICDs is that they are not able to choke the water back after breakthrough. Since passive ICDs have no ability to choke the water back after breakthrough, RCP valves have been developed as a robust alternative. RCPs have a moveable disk and they can be partially closed for low viscous fluids like water and gas. As a result, in addition to delaying the water or gas breakthrough, RCPs can autonomously reduce the production of water or gas after breakthrough. Since the RCP valve opening is sensitive to the fluid viscosity, these valves have a better capability for chocking the unwanted fluids when there is a considerable difference between the viscosity of oil and the unwanted fluids. Therefore, practically, RCP valves have a better performance when they are used for chocking gas in a reservoir with light oil or chocking water in a reservoir with heavy oil. In the JSF, the viscosity of oil is 3 cP and since there is not a big difference between the oil and water (0.45 cP) viscosity in this field, the maximum potential of the RCP technology for improving the oil recovery cannot be achieved. However, using RCP valves for the JSF condition can be highly beneficial.

According to the simulation results, for both homogeneous and heterogeneous reservoirs, by completion of the well 16/2-D-12 with RCP valves, the water production considerably decreases compared to using ICDs. Moreover, using RCP valves has a negligible impact on oil production from this well compared to using ICDs, for the first 750 days of production. Therefore, by the completion of this well with RCP valves more cost-effective oil production can be achieved.

# 8 Conclusion

This master's thesis has been conducted for developing a simulation model for cost-effective and safe oil production from existing and near-future oil fields by a special focus on the Johan Sverdrup oil field.

To achieve the main objectives of the thesis, there were two main challenges. One of these challenges was the lack of information in the literature about the characteristics of the Johan Sverdrup field and the pressure drawdown for the production wells in this field. The other one was the difficulties related to the implementation of the autonomous behavior of the RCP valves in OLGA.

Based on the literature study carried out for the evaluation of the technical potential of different EOR methods for 27 fields on the Norwegian continental shelf, it can be concluded that low salinity/polymer flooding, as well as miscible WAG injection with CO2 or hydrocarbon gas, have the highest technical potential for enhancing oil recovery in these fields. Moreover, it can be concluded that the implementation of offshore EOR projects has a huge capital cost but compared to conventional methods, extra oil recovery can be yielded later on. The total capital cost of different EOR methods depends on several factors. However, it can be roughly said that the EOR methods that need $CO_2$ or low salinity water injection have the highest capital cost. Besides, it can be argued that the operational cost of injecting polymers, surfactants, gels, and alkalines is higher compared to the other EOR methods. Therefore, choosing the most cost-effective method of EOR for each oil field requires doing a comprehensive cost estimation by assessing different aspects of technical, financial, and operational conditions.

By investigation of the horizontal well technology, it can be concluded that horizontal wells can delay water or gas breakthrough because of lower pressure drawdown for a given production rate. They also can increase the well productivity due to the greater wellbore length exposed to the pay zone. Moreover, this technology can reduce sand production because of lower pressure drop and fluid velocities around the wellbore. By using horizontal wells, a larger and better drainage pattern can be achieved and as a result, overall reserves recovery will be improved. Another advantage of this technology is reducing the required number of offshore platforms and consequently, minimizing the footprint on the surface. Horizontal wells also help to reach difficult targets under residential areas where conventional drilling is impossible. However, water or gas coning owing to the heel-toe effect and heterogeneity along the horizontal well is the major challenge related to this technology.

Based on the grid sensitivity analysis by considering the length of the horizontal well in the *x*-direction, it can be concluded that the simulation results are noticeably sensitive to decrease the number of grids in the *z*-direction (depth of the near-well reservoir). However, the results do not have a considerable sensitivity to decrease the number of grids in the *y*-direction (width of the reservoir). As a result, to achieve an optimum grid setup, in addition to increasing the mesh resolution near the wellbore, the resolution of mesh in the *z*-direction must be higher compared to the *y*-direction. The width of the near-well reservoir affects the results but the results have a converging pattern with respect to increasing the near-well reservoir width. Therefore, in order to achieve a true picture of oil production from a well, determining the optimum width of the drainage area near the well is highly important.

# 8 Conclusion

The obtained results show that for both the open-hole well and the well with inflow control devices in the homogeneous reservoir, water begins to enter the well from the heel side due to the heel-toe effect. Moreover, due to the faster development of the water cone in the high permeable zones, the early water breakthrough in the heterogeneous reservoir takes place sooner compared to the homogeneous reservoir. Early water breakthrough leads to a significant drop in oil production, and this problem must be tackled to achieve cost-effective oil production. Both ICDs and RCPs can effectively even out the flow influx along the horizontal well and consequently delay the water breakthrough significantly. Since RCPs remain fully open before the water breakthrough occurs, there is no difference between the functionality of ICDs and RCP valves in delaying the time of water breakthrough. In addition, by comparing the simulation results, it can be concluded that the use of these inflow control devices in the heterogeneous reservoir is more effective than in the homogeneous reservoir. Simulation results showed that, by using inflow control devices for the well 16/2-D-12, the time of water breakthrough can be delayed by 253 days in the homogeneous reservoir and 255 days in the heterogeneous reservoir compared to the open-hole well.

There is no option in OLGA for the implementation of the autonomous behavior of RCPs. Due to the performance of the PID controller based on a fixed setpoint and the difficulties in properly tuning them, choosing the PID controllers for the implementation of the behavior of the RCP valves in OLGA leads to some errors. Therefore, in this thesis, a mathematical model and a control function for the RCP valves were developed and implemented in OLGA. The model is based on experimental data and the autonomous behavior of the RCPs. According to the simulation results, it can be argued that the new method of implementing the RCP valves in OLGA works very well and can appropriately simulate the autonomous behavior of the RCP valves in choking the water back over the range of water cut variations.

Since there is a good consistency between the simulation results for the value of oil production and the initial estimated value of oil production from the well 16/2-D-12 (with only about 7.5 % difference), it can be concluded that the calculated value of the pressure drawdown for developing the OLGA/ROCX model has been closed to target.

ICDs are used for delaying early water breakthrough, but since passive ICDs have no ability to choke the water back after breakthrough, RCP valves which can partially be closed for low viscous fluids have been developed. As a result, in addition to delaying the water or gas breakthrough, RCPs can autonomously reduce the production of water or gas after breakthrough. Since the RCP valve opening is sensitive to the fluid viscosity, these valves have a better capability for chocking the unwanted fluids when there is a considerable difference between the viscosity of the oil and the unwanted fluids. In the JSF, since there is not a significant difference between the oil and water viscosity, the maximum potential of the RCP technology for improving the oil recovery can not be yielded. However, using RCP valves for the JSF condition can significantly reduce water production. According to the simulation results for the homogeneous and heterogeneous reservoirs, by completion of the well 16/2-D-12 with RCP valves, the accumulated water production can be reduced by 12.1% and 11.9% respectively during the first 750 days of production. Besides, using RCP valves can reduce the flow rate of water production by 13.3% in the homogeneous and 13.4% in the heterogeneous reservoir after 750 days. In addition to that, for both homogeneous and heterogeneous reservoirs the outlet water cut can be reduced by 2.9% resulting in more cost-effective oil production from this well by using RCP valves. Furthermore, by evaluating the simulation results it can be concluded that using RCP valves has a negligible impact on both the

accumulated oil production and flow rate of oil production from this well compared to using ICDs. Therefore, by the completion of the well 16/2-D-12 with RCP valves more cost-effective oil production can be achieved.

In this study, the functionality of the RCP valves compared to the ICDs in the homogeneous and heterogeneous reservoirs was evaluated. For future works, the functionality of the RCP valves based on the new method of implementation can also be tested in the fractured reservoir. The performance of the RCP valves based on this new method of implementation can also be investigated for a reservoir with heavy oil in future studies. It is suggested that in order to validate the accuracy of the developed method of implementation of the RCP valves in OLGA, the same simulations also be carried out by using NETool, which has a special option for implementing RCP valves.

# References


[1] T. E. L. Council. (2015). *Petroleum History*. Available: https://enviroliteracy.org/energy/fossil-fuels/petroleum-history/

[2] D. GL. (2019). *Energy Transition Outlook 2019*. Available: https://eto.dnvgl.com/2019

[3] N. D. Petroleum. (14.06.2017). *Enhanced oil recovery (EOR) methods*. Available: https://www.npd.no/contentassets/516ed5b967e9454791c23b0412fad58f/technical-potential.pdf

[4] H. Aakre, "The impact of autonomous inflow control valve on increased oil production and recovery," University College of Southeast Norway, Faculty of Technology, Natural Sciences and Maritime Sciences, Kongsberg, 2017.

[5] Equinor. (2020). *Johan Sverdrup field*. Available: https://www.equinor.com/en/what-we-do/johan-sverdrup.html

[6] Wikipedia. (27.04.2020). *Extraction of petroleum*. Available: https://en.wikipedia.org/wiki/Extraction_of_petroleum#Primary_recovery

[7] Wikipedia. (12.01.2020). *Enhanced oil recovery*. Available: https://en.wikipedia.org/wiki/Enhanced_oil_recovery

[8] E. C. Donaldson, G. V. Chilingarian, and T. F. Yen, *Enhanced oil recovery, II: Processes and operations*. Elsevier, 1989.

[9] N. P. Directorate. (14.04.2017). *A brief description of EOR methods*.

[10] S. Afzali, N. Rezaei, and S. J. F. Zendehboudi, "A comprehensive review on enhanced oil recovery by water alternating gas (WAG) injection," vol. 227, pp. 218-246, 2018.

[11] A. Katende and F. J. J. o. M. L. Sagala, "A critical review of low salinity water flooding: mechanism, laboratory and field application," vol. 278, pp. 627-649, 2019.

[12] A. Samanta, K. Ojha, A. Sarkar, A. J. A. i. P. E. Mandal, and Development, "Surfactant and surfactant-polymer flooding for enhanced oil recovery," vol. 2, no. 1, pp. 13-18, 2011.

[13] L. Yu, Q. Sang, M. J. O. Dong, G. Science, and T. R. d. I. E. nouvelles, "Enhanced oil recovery ability of branched preformed particle gel in heterogeneous reservoirs," vol. 73, p. 65, 2018.

[14] J. J. Sheng, *Modern chemical enhanced oil recovery: theory and practice*. Gulf Professional Publishing, 2010.

[15] A. Satter and G. M. Iqbal, *Reservoir engineering: the fundamentals, simulation, and management of conventional and unconventional recoveries*. Gulf Professional Publishing, 2015.

[16] E. Education. (29.08.2017). *Horizontal well*. Available: https://energyeducation.ca/encyclopedia/Horizontal_well

[17] PetroWiki. (15.01.2018). *Horizontal wells*. Available: https://petrowiki.org/Horizontal_wells

[18] F. Jahn, M. Cook, and M. J. D. i. P. S. Grahm, "Drilling Engineering," vol. 55, pp. 47-81, 2008.

[19] T. H. Ahmed, *Gas and Water Coning*, 4th ed. ed. Amsterdam ;, 2010, pp. 583-649.

[20] Salamander. (2020). *BoostWell™ - Viscosity Improvement*. Available: https://www.salamandersolutions.com/applications/boostwell-viscosity-improvement

[21] L.-B. Ouyang, "Practical consideration of an inflow-control device application for reducing water production," in *SPE Annual Technical Conference and Exhibition*, 2009: Society of Petroleum Engineers.

[22] O. Chammout, B. Ghosh, M. Y. J. J. o. P. Alklih, and G. Engineering, "Downhole flow controllers in mitigating challenges of long reach horizontal wells: A practical outlook with case studies," no. 8, pp. 97-110, 2017.

[23] V. Mathiesen, B. Werswick, H. Aakre, and G. Elseth, "Autonomous Valve, A Game Changer Of Inflow Control In Horizontal Wells," in *Offshore Europe*, 2011: Society of Petroleum Engineers.

[24] S. M. Askvik and I. L. J. Sørheim, "Dynamic Autonomous Inflow Control Device-Performance prediction and experimental investigation of a specific rate controlled production valve design," NTNU, 2017.

[25] M. Halvorsen, G. Elseth, and O. M. Nævdal, "Increased oil production at Troll by autonomous inflow control with RCP valves," in *SPE Annual Technical Conference and Exhibition*, 2012: Society of Petroleum Engineers.

[26] SINTEF. (2011). *Carbon Capture and Storage*. Available: https://www.sintef.no/globalassets/project/oilandgas/pdf/co2transportcapabilitiesstatement.pdf

[27] Halliburton. (2020). *NETool Softare*. Available: https://www.landmark.solutions/NETool

[28] Schlumberger. (2020). *OLGA ROCX*. Available: https://www.software.slb.com/products/olga/olga-wells-management/rocx

[29] A. Malagalage, "Near well simulation and modelling of oil production from heavy oil reservoirs," Høgskolen i Telemark, 2015.

[30] R. Aryal, "Near well simulation of oil production from heavy oil reservoirs," Høgskolen i Telemark, 2015.

[31] M. P. Ediriweera, "Near well simulation of heavy oil reservoir with water drive," Høgskolen i Telemark, 2015.

[32] R. Timsina, "Near-well simulations and modelling of oil production from reservoir," Høgskolen i Sørøst-Norge, 2017.

[33] L. S. Raastad, "Near well simulation of oil production from conventional heterogeneous oil," Høgskolen i Telemark, 2015.

[34] Wikipedia. (16.04.2020). *Petroleum reservoir*. Available: https://en.wikipedia.org/wiki/Petroleum_reservoir

[35] A. Y. Dandekar, *Petroleum reservoir rock and fluid properties*. CRC press, 2013.

[36] C. Ayan *et al.*, "Measuring permeability anisotropy: the latest approach," vol. 6, no. 4, pp. 24-35, 1994.

[37] S. A. J. E. J. o. P. Shedid, "Vertical-horizontal permeability correlations using coring data," vol. 28, no. 1, pp. 97-101, 2019.

[38] K. Moncada *et al.*, "Determination of vertical and horizontal permeabilities for vertical oil and gas wells with partial completion and partial penetration using pressure and pressure derivative plots without type-curve matching," vol. 3, no. 1, pp. 77-94, 2005.

[39] T. Yildiz and E. Ozkan, "Influence of Areal Anisotropy on Horizontal Well Performance," in *SPE Annual Technical Conference and Exhibition*, 1997: Society of Petroleum Engineers.

[40] P. C. Iheanacho, D. Tiab, and A. O. Igbokoyi, "Vertical-Horizontal permeability relationships for sandstone reservoirs," in *Nigeria annual international conference and exhibition*, 2012: Society of Petroleum Engineers.

[41] F. Associates. (2014). *Relative Permeability*. Available: http://www.fekete.com/SAN/WebHelp/FeketeHarmony/Harmony_WebHelp/Content/HTML_Files/Reference_Material/General_Concepts/Relative_Permeability.htm

[42] E. P. Geology. (24.11.2014). *Oil and water wet relative permeabilities*. Available: http://www.epgeology.com/gallery/image.php?album_id=12&image_id=269

[43] F. Associates. (2014). *Relative Permeability Correlations*. Available: http://www.fekete.com/SAN/WebHelp/FeketeHarmony/Harmony_WebHelp/Content/HTML_Files/Reference_Material/Calculations_and_Correlations/Relative_Permeability_Correlations.htm

[44] Wikipedia. (13.04.2020). *API gravity*. Available: en.wikipedia.org/wiki/API_gravity

[45] J. Bellarby, *Well completion design*. Elsevier, 2009.

[46] J. J. Velarde, "Correlation of black oil properties at pressures below the bubble-point," Texas A&M University, 1996.

[47] Schlumberger. (2020). *Oilfield Glossary/water cut*. Available: https://www.glossary.oilfield.slb.com/en/Terms/w/water_cut.aspx

[48] Schlumberger. (2020). *Oilfield Glossary/GOR*. Available: glossary.oilfield.slb.com/en/Terms/g/gas-oil-ratio.aspx

[49] Schlumberger. (2020). *Oilfield Glossary/GLR*. Available: https://www.glossary.oilfield.slb.com/en/Terms/g/glr.aspx

[50] Schlumberger. (2020). *Oilfield Glossary/productivity index*. Available: https://www.glossary.oilfield.slb.com/en/Terms/p/productivity_index_pi.aspx

[51] ScienceDirect. (2020). *Formation Volume Factor*. Available: https://www.sciencedirect.com/topics/engineering/formation-volume-factor

[52] PetroWiki. (12.06.2015). *Estimating horizontal well productivity*. Available: https://petrowiki.org/Estimating_horizontal_well_productivity

[53] Wikipedia. (27.04.2020). *Darcy friction factor formulae*. Available: https://en.wikipedia.org/wiki/Darcy_friction_factor_formulae

[54] M. J. Economides, A. D. Hill, C. Ehlig-Economides, and D. Zhu, *Petroleum production systems*. Pearson Education, 2013.

[55] M. Mgimba, "Numerical Study on Autonomous Inflow Control Devices: Their Performance and Effects on the Production from Horizontal Oil Wells with an Underlying Aquifer," NTNU, 2018.

[56] T. E. ToolBox. (2004). *Orifice, Nozzle and Venturi Flow Rate Meters*. Available: file:///C:/Users/alimo/OneDrive/Skrivebord/Orifice/Orifice,%20Nozzle%20and%20Venturi%20Flow%20Rate%20Meters.html

[57] M. Halvorsen, M. Madsen, M. Vikøren Mo, I. Isma Mohd, and A. Green, "Enhanced oil recovery on troll field by implementing autonomous inflow control device," in *SPE Bergen One Day Seminar*, 2016: Society of Petroleum Engineers.

[58] B. A. Voll, I. M. Ismail, and I. Oguche, "Sustaining Production by Limiting Water Cut and Gas Break Through With Autonomous Inflow Control Technology," in *SPE Russian Oil and Gas Exploration & Production Technical Conference and Exhibition*, 2014: Society of Petroleum Engineers.

[59] I. L. J. Sørheim, S. M. Askvik, and H. A. Asheim, "Performance Prediction for Dynamic Autonomous Flow Control Valves," in *SPE Europec featured at 80th EAGE Conference and Exhibition*, 2018: Society of Petroleum Engineers.

[60] Wikipedia. (25.04.2020). *Linear regression*. Available: https://en.wikipedia.org/wiki/Linear_regression

[61] N. Petroleum. (2020). *Johan Sverdrup*. Available: https://www.norskpetroleum.no/en/facts/field/johan-sverdrup/

[62] Wikipedia. (08.04.2020). *Johan Sverdrup oil field*. Available: https://en.wikipedia.org/wiki/Johan_Sverdrup_oil_field

[63] Equinor. (30.03.2020). *Expecting faster ramp-up to higher plateau production on Johan Sverdrup*. Available: https://www.equinor.com/en/news/2020-03-30-johan-sverdrup-plateau-production.html

[64] N. P. Directorate. (2020). *Fact pages/Johan Sverdrup*. Available: https://factpages.npd.no/en/field/pageview/all/26376286

[65] Equinor. (2020). *Crude oil assays*. Available: https://www.equinor.com/no/what-we-do/crude-oil-and-condensate-assays.html

[66] H.-M. Kaspersen, "Reservoir Characterization of Jurassic Sandstones of the Johan Sverdrup Field, Central North Sea," 2016.

[67] F. Wesenlund and D. Karlsen, "The petroleum geochemistry of the Johan Sverdrup field, Southern Utsira High, Norwegian North Sea," MSc thesis, University of Oslo, Oslo, Norway, 2016.

[68] H. Olsen, N. A. Briedis, D. J. M. Renshaw, and P. Geology, "Sedimentological analysis and reservoir characterization of a multi-darcy, billion barrel oil field–The Upper Jurassic shallow marine sandstones of the Johan Sverdrup field, North Sea, Norway," vol. 84, pp. 102-134, 2017.

[69] W. Fang, "Evaluation of low salinity injection EOR potential in Johan Sverdrup Field," University of Stavanger, Norway, 2017.

[70] M. Tangen, "Wettability Variations within the North Sea Oil Field Frøy," Institutt for petroleumsteknologi og anvendt geofysikk, 2012.

[71] N. Hadia, H. H. Lehne, K. G. Kumar, K. A. Selboe, F. Å. Stensen, and O. Torsater, "Laboratory Investigation of Low Salinity Waterflooding on Reservoir Rock Samples from the Fr? y Field," in *SPE Middle East Oil and Gas Show and Conference*, 2011: Society of Petroleum Engineers.

[72] Wikipedia. (11.11.2019). *Temperature dependence of viscosity*. Available: https://en.wikipedia.org/wiki/Temperature_dependence_of_viscosity

[73] Schlumberger. (2020). *Oilfield Glosaary/true vertical depth*. Available: https://www.glossary.oilfield.slb.com/en/Terms/t/true_vertical_depth.aspx

[74] EnggCyclopedia. *Absolute roughness of a pipe*. Available: https://www.enggcyclopedia.com/2011/09/absolute-roughness/

[75] Collins. (2020). *pressure drawdown*. Available: https://www.collinsdictionary.com/dictionary/english/pressure-drawdown

[76] PetroWiki. (19.01.2016). *Controlling excess water production*. Available: https://petrowiki.org/Controlling_excess_water_production

[77] Neutrium. (2020). *CV VERSUS ORIFICE SIZE*. Available: https://neutrium.net/fluid_flow/cv-versus-orifice-size/

# Appendices

**Appendix A: Task description**
**Appendix B: General information of the well 16/2-D-12**
**Appendix C: General information of the well 16/2-8**
**Appendix D: Formation pressure data of the well 16/2-8**
**Appendix E: Equinor's crude summary report for the Johan Sverdrup field**
**Appendix F: Physical properties of the core plugs collected from Frøy field**
**Appendix G: MATLAB code for extrapolating the value of crude oil viscosity**
**Appendix H: Calculation procedures**
**Appendix I: List of the production wells in the JSF**
**Appendix J: MATLAB code for calculating the pressure drop**
**Appendix K: Application of GetData Graph Digitizer for extracting data**
**Appendix L: MATLAB code for developing the mathematical model of RCPs**
**Appendix M: MATLAB code for calculating the valve opening and control table**
**Appendix N: MATLAB code for creating values for implementing heterogeneity**
**Appendix O: Reservior model in ROCX**
**Appendix P: Well model in OLGA**

# Appendix A: Task description

University of South-Eastern Norway

Faculty of Technology, Natural Sciences and Maritime Sciences, Campus Porsgrunn

## FMH606 Master's Thesis

**Title**: Cost effective and safe oil production from existing and near-future oil fields

**USN supervisor**: Prof. Britt M. E. Moldestad

**External partner**: -

**Task background**:
The global energy demand has increased over the last decades, and there is an urgent need to promote the use of sustainable alternatives to fossil fuels in order to limit the Earth's global warming. However, the use of fossil fuels cannot stop over the night, but the focus can be on making the oil production more energy and cost effective.

Cost effective and safe oil production from existing and near-future oil fields is of key importance in a transition towards sustainable energy economies. Oil production must maximize the profit to help the funding of needed, new sustainable energy technology, while minimizing the energy footprint.

**Task description**:

1. Literature study
   - New technologies for enhanced and cost effective oil recovery from mature and new oil reservoirs.
   - Long horizontal wells
   - Modelling and simulation of oil production

2. Modelling and simulation of cost effective oil production
   - Different software (available at USN) to concider:
     - OLGA in combination with ROCX
     - Eclipse
     - NETool
3. Use different new technologies for enhanced oil recovery in the simulations. Compare the results regarding cost effective production.

**Student category**: EET and PT students

**Practical arrangements**:
Necessary software will be provided by USN.

**Supervision**:
As a general rule, the student is entitled to 15-20 hours of supervision. This includes necessary time for the supervisor to prepare for supervision meetings (reading material to be discussed, etc).

**Signatures**:

Supervisor (date and signature): 17.05.2020 Britt Moldestad

Student (write clearly in all capitalized letters): ALI MORADI

Student (date and signature): Ali Moradi 17.05.2020

# Appendix B: General information of the well 16/2-D-12

**NPD Factpages**

**Wellbore / Development**

Printed: 3.5.2020 - 23:40

**General information**

| | |
|---|---|
| Wellbore name | 16/2-D-12 |
| Type | DEVELOPMENT |
| Purpose | PRODUCTION |
| Status | PRODUCING |
| Multilateral | NO |
| Factmaps in new window | link |
| Main area | NORTH SEA |
| Field | JOHAN SVERDRUP |
| Discovery | 16/2-6 Johan Sverdrup |
| Well name | 16/2-D-12 |
| Drilled in production licence | 265 |
| Drilling operator | Statoil Petroleum AS |
| Drill permit | 4028-P |
| Drilling facility | DEEPSEA ATLANTIC |
| Production facility | JOHAN SVERDRUP D |
| Drilling days | 21 |
| Entered date | 24.04.2016 |
| Completed date | 05.06.2016 |
| Release date | 05.06.2018 |
| Predrilled entry date | 05.04.2016 |
| Predrilled completion date | 07.04.2016 |
| Purpose - planned | PRODUCTION |
| Content | OIL |
| Discovery wellbore | NO |
| Kelly bushing elevation [m] | 30.0 |
| Water depth [m] | 113.4 |
| Total depth (MD) [m RKB] | 3875.0 |
| Final vertical depth (TVD) [m RKB] | 1876.0 |
| Geodetic datum | ED50 |
| NS degrees | 58° 50' 9.44" N |
| EW degrees | 2° 33' 12.77" E |
| NS UTM [m] | 6522021.74 |
| EW UTM [m] | 474227.20 |
| UTM zone | 31 |
| NPDID wellbore | 7903 |

# Appendix C: General information of the well 16/2-8

**NPD Factpages**
**Wellbore / Exploration**
Printed: 4.5.2020 - 04:55

**General information**

| | |
|---|---|
| Wellbore name | 16/2-8 |
| Type | EXPLORATION |
| Purpose | APPRAISAL |
| Status | P&A |
| Press release | link |
| Factmaps in new window | link |
| Main area | NORTH SEA |
| Field | JOHAN SVERDRUP |
| Discovery | 16/2-6 Johan Sverdrup |
| Well name | 16/2-8 |
| Seismic location | LN0902-inline 2120 & crossline 6672 |
| Drilled in production licence | 265 |
| Drilling operator | Statoil Petroleum AS |
| Drill permit | 1346-L |
| Drilling facility | TRANSOCEAN LEADER |
| Drilling days | 34 |
| Entered date | 17.07.2011 |
| Completed date | 19.08.2011 |
| Release date | 19.08.2013 |
| Publication date | 19.08.2013 |
| Purpose - planned | WILDCAT |
| Reentry | NO |
| Content | OIL |
| Discovery wellbore | NO |
| 1st level with HC, age | LATE JURASSIC |
| 1st level with HC, formation | INTRA DRAUPNE FM SS |
| 2nd level with HC, age | MIDDLE JURASSIC |
| 2nd level with HC, formation | HUGIN FM |
| Kelly bushing elevation [m] | 23.5 |
| Water depth [m] | 112.0 |
| Total depth (MD) [m RKB] | 2140.0 |
| Final vertical depth (TVD) [m RKB] | 2140.0 |
| Maximum inclination [°] | 1 |
| Bottom hole temperature [°C] | 81 |
| Oldest penetrated age | LATE TRIASSIC |
| Oldest penetrated formation | SKAGERRAK FM |
| Geodetic datum | ED50 |
| NS degrees | 58° 48' 57'' N |

OLJEDIREKTORATET

# 16 / 2.8

16.08.2011 Statoil Petroleum AS, operator of production license 265, is finishing drilling of exploration well 16 / 2-8 ("Aldous Major South"). The well is drilled about 4 kilometers west of the oil discovery 16 / 2-6 (Avaldsnes) in the middle part of the North Sea.

The primary exploration goal for the well was to detect petroleum in upper to middle Jurassic reservoir rocks (the Draupne, Hugin and Sleipner formations), and clarify communication to 16 / 2-6 (Avaldsnes). Secondary exploration targets were to detect petroleum in the Upper Triassic (Skagerrak Formation) and in Upper Cretaceous (Shetland Group). An oil column of 65 meters was found in the coarse-grained and unconsolidated sandstone in the Draupne Formation of better reservoir quality than expected. Preliminary calculation of the size of the discovery is between 30 and 65 million Sm $^{3}$ of recoverable oil with potential for additional resources near the discovery. The gas / oil ratio is 44 (Sm $^{3}$ / Sm $^{3}$ ) and the density calculated at 0.82 g / cm $^{3}$. The well was not formation tested, but extensive data collection and sampling has been carried out.

The well data collected provide the same oil / water contact as in the oil discovery 16 / 2-6 (Avaldsnes) and indicate communication between the finds. If appraisal wells in production licenses 265 (Aldous Major South) and 501 (Avaldsnes) confirm the connection between these discoveries, the total resources may be between 80 and 190 million Sm $^{3}$ of recoverable oil.

The well is the fifth exploration well in production license 265 . The permit was granted in the North Sea awards 2000.

16 / 2-8 was drilled to a vertical depth of 2083 meters below sea level, and was completed in the Skagerrak formation in the upper Triassic. The sea depth is 112 meters. The well is now permanently plugged and abandoned.

Well 16 / 2-8 was drilled by the *Transocean Leader* drilling facility which will continue drilling of exploration well 16 / 2-9 S in the same production license.

**Contact person at the Norwegian Petroleum Directorate**
Eldbjørg Vaage Melberg, tel. 51 87 61 00

# Appendix D: Formation pressure data of the well 16/2-8

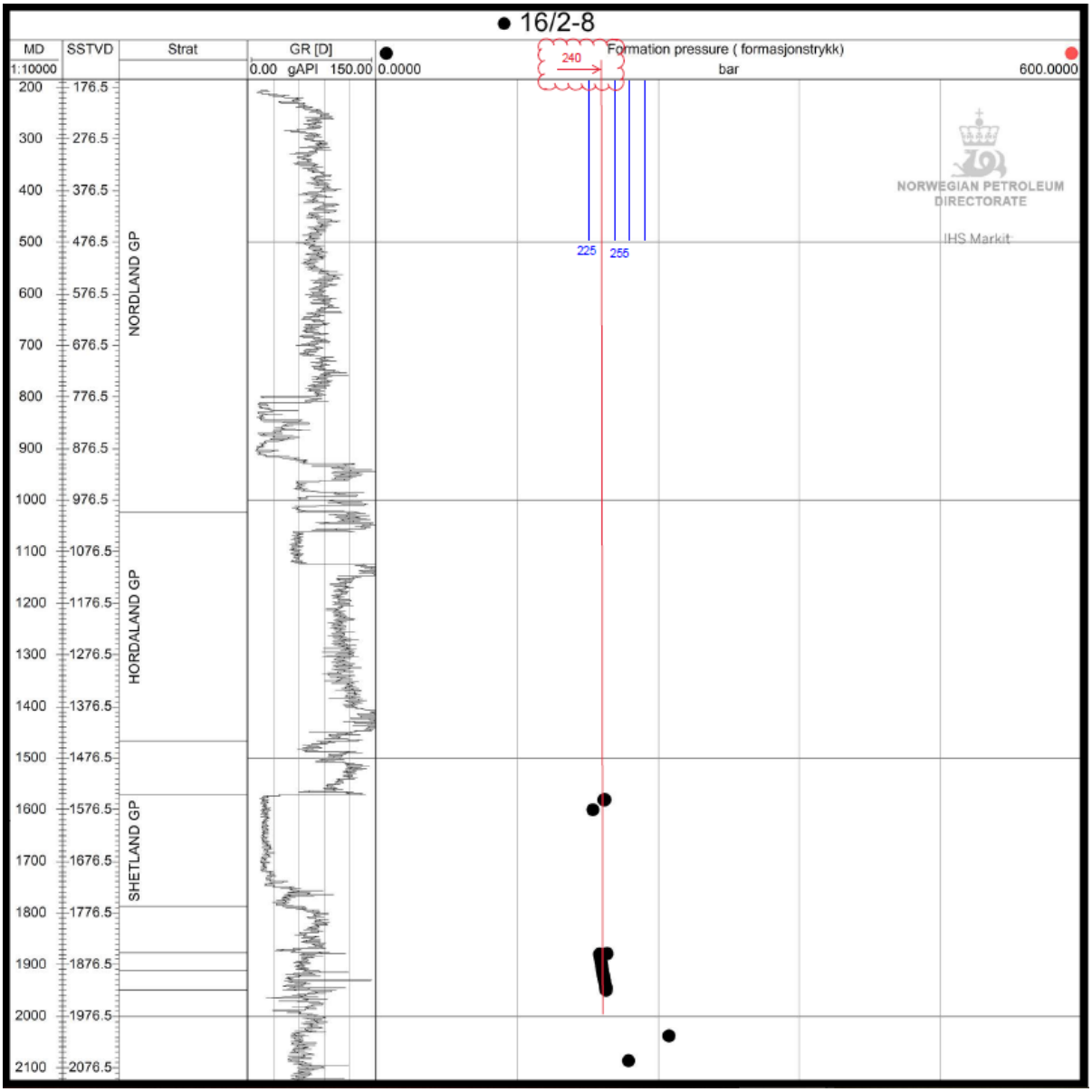


From NPD's fact pages [64].

# Appendix E: Equinor's crude summary report for the Johan Sverdrup field

equinor

Crude: **JOHAN SVERDRUP 2013 05**
Reference: **JOHANSVERDRUP201305**

## Crude Summary Report

| General Information | | Molecules (% wt on crude) | | Whole Crude Properties | |
|---|---|---|---|---|---|
| Name: | JOHAN SVERDRUP 2013 05 | methane + ethane | 0.04 | Density @ 15°C (g/cc) | 0.887 |
| Reference: | JOHANSVERDRUP201305 | propane | 0.37 | API Gravity | 28.0 |
| Traded Crude: | Johan Sverdrup | isobutane | 0.23 | Total Sulphur (% wt) | 0.80 |
| Origin: | Norway | n-butane | 0.68 | Pour Point*, min/max (°C) | <-36/-3 |
| Sample Date: | 11 May 2013 | isopentane | 0.52 | Viscosity @ 20°C (cSt) | 26 |
| Assay Date: | 06 February 2013 | n-pentane | 0.73 | Viscosity @ 40°C (cSt) | 12 |
| Issue Date: | 06 September 2013 | cyclopentane | 0.09 | Nickel (ppm) | 3.7 |
| Comments: | Pre-production assay. Well 16/2-17S DST2 | $C_6$ paraffins | 1.36 | Vanadium (ppm) | 11.9 |
| | | $C_6$ naphthenes | 0.87 | Total Nitrogen (ppm) | 2196 |
| | | benzene | 0.06 | Total Acid Number (mgKOH/ | 0.32 |
| | | $C_7$ paraffins | 1.18 | Mercaptan Sulphur (ppm) | 2 |
| | | $C_7$ naphthenes | 1.38 | Hydrogen Sulphide (ppm) | 0.0 |
| | | toluene | 0.38 | Reid Vapour Pressure (psi) | 5.2 |

| Cut Data | | | Atmospheric Cuts | | | | | | | | | Vacuum Cuts | | | |
|---|---|---|---|---|---|---|---|---|---|---|---|---|---|---|---|
| Start (°C) | IBP | IBP | C5 | 65 | 100 | 150 | 200 | 250 | 300 | 350 | 370 | 370 | 450 | 500 | 550 |
| End (°C) | FBP | C4 | 65 | 100 | 150 | 200 | 250 | 300 | 350 | 370 | FBP | 450 | 500 | 550 | FBP |
| Yield (% wt) | | 1.3 | 2.0 | 3.2 | 5.1 | 6.3 | 8.6 | 9.6 | 9.6 | 3.4 | 51.0 | 12.3 | 8.8 | 7.8 | 22.0 |
| Yield (% vol) | | 2.1 | 2.8 | 3.9 | 5.9 | 6.9 | 9.1 | 9.8 | 9.6 | 3.3 | 46.5 | 11.9 | 8.4 | 7.3 | 19.0 |
| Cumulative Yield (% wt) | | 1.3 | 3.3 | 6.5 | 11.6 | 17.9 | 26.4 | 36.0 | 45.6 | 49.0 | 100.0 | | | | |
| Density @ 15°C (g/cc) | 0.887 | | ### | 0.714 | 0.770 | 0.796 | ### | 0.864 | 0.888 | 0.901 | 0.968 | 0.917 | ### | 0.945 | 1.026 |
| API Gravity | 28.0 | | 88.2 | 66.7 | 52.1 | 46.1 | 33.2 | 32.2 | 27.8 | 25.5 | 14.5 | 22.7 | 20.6 | 18.1 | 6.3 |
| UOPK | 11.8 | | | | 11.6 | 11.7 | 11.6 | 11.5 | 11.5 | 11.6 | 11.8 | 11.7 | 11.9 | 11.9 | 11.7 |
| Total Sulphur (% wt) | 0.80 | | ### | 0.001 | 0.004 | 0.023 | ### | 0.295 | 0.68 | 0.84 | 1.32 | 0.85 | 0.98 | 1.20 | 1.76 |
| Mercaptan Sulphur (ppm) | 2 | | 0.0 | 0.1 | 0.2 | 0.5 | 1.3 | 3.2 | | | | | | | |
| Total Nitrogen (ppm) | 2196 | | | | | | 1 | 13 | 211 | 644 | 4223 | 1179 | 2005 | 3224 | 7167 |
| Basic Nitrogen (ppm) | 573 | | | | | | 1.95 | 12.7 | 87 | 213 | 1091 | 351 | 491 | 790 | 1851 |
| Total Acid Number (mgKOH/ | 0.32 | | 0.00 | 0.00 | 0.00 | 0.02 | 0.04 | 0.09 | 0.30 | 0.47 | 0.47 | 0.50 | 0.54 | 0.59 | 0.39 |
| Viscosity @ 20°C (cSt) | 26.1 | | | | | 1.20 | | | | | | | | | |
| Viscosity @ 40°C (cSt) | 12.0 | | | | | 0.95 | 1.67 | 3.05 | 6.57 | 13.9 | | | | | |
| Viscosity @ 50°C (cSt) | 8.75 | | | | | | 1.44 | 2.48 | 4.98 | 9.86 | 1243 | 30.7 | 74.7 | 222 | |
| Viscosity @ 60°C (cSt) | | | | | | | | | | | 591 | 20.4 | 45.8 | 124 | |
| Viscosity @ 100°C (cSt) | | | | | | | | | | | 68.7 | 6.24 | 11.1 | 23.1 | 8100 |
| Viscosity @ 130°C (cSt) | | | | | | | | | | | | | | | 1085 |
| RON (Clear) | | | 77.9 | 55.9 | 60.7 | 42.1 | | | | | | | | | |
| MON (Clear) | | | 77.2 | 53.9 | 57.8 | 39.7 | | | | | | | | | |
| Paraffins (% wt) | 26.5 | | 95.5 | 59.0 | 39.7 | 41.8 | | | | | | | | | |
| Naphthenes (%wt) | 37.7 | | 4.5 | 39.0 | 37.7 | 35.2 | | | | | | | | | |
| Aromatics (% wt) | 35.8 | | 0.0 | 2.0 | 22.5 | 23.0 | | | | | | | | | |
| Pour Point*, max (°C) | -3 | | | | | | -40 | -25 | -4 | 11 | 32 | 27 | 38 | 46 | 54 |
| Pour Point*, min (°C) | <-36 | | | | | | | | | | | | | | |
| Cloud Point (°C) | | | | | | | -39 | -25 | -4 | | | | | | |
| Freeze Point (°C) | | | | | | -55 | -35 | -22 | | | | | | | |
| Smoke Point (mm) | | | | | | 22 | 19 | 16 | | | | | | | |
| Cetane Index | | | | | | 36 | 41 | 43 | 48 | 52 | | | | | |
| Naphthalenes (% vol) | | | | | | 0.1 | 4.0 | 11.3 | 18.1 | | | | | | |
| Aniline Point (°C) | | | | | 58.3 | 62.1 | 65.8 | 69.8 | 74.4 | 76.7 | | 78.3 | 83.4 | 87.7 | |
| Hydrogen (% wt) | | | 16.5 | 15.3 | 13.8 | 13.8 | 13.3 | 12.9 | 12.7 | 12.6 | | 12.5 | 12.3 | 12.2 | |
| Wax (% wt) | 8.2 | | | | | | | | | | 14.6 | 8.3 | 13.1 | 16.6 | 18.0 |
| $C_7$ Asphaltenes (% wt) | 2.0 | | | | | | | | | | 3.9 | | 0.0 | 0.0 | 9.1 |
| Micro Carbon Residue (% wt | 5.0 | | | | | | | | | | 9.8 | | 0.1 | 1.1 | 22.3 |
| Ramsbottom Carbon Residue (% wt | 4.2 | | | | | | | | | | 8.2 | | 0.1 | 1.0 | 18.5 |
| Vanadium (ppm) | 11.9 | | | | | | | | | | 23.4 | | 0.0 | 0.0 | 54.1 |
| Nickel (ppm) | 3.7 | | | | | | | | | | 7.3 | | 0.0 | 0.0 | 16.8 |

# Appendix F: Physical properties of the core plugs collected from Frøy field

Table 2. Physical properties of the core plugs.

| Core # | Well # | Depth [m] | Length cm | Diameter cm | Porosity % | Permeability mD | $S_{wi}$ % PV | Remarks |
|---|---|---|---|---|---|---|---|---|
| B8894 | 25/5-A-7 | 4487.83 | 8.51 | 3.81 | 22.6 | 4800 | 23.4 | |
| B8895 | 25/5-A-7 | 4487.88 | 8.67 | 3.81 | 22.2 | 4500 | 16.6 | |
| B8896 | 25/5-A-7 | 4487.93 | 7.55 | 3.81 | 21.7 | 3900 | 14.8 | Flooded with 10% and 1% IB only |
| B8897 | 25/5-A-7 | 4511.40 | 4.81 | 3.81 | 25.0 | 2330 | | Used for wettability measurement |
| B8898 | 25/5-A-7 | 4511.45 | 8.46 | 3.81 | 25.4 | 3050 | 30.2 | $S_{wi}$ was established by flooding method |
| B8899 | 25/5-A-7 | 4511.50 | 8.85 | 3.81 | 25.1 | 3070 | 21.6 | $S_{wi}$ was established by flooding method |
| B8931 | 25/5-A-7 | 4516.71 | 7.18 | 3.81 | 25.3 | 940 | 16.7 | |
| B8932 | 25/5-A-7 | 4516.75 | 8.35 | 3.81 | 24.7 | 706 | 17.1 | |
| B8933 | 25/5-A-7 | 4516.79 | 8.73 | 3.81 | 24.2 | 603 | 25.1 | Flooded with 1% IB only |
| B8900 | 25/5-A-1 | 3228.62 | 7.80 | 3.80 | 23.1 | 590 | 36.3 | $S_{wi}$ was established by flooding method |
| B8928 | 25/5-A-1 | 3227.62 | 8.76 | 3.81 | 19.1 | 650 | 26.1 | |
| B8929 | 25/5-A-1 | 3227.67 | 8.59 | 3.81 | 16.1 | 88 | 25.5 | Showed some heterogeneity |
| NS1 | 25/5-A-1 | 3228.92 | 8.16 | 3.81 | 12.1 | 11 | 40.2 | |
| NS2 | 25/5-A-1 | 3186.57 | 7.51 | 3.81 | 18.4 | 28 | 20.3 | |
| NS3 | 25/5-A-1 | 3232.67 | 8.11 | 3.81 | 20.3 | 937 | 46.3 | |

From [71].

# Appendix G: MATLAB code for extrapolating the value of crude oil viscosity

```
clear
clc

T=[293;313;323]; % Temperature in K
Mu=[23.15;10.64;7.76];
Mu_ln=log(Mu); % Logaritm of viscosity

% if Mu=A*exp(B/T) then ln(Mu)= ln(A)+B/T
Phi=[1 1/T(1);1 1/T(2);1 1/T(3)];
Phi_T=Phi';
Theta=inv(Phi_T*Phi)*Phi_T*Mu_ln;

% Theta(1)=ln(A) & Theta(2)=B
T_unknown= 354 % K
Mu_unknown=exp(Theta(1)+Theta(2)/T_unknown) % calculation of the unknown Mu

plot(T,Mu,'r*',T_unknown,Mu_unknown,'green*')
hold on
T_curve=[290:1:360];
Mu_curve=exp(Theta(1)+Theta(2)./T_curve);
plot(T_curve,Mu_curve,'b--')
```

```
T_unknown =

   354


Mu_unknown =

    2.9976
```

# Appendix H: Calculation procedures

## 1) Calculation of the permeability anisotropy near the well 16/2-D-12

Based on subchapter 4.2.3.3 the absolute permeability of the JSF is 14.7 D or $k = 14.7$. Besides, according to subchapter 4.2.3.2, the average effective porosity for the JSF is 0.27, which means that $\varphi_{e,average} = 0.27$. Moreover, by using the given values in Table 4.3, the average shale volume can be calculated as:

$$V_{sh,average} = \frac{h_{zone1} \cdot V_{sh\_zone1} + h_{zone2} \cdot V_{sh\_zone2}}{h_{zone1} + h_{zone2}} = \frac{32.46 \times 0.09 + 22.86 \times 0.122}{32.46 + 22.86} = 0.103 \text{ m}$$

As a result, by using Equation 3.9 it can be written that:

$$k_z = 0.0718 \times \sqrt{\left[\frac{k_H(1-V_{sh})}{\phi_e}\right]^{2.0901}} = 0.0718 \times \sqrt{\left[\frac{k_H(1-0.103)}{0.27}\right]^{2.0901}} = 0.252 \times k_H^{1.045}$$

Based on Equations 3.7, 3.8, and the previous equation for $k_z$, it can be written that:

$$k = \sqrt[3]{k_x k_y k_z} \text{ and } k_H = \sqrt{k_x k_y} \Rightarrow k = \sqrt[3]{k_H^2 k_z} \Rightarrow k = \sqrt[3]{k_H^2 \times 0.252 \times k_H^{1.045}}$$

$$\Rightarrow 14.7^3 = 0.252 \times k_H^{3.045} \Rightarrow k_H = \sqrt[3.045]{\frac{14.7^3}{0.252}} = 22.2 \text{ D}$$

$$\Rightarrow k_v = k_z = 0.252 \times 22.2^{1.045} = 6.4 \text{ D}$$

$$\text{If } k_x = k_y \Rightarrow k_H = \sqrt{k_x k_y} = \sqrt{k_x^2} \Rightarrow k_x = k_y = 22.2 \text{ D}$$

Therefore, the permeability anisotropy, *a*, can be calculated as:

$$a = \frac{k_v}{k_H} = \frac{6.4}{22.2} \approx 0.3$$

## 2) Calculation of the length of the horizontal section in the well 16/2-D-12

As it is mentioned in the subchapter 4.1, the measured depth of the well 16/2-D-12 is 3875 m and it has the final vertical depth of 1876 m.

There is no information about the exact geometry of the well 16/2-D-12 in the literature. Therefore, based on the classification of horizontal wells represented in Figure 2.6, in subchapter 2.2.1, it is assumed that the well 16/2-D-12 is a medium radius horizontal well with the maximum radius in the kickoff section which means $R_{kickoff} = 1000 \text{ ft} = 304.8 \text{ m}$. As a result, the length of the horizontal section of this well, $L_{horizontal}$, can be calculated as:

$$L_{MD} = L_{TVD} + L_{kickoff} + L_{horizontal}$$

$$L_{kickoff} = R_{kickoff} \times \frac{4}{\pi} = 304.8 \times \frac{4}{\pi} = 388 \text{ m}$$

$$\Rightarrow L_{horizontal} = 3875 - 1876 - 388 = 1611 \text{ m} \approx 1612^{*} \text{ m}$$

* For the modeling and simulation, if it is assumed that the horizontal section of the well consists of 13 joints, each 124 m long, the length of the horizontal section of the well can be considered: $L_{horizontal} = 13 \times 124 = 1612 \text{ m}$.

## 3) Calculation of the productivity index for the well 16/2-D-12

Based on the reservoir rock and fluid properties, and comparing the Odeh's model parameters shown in Figure 3.10 with the geometry of the reservoir considered for developing the model in this thesis shown in Figure 6.2, the Odeh's model is used by considering the following values:

$$a = 120 \text{ m} = 394 \text{ ft}, \; b = L_w = 1612 \text{ m} = 5287 \text{ ft}$$

$$h = 55.5 \text{ m} = 182 \text{ ft}$$

$$d_x = 60 \text{ m} = 197 \text{ ft}, \; d_y = 0, \; d_z = 5.5 \text{ m} = 20 \text{ ft}, \; r_w = 0.108 \text{ m} = 0.354 \text{ ft}$$

$$k_x = k_y = 22200 \text{ mD}, \; k_z = 6400 \text{ mD}$$

$$B = \frac{V_{res.}}{V_{st}} \approx \frac{0.887}{0.82} = 1.08$$

$$\mu = 3 \text{ cP}$$

To check the conditions of Equation 3.30, it can be written:

$$\frac{b}{\sqrt{k_y}} = \frac{5278}{\sqrt{22200}} = 35.5 > \frac{1.33a}{\sqrt{k_x}} = \frac{1.33 \times 394}{\sqrt{22200}} = 3.5 \gg \frac{0.75h}{\sqrt{k_z}} = \frac{0.75 \times 182}{\sqrt{6400}} = 1.7$$

As a result, Equations 3.31 and 3.35 are valid and can be used. Based on the geometry of the reservoir and using Equations 3.323.33 and 3.34, it can be concluded:

$$b = L_w \Rightarrow P_{xyz} = P_{xy} = 0$$

$$d_y = 0 \Rightarrow y_m = \frac{L_w}{2} \Rightarrow P_x = 0$$

Therefore, based on Equation 3.31:

$$S_r = P_{xyz} + P_y + P_{xy} = 0$$

Moreover, by considering Equation 3.35 it can be written:

$$\ln C_H = \frac{6.28 \times 394}{182}\sqrt{\frac{6400}{22200}}\left(\frac{1}{3} - \frac{197}{394} + \frac{197^2}{394^2}\right) - \ln\left(\sin\frac{\pi \times 20}{182}\right) - 0.5\ln\left[(394/182)\sqrt{\frac{6400}{22200}}\right] - 1.088$$

$$\Rightarrow \ln C_H = 0.529 \Rightarrow C_H = e^{0.529} = 1.696$$

Using the value of $C_H$ and $S_r$ and Equation 3.29, the productivity index for the well 16/2-D-12 considered for simulation can be calculated as:

$$J = \frac{7.08 \times 10^{-3} \times 5287 \times \sqrt{22200 \times 6400}}{1.08 \times 3 \times (\ln(1.696\sqrt{394 \times 182}/0.354) - 0.75 + 0} = 19885 \text{ stb/d/psi} = 46133 \text{ m}^3\text{/d/bar}$$

## 4) Calculation of the average pressure drop across the TR7 RCP valve and the number of them for the well 16/2-D-12

In subchapter 5.3.2 the production of the well 16/2-D-12 is estimated to be 20000 bbl/d =3200 $m^3$/day. The length of the well is 1612 m and it is considered that it consists of 130 joints, each 12.4 m long. Two TR7 RCP valves are considered to be installed on each joint, As a result:

$$N_{RCP} = 130 \times 2 = 260$$

where $N_{RCP}$ is the required number of the TR7 RCP valve for the well 16/2-D-12. Therefore, the estimated flow rate of oil passing through an RCP valve, $\dot{Q}_{RCP,estimation}$ , for this well can be calculated as:

$$\dot{Q}_{RCP,estimation} = \frac{\dot{Q}_{oil,estimation}}{N_{RCP}} = \left(\frac{3200\text{m}^3\text{/d}}{260}\right)/24\text{h} = 0.513 \text{ m}^3\text{/h}$$

In order to estimate the pressure drop across a TR7 RCP valve, $\Delta P_{RCP,estimation}$, in the well 16/2-D-12 based on the estimated flow rate passing through it, the mathematical model for TR7 RCP valve, presented by Equation 5.13 can be used as:

$$\rho_{mix} = \rho_{oil} = 820 \text{ kg/m}^3, \mu_{mix} = \mu_{oil} = 3 \text{ cP}, \dot{Q} = \dot{Q}_{RCP,estimation} = 0.513 \text{ m}^3/\text{h}$$

$$\Rightarrow \Delta P_{RCP} = 0.7624 \cdot \left(\frac{\rho^2{}_{mix}}{10000}\right) \cdot \left(\frac{1}{\mu_{mix}}\right)^{0.1097} \cdot \dot{Q}_{RCP}^{2.1554} = 0.7624 \cdot \left(\frac{820^2}{10000}\right) \cdot \left(\frac{1}{3}\right)^{0.1097} \cdot 0.513^{2.1554} = 10.78$$

$$\Rightarrow \Delta P_{RCP,estimation} = 10.78 \text{ bar}$$

## 5) Calculation of the Cross-sectional area and diameter of the equivalent orifice hole

In order to estimate the corresponding diameter of the equivalent orifice valve, it is considered that the orifice valve is fully open and as a result $a = 1$. The valve is fully open when only oil is passing through the valve, and therefore in this condition, it can be written that:

$$\rho_{mix} = \rho_{oil} = 820 \text{ kg/m}^3 \text{ and } \mu_{mix} = \mu_{oil} = 3 \text{ cP}$$

Moreover, for a thin orifice plate, $C_d \approx 0.61$[77] and by using Equation 5.14 it can be written that:

$$A_{orifice} = A_2 = \frac{20 \times \left[\frac{10.78 \times 10^5}{10^5 \times 0.7624 \times (820^2/10000) \times (1/3)^{0.1097}}\right]^{\frac{1}{2.1554}}}{3600 \times 0.61 \times \sqrt{\frac{2 \times 10.78 \times 10^5}{820}}} = 9.1 \times 10^{-5} \text{ m}^2$$

$$\Rightarrow d_{orifice} = \sqrt{\frac{4A_2}{\pi}} = \sqrt{\frac{4 \times 9.1 \times 10^{-5}}{\pi}} = 0.0108m = 10.8 \text{ mm}$$

## 6) Calculation of the pressure drawdown and outlet pressure of the tubing

In order to calculate the pressure drawdown for the well 16/2-D-12, $\dot{Q}_{oil}$, $\Delta P_{pipe,friction}$, $J$ and $\Delta P_{RCP,average}$ were calculated in sub-chapters 5.3.25.4, 5.5 and 5.7 respectively as:

$$\dot{Q}_{oil} = \dot{Q}_{oil,estimation} = 3200 \text{ m}^3/\text{d}$$
$$\Delta P_{pipe,friction} = 2.1 \text{ bar}$$
$$J = 46133 \text{ m}^3/\text{d/bar}$$
$$\Delta P_{RCP,average} = \Delta P_{RCP,estimation} = 10.78 \text{ bar}$$

Therefore, the pressure drawdown for the well 16/2-D-12 in JSF based on estimated oil production of 20000 bbl/d = 3200 $m^3$/d and considering 260 TR7 RCP valves for this well, can be calculated by using Equation 5.22. Moreover, the outlet pressure of the tubing for the well 16/2-D-12 used for developing the OLGA/ROCX model can be calculated by Equation 3.21 as:

$$\Delta P_{drawdown} = \Delta P_{RCP,average} + \frac{\Delta P_{pipe,friction}}{2} + \frac{\dot{Q}_{oil,estimation}}{J} = 10.78 + \frac{2.1}{2} + \frac{3200}{46133} = 11.9 \text{ bar} \approx 12 \text{ bar}$$

Moreover, the outlet pressure of production tubing in the OLGA/ROCX model is calculated as:

$$P_{tubing,outlet} = P_{reservior} - \Delta P_{drawdown} = 240 - 12 = 228 \text{ bar}$$

# Appendix I: List of the production wells in the JSF

| Well path name | Drilling | Drilling End | purpose | Contents |
|---|---|---|---|---|
| 16/2 D-1 | | | PRODUCTION | |
| 16/2 D-2 | | | PRODUCTION | |
| 16/2 D-3 | | | PRODUCTION | |
| 16/2 D-4 | | | PRODUCTION | |
| 16/2 D-5 | | | PRODUCTION | |
| 16/2 D-6 | 02/24/2020 | | PRODUCTION | |
| 16/2 D-7 | | | PRODUCTION | |
| 16/2 D-8 | | | PRODUCTION | |
| 16/2 D-9 | 04/21/2016 | 06/25/2016 | PRODUCTION | OIL |
| 16/2 D-10 | 04/14/2016 | 08/14/2016 | PRODUCTION | OIL |
| 16/2 D-11 | 03/04/2016 | 03/31/2016 | PRODUCTION | OIL |
| 16/2 D-12 | 04/24/2016 | 05/06/2016 | PRODUCTION | OIL |
| 16/2 D-13 | 04/10/2016 | 02/08/2016 | PRODUCTION | OIL |
| 16/2 D-14 | 08/21/2016 | 01/11/2016 | PRODUCTION | OIL |
| 16/2 D-15 | 04/17/2016 | 07/15/2016 | PRODUCTION | OIL |
| 16/2 D-16 | 08/25/2016 | 10/25/2016 | PRODUCTION | OIL |
| 16/2 D-17 | | | PRODUCTION | |
| 16/2 D-18 | 01/08/2020 | 02/09/2020 | PRODUCTION | OIL |
| 16/2 D-19 | | | PRODUCTION | |
| 16/2 D-20 | | | PRODUCTION | |
| 16/2 D-22 | | | OBSERVATION | |
| 16/2 D-23 | | | PRODUCTION | |
| 16/2 D-32 | | | PRODUCTION | |

From [64].

# Appendix J: MATLAB code for calculating the pressure drop

```
clear
clc

D=0.1397; % m
Rho=820; % kg/m^3
Mu=3; % cp
Mu=3*0.001; % pa.s
Eps=15e-6; % m
Qdot=20000; % b/d
L=1612; % m
k=124;
j=round(L/k); % number of sections
Qdot_i=Qdot/j;

for i=1:j
Qdot_s=i*Qdot_i*0.16/(3600*24); % m3/s
A=3.14*D^2/4; % m^2
V=Qdot_s/A; % m/s
Re=Rho*V*D/Mu;
syms f % Darcy friction factor
eq= 1/sqrt(f)==1.74-2*log10((2*Eps/D)+(18.7/(Re*sqrt(f)))); % Colebrook-White equation
f=vpasolve(eq,f);
Delta_P(i)=((f*Rho*k*V^2)/(2*D))*1e-5;
end

Delta_P=sum(Delta_P(:)) % bar
```

```
Delta_P =

2.0667
```

# Appendix K: Application of GetData Graph Digitizer for extracting data

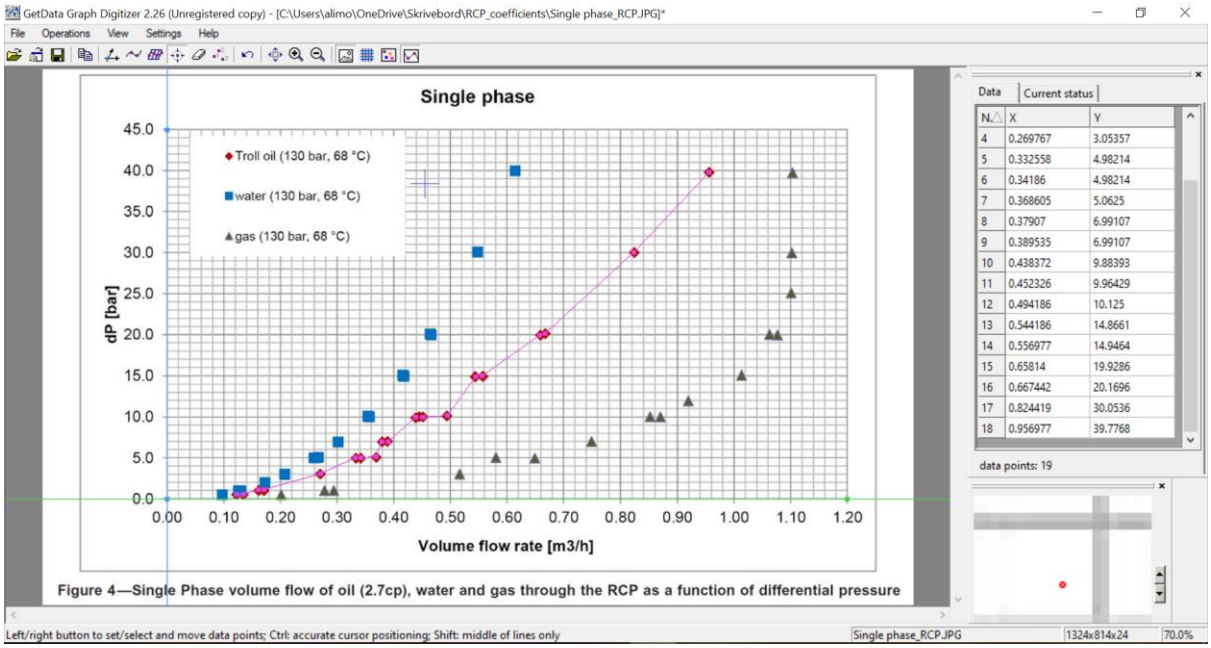

# Appendix L: MATLAB code for developing the mathematical model of RCPs

```
clear
clc
Rho_oil=890; % kg/m3
Mu_oil=2.7; % cP
Mu_cal=1
Rho_cal=10000
Q_oil=[0.12;0.13;0.16;0.17;0.27;0.33;0.34;0.37;0.38;0.39;0.44;0.45;0.49;...
    0.54;0.56;0.66;0.67;0.82;0.96]; % oil flow rate_single phase _experimental data
DP_oil=[0.48;0.56;1.04;1.04;3.05;4.98;4.98;5.06;6.99;6.99;9.88;9.96;10.13;14.87;14.95;...
    19.93;20.17;30.05;39.78]; % oil pressure drop across RCP_single phase _experimental data
Q_log=log10(Q_oil);
Y=log10(DP_oil*Rho_cal/(Rho_oil^2));
a=ones(19,1);
b=log10(Mu_cal/Mu_oil)*ones(19,1);
Phi=[a b Q_log];
Phi_T =Phi';
Theta=inv(Phi_T*Phi)*Phi_T*Y;
a_AICD=10^Theta(1)
y=Theta(2)
x=Theta(3)
Q_oil_curve=[0:0.01:0.96];
DP_curve_oil=a_AICD*((Rho_oil^2)/Rho_cal)*((Mu_cal/Mu_oil)^y).*(Q_oil_curve.^x);
plot(Q_oil,DP_oil,'red*',Q_oil_curve,DP_curve_oil,'black')
Rho_water=1100; % kg/m3
Mu_water=0.45; % cP
Q_water=[0.10;0.13;0.17;0.21;0.26;0.30;0.36;0.42;0.47;0.55;0.61];...
    % water flow rate_single phase _experimental data [m3/h]
DP_water=[0.48;0.88;2.01;2.97;5.06;6.99;10.04;15.03;20.09;30.13;40.02];...
    % water pressure drop across RCP_single phase _experimental data [bar]
Q_water_curve=[0:0.01:0.72];
DP_curve_water=a_AICD*((Rho_water^2)/Rho_cal)*((Mu_cal/Mu_water)^y).*(Q_water_curve.^x);
hold on
plot(Q_water,DP_water,'blue*',Q_water_curve,DP_curve_water,'green')
```

```
Mu_cal =

     1


Rho_cal =

     10000


a_AICD =

    0.7624


y =

    0.1097


x =

    2.1554
```

# Appendix M: MATLAB code for calculating the valve opening and control table

```
clear
clc
WC=[0:0.05:1];
Rho_water=971; % kg/m3
Rho_oil=820; % kg/m3
Mu_water=0.361; % cp
Mu_oil=3; % cp
Rho_mix=WC.*Rho_water+(1-WC).*Rho_oil; % kg/m3
Mu_mix=WC.*Mu_water+(1-WC).*Mu_oil; % cp
DP=10.78; % bar
Q=(10.78./(0.7624*((Rho_mix.^2)/10000).*((1./Mu_mix).^0.1097))).^(1/2.1554); % m3/h
Number_valve=20;
Q_valve=Number_valve*Q/3600; % m3/s
DP_valve=DP*10^5;
CD=0.61;
A_orifice=Q_valve./(CD*sqrt(2*DP_valve./Rho_mix));
d_orifice_initial=sqrt(4*A_orifice(1)/3.14)
valve_opening_signal=A_orifice./A_orifice(1);
plot(WC,valve_opening_signal)
for i=0:20
    j=2*i+1;
    k=2*i+2;
control_table(j)=WC(i+1);
control_table(k)=valve_opening_signal(i+1);
end
control_table
```

```
d_orifice_initial =

    0.0108

control_table =

  Columns 1 through 7

         0    1.0000    0.0500    0.9938    0.1000    0.9876    0.1500

  Columns 8 through 14

    0.9813    0.2000    0.9750    0.2500    0.9686    0.3000    0.9621

  Columns 15 through 21

    0.3500    0.9556    0.4000    0.9489    0.4500    0.9420    0.5000

  Columns 22 through 28

    0.9350    0.5500    0.9278    0.6000    0.9203    0.6500    0.9125

  Columns 29 through 35

    0.7000    0.9043    0.7500    0.8956    0.8000    0.8863    0.8500

  Columns 36 through 42

    0.8761    0.9000    0.8646    0.9500    0.8514    1.0000    0.8352
```

# Appendix N: MATLAB code for creating values for implementing heterogeneity

```
clear all
clc
nx=13; ny=25; nz=15;
permx=22200*ones(1,13);
permy=22200*ones(1,25);
permz=6400*ones(1,15);
counter=1;
for k=1:nz
    for j=1:ny
        for i=1:nx
            if i==2 && (k==3 || k==4 || k==5 || k==6 || k==7 || k==8 || k==9 || k==10 || k==11)
                array(:,:,counter)=[44400 44400 12800];
            elseif i==11 && (k==1 || k==2 || k==3 || k==4 || k==5 || k==6 || k==7 || k==8 || k==9 || k==10 || k==11 || k==12 || k==13)
                array(:,:,counter)=[33300 33300 9600];
            elseif k==14 && (i==6 || i==7 || i==8 || i==9 )
                array(:,:,counter)=[44400 44400 12800];
            elseif k==13 && (i==3 || i==4)
                array(:,:,counter)=[33300 33300 9600];
            elseif (i==4 && (k==7 || k==8)) || (i==5 && (k==8 || k==9)) || (i==6 && (k==9 || k==10)) || (i==7 && (k==10 || k==11)) || (i==8 && k==11)
                array(:,:,counter)=[55500 55500 16000];
            else
            array(:,:,counter)=[permx(i) permy(j) permz(k)];
            end
            counter=counter+1;
        end
    end
end
array_x=array(:,1,:);
array_y=array(:,2,:);
array_z=array(:,3,:);
dlmwrite('ijk_permx.txt',array_x)
dlmwrite('ijk_permy.txt',array_y)
dlmwrite('ijk_permz.txt',array_z)
```

# Appendix O: Reservior model in ROCX

```
#  Version: 2016.1.1.0
#  Input file created by Input File Editor.
#  5/13/2020 11:50:58 PM


*GEOMETRY RECTANGULAR


#  Number of grid blocks in horizontal and vertical direction
#  ----------------------------------------------------------
#  nx   ny   nz
   13   25   15


   dx   const   124
   dy   j   9.5   9   8   7   6   5   4   3   2.5   2   2   1.5   1   1.5   2   2   2.5   3   4   5
   6   7   8   9   9.5
   dz   k   2   2   1.5   1   1.5   2   2   2.5   3   4   5   6   7   8   8


#  Direction vector for gravity
#  ----------------------------
#  gx   gy   gz
   0   0   1


*FLUID_PARAMETERS


   blackoil


#  Black oil option data
#  ---------------------
   gormodel   Lasater
   massfrac
```

```
   rsgo_bp_tuning off

   oilvisc_tuning on

   gor    44
   gasspecificgravity    0.64
   oilspecificgravity    0.82
   oilvisc    3
   visctemp    81
   viscpress    240

#   Black oil component data
#   ------------------------
   ncomp    3

   label    BO_Oil_0
   type    oil
   oilspecificgravity    0.82

   label    BO_Gas_0
   type    gas
   gasspecificgravity    0.64
#      h2smolefraction    Not used
#      co2molefraction    Not used
#      n2molefraction    Not used

   label    BO_Water_0
   type    water
   waterspecificgravity    0.97


#   Black oil feed data
```

```
#  ------------------
   nfeed    2

   label    Feed_Oil
   oilcomponent    BO_Oil_0
   gascomponent    BO_Gas_0
   gor    44

   watercomponent    BO_Water_0
   watercut    0.0001
   label    Feed_Water
   oilcomponent    BO_Oil_0
   gascomponent    BO_Gas_0
   glr    0.0001

   watercomponent    BO_Water_0
   watercut    0.99

*RESERVOIR_PARAMETERS

#  Permeability (mDarcy) in principal directions
#  ---------------------------------------------
   permx    const    22200
   permy    const    22200
   permz    const    6400

#  Porosity
#  --------
   por    const    0.27

#              compr    reference_pressure
   rock_compr    0    0
```

```
# swc   sor   sgr
  0.12   0.05   0

  stone

  table

# som   krowc
  0.05   1

# $GUI krwoc=0.4   nw=2
  krw
  0   0
  0.12   0
  0.15   0.000522572216577153
  0.2   0.00371606909565975
  0.25   0.00981274495572652
  0.3   0.0188125997967775
  0.35   0.0307156336188126
  0.4   0.0455218464218319
  0.45   0.0632312382058354
  0.5   0.083843808970823
  0.55   0.107359558716795
  0.6   0.133778487443751
  0.65   0.163100595151691
  0.7   0.195325881840616
  0.75   0.230454347510524
  0.8   0.268485992161417
  0.85   0.309420815793294
  0.9   0.353258818406155
  0.95   0.4
```

1 1 /

# $GUI krgom=1 ng=2

krg

0 0

0.05 0.00277008310249308

0.1 0.0110803324099723

0.15 0.0249307479224377

0.2 0.0443213296398892

0.25 0.0692520775623269

0.3 0.0997229916897507

0.35 0.135734072022161

0.4 0.177285318559557

0.45 0.224376731301939

0.5 0.277008310249307

0.55 0.335180055401662

0.6 0.398891966759003

0.65 0.46814404432133

0.7 0.542936288088643

0.75 0.623268698060942

0.8 0.709141274238227

0.85 0.800554016620499

0.9 0.897506925207757

0.95 1

1 1 /

# $GUI krowc=1 now=4

krow

0 1

0.12 1

0.15 0.863073095232341

0.2 0.666703421724506

0.25 0.50591760294259

```
0.3    0.37613267018022
0.35    0.273081721538358
0.4    0.192813921925304
0.45    0.131694503056693
0.5    0.0864047634554961
0.55    0.0539420684520213
0.6    0.0316198501839119
0.65    0.0170676075961473
0.7    0.00823090644104327
0.75    0.00337137927825132
0.8    0.0010667254747592
0.85    0.000210711204890706
0.9    1.3169450305669E-05
0.95    0
1    0    /

krog
0    1
1    0    /

Pcow
0.12    1
1    0    /

Pcgo
0    0
0.95    1    /

*BOUNDARY_CONDITIONS

manual

#    Injection flow rates
```

```
#  --------------------
#  nsource
   0

#  ix   iy   iz   ntime   time   mw   mo   mg   temp

#  Production pressures
#  --------------------
#  npres_bou
   14

#  i   j   k   idir   type   name   ntime   time   pres_bou   temp_bou   Sw_bou   So_bou   Sg_bou   Feeds
   1-13   1-25   15   3   res   I1   1   0   240   81   1   0   0   [Feed_Water 1]
#  i   j   k   idir   type   rw   name   ntime   time   skin   WIFoil   WIFgas   WIFwater   pres_bou   temp_bou
Sw_bou   So_bou   Sg_bou
   13   13   4   1   well   0.2159   P13   1   0   0   1   1   1   240   81   0.062   0.938   0   [Feed_Oil 1]
   12   13   4   1   well   0.2159   P12   1   0   0   1   1   1   240   81   0.062   0.938   0   [Feed_Oil 1]
   11   13   4   1   well   0.2159   P11   1   0   0   1   1   1   240   81   0.062   0.938   0   [Feed_Oil 1]
   10   13   4   1   well   0.2159   P10   1   0   0   1   1   1   240   81   0.062   0.938   0   [Feed_Oil 1]
   9   13   4   1   well   0.2159   P9   1   0   0   1   1   1   240   81   0.062   0.938   0   [Feed_Oil 1]
   8   13   4   1   well   0.2159   P8   1   0   0   1   1   1   240   81   0.062   0.938   0   [Feed_Oil 1]
   7   13   4   1   well   0.2159   P7   1   0   0   1   1   1   240   81   0.062   0.938   0   [Feed_Oil 1]
   6   13   4   1   well   0.2159   P6   1   0   0   1   1   1   240   81   0.062   0.938   0   [Feed_Oil 1]
   5   13   4   1   well   0.2159   P5   1   0   0   1   1   1   240   81   0.062   0.938   0   [Feed_Oil 1]
   4   13   4   1   well   0.2159   P4   1   0   0   1   1   1   240   81   0.062   0.938   0   [Feed_Oil 1]
   3   13   4   1   well   0.2159   P3   1   0   0   1   1   1   240   81   0.062   0.938   0   [Feed_Oil 1]
   2   13   4   1   well   0.2159   P2   1   0   0   1   1   1   240   81   0.062   0.938   0   [Feed_Oil 1]
   1   13   4   1   well   0.2159   P1   1   0   0   1   1   1   240   81   0.062   0.938   0   [Feed_Oil 1]

*INITIAL_CONDITIONS

#  Feed
   feed const [Feed_Oil 1] /
```

```
manual

#  Saturations
#  ----------
   sw   k   0.062   0.062   0.062   0.062   0.062   0.062   0.062   0.062   0.062   0.062   0.062   0.062   0.322
0.322   0.322
   so   k   0.938   0.938   0.938   0.938   0.938   0.938   0.938   0.938   0.938   0.938   0.938   0.938   0.678
0.678   0.678
   sg   const   0

#  Pressures
#  ---------
   Po   const   240

#  Temperatures
#  ------------
   T   const   81

*TEMPERATURE off

*INTEGRATION

#  tstart   tstop
   0   0

#  dtmin   dtmax   dtstart   dtfac   cflfac
   0.1   20   0.1   10   1

implicit Linsolver

*WELL_COUPLING_LEVEL
   2
```

```
*OUTPUT

#  cof_time   cof_rate
   1   1

#  ntplot
   13
   P13
   P12
   P11
   P10
   P9
   P8
   P7
   P6
   P5
   P4
   P3
   P2
   P1

   Dt_Trend
   0   86400   /

   Dt_Prof
   0   259200   /

   screen_info   0

*END
```

# Appendix P: Well model in OLGA

## 1. Introduction

| | |
|---|---|
| **Project** | MASTER'S THESIS |
| **Case description** | RCP-case1 |
| **Date** | |
| **Author** | ALI MORADI |
| **PVT File** | ./3phase.tab |

## 2. Simulation Options

| | | |
|---|---|---|
| **Overall setting** | Flow model | OLGA |
| | Mass eq scheme | 1STORDER |
| | Compositional model | BLACKOIL |
| | Debug | ON |
| | Drilling | OFF |
| | Phase | THREE |
| | Elastic walls | OFF |
| | Void in slug | SINTEF |
| | Steady state | OFF |
| | User defined plug-in | OFF |
| | Temp. calc. | WALL |
| | Wax deposition | OFF |
| | Restart | OFF |
| **Integration** | Simulation starttime | 0 s |
| | Simulation stoptime | 250 d |
| | Minimum time step | 1 s |
| | Maximum time step | 3600 s |

## 3. System Layout - Graphics

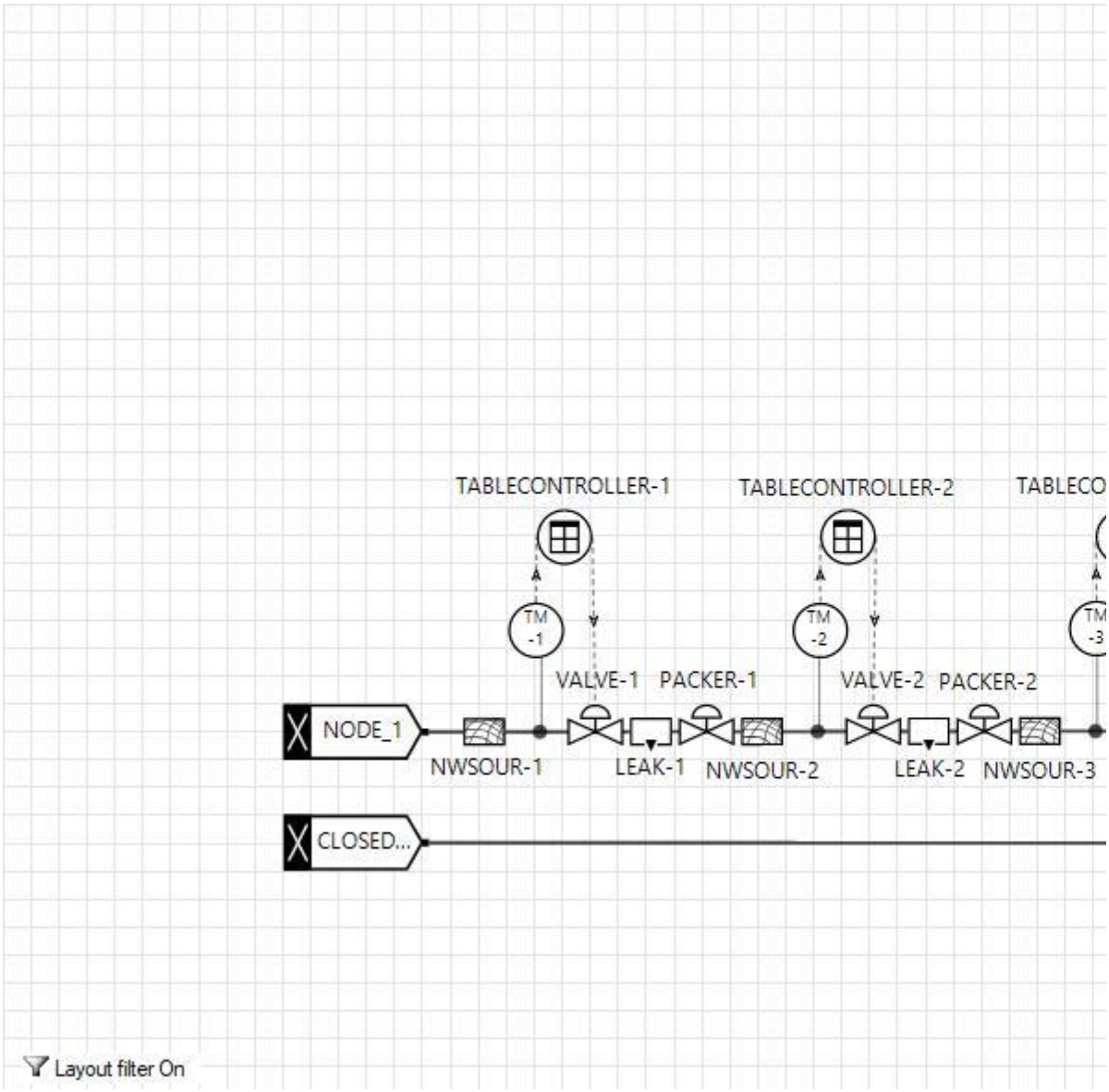


## 4. System Layout - Table

### 4.1 Summary

#### 4.1.1 Overall

| No. of Branches | No. of Pipes | No. of Sections |
|---|---|---|
| 2 | 2 | 78 |

#### 4.1.2 Flows

| Branches | No. of Pipes | No. of Sections | Min. Section Length | At | Max. Section Length | At |
|---|---|---|---|---|---|---|

| | | | | | | |
|---|---|---|---|---|---|---|
| FLOWPATH | 1 | 26 | 62 m | PIPE-1 | 62 m | PIPE-1 |
| PIPELINE | 1 | 26 | 62 m | PIPE-1 | 62 m | PIPE-1 |

### 4.2 Layout

| Pipe no. | Branch | Label | Diameter | Roughness | XEnd | YEND | Wall |
|---|---|---|---|---|---|---|---|
| 1 - 1 | FLOWPATH | PIPE-1 | 0.14 M | 0.015 mm | 1612 m | 0 M | WALL-1 |
| 2 - 1 | PIPELINE | PIPE-1 | 0.216 M | 0.015 mm | 1612 m | 0 M | WALL-1 |

## 5. Insulation and Walls

### 5. 1 Material

| Label | Density | Conductivity | Heat Capacity |
|---|---|---|---|
| MATER-1 | 7850 kg/m3 | 50 W/m-C | 500 J/kg-C |
| MATER-2 | 2500 kg/m3 | 1 W/m-C | 880 J/kg-C |

### 5. 2 Walls

| Label | Material | Wall thickness | Elastic |
|---|---|---|---|
| WALL-1 | MATER-1 | 0.009 m | OFF |
| | MATER-2 | 0.02 m | |
| | MATER-2 | 0.02 m | |
| WALL-2 | MATER-1 | 0.0075 m | OFF |
| | MATER-2 | 0.02 m | |
| | MATER-2 | 0.02 m | |

## 6. Boundary Conditions

### 6. 1 Nodes

| Label | Type | Pressure | Temperature | GMF |
|---|---|---|---|---|
| CLOSED_3 | CLOSED | | | -1 |
| OUTLET | PRESSURE | 228 bara | 81 C | -1 |
| NODE_2 | CLOSED | | | -1 |

| | | | | |
|---|---|---|---|---|
| NODE_1 | CLOSED | | | -1 |

### 6. 2 Heattransfer

| Branch | Pipe | Interpolation | Houteroption. | Hambient | Tambient |
|---|---|---|---|---|---|
| FLOWPATH | PIPE-1 | SECTIONWISE | AIR | | 81 C |
| PIPELINE | PIPE-1 | SECTIONWISE | AIR | 1E-06 W/m2-C | 81 C |

### 6. 3 Initial Conditions

| Branch | Pipe | Mass Flow | VoidFraction | WaterCut |
|---|---|---|---|---|
| FLOWPATH | ALL | 0 | 1 - | 0 |
| PIPELINE | PIPE-1 | 0 | 1 - | 0 |

## 7. Equipment

### 7. 1 Valves

| Label | Branch | Pipe | Section | Diameter | Opening | CD |
|---|---|---|---|---|---|---|
| VALVE-1 | PIPELINE | PIPE-1 | 2 | 0.011 m | 1 | 0.61 - |
| PACKER-1 | PIPELINE | PIPE-1 | 3 | 0.12 m | 0 | 0.84 |
| VALVE-2 | PIPELINE | PIPE-1 | 4 | 0.011 m | 1 | 0.61 - |
| VALVE-3 | PIPELINE | PIPE-1 | 6 | 0.011 m | 1 | 0.61 - |
| VALVE-5 | PIPELINE | PIPE-1 | 10 | 0.011 m | 1 | 0.61 - |
| VALVE-6 | PIPELINE | PIPE-1 | 12 | 0.011 m | 1 | 0.61 - |
| VALVE-8 | PIPELINE | PIPE-1 | 16 | 0.011 m | 1 | 0.61 - |
| VALVE-9 | PIPELINE | PIPE-1 | 18 | 0.011 m | 1 | 0.61 - |
| VALVE-10 | PIPELINE | PIPE-1 | 20 | 0.011 m | 1 | 0.61 - |
| VALVE-11 | PIPELINE | PIPE-1 | 22 | 0.011 m | 1 | 0.61 - |
| VALVE-12 | PIPELINE | PIPE-1 | 24 | 0.011 m | 1 | 0.61 - |
| VALVE-13 | PIPELINE | PIPE-1 | 26 | 0.011 m | 1 | 0.61 - |
| PACKER-2 | PIPELINE | PIPE-1 | 5 | 0.12 m | 0 | 0.84 |
| PACKER-3 | PIPELINE | PIPE-1 | 7 | 0.12 m | 0 | 0.84 |
| VALVE-4 | PIPELINE | PIPE-1 | 8 | 0.011 m | 1 | 0.61 - |
| VALVE-7 | PIPELINE | PIPE-1 | 14 | 0.011 m | 1 | 0.61 - |

| | | | | | | |
|---|---|---|---|---|---|---|
| PACKER-4 | PIPELINE | PIPE-1 | 9 | 0.12 m | 0 | 0.84 |
| PACKER-5 | PIPELINE | PIPE-1 | 11 | 0.12 m | 0 | 0.84 |
| PACKER-6 | PIPELINE | PIPE-1 | 13 | 0.12 m | 0 | 0.84 |
| PACKER-7 | PIPELINE | PIPE-1 | 15 | 0.12 m | 0 | 0.84 |
| PACKER-8 | PIPELINE | PIPE-1 | 17 | 0.12 m | 0 | 0.84 |
| PACKER-9 | PIPELINE | PIPE-1 | 19 | 0.12 m | 0 | 0.84 |
| PACKER-10 | PIPELINE | PIPE-1 | 21 | 0.12 m | 0 | 0.84 |
| PACKER-11 | PIPELINE | PIPE-1 | 23 | 0.12 m | 0 | 0.84 |
| PACKER-12 | PIPELINE | PIPE-1 | 25 | 0.12 m | 0 | 0.84 |

### 7. 2 Position

| Label | Branch | Pipe | Section |
|---|---|---|---|
| POS-1 | FLOWPATH | PIPE-1 | 2 |
| POS-2 | FLOWPATH | PIPE-1 | 4 |
| POS-3 | FLOWPATH | PIPE-1 | 6 |
| POS-4 | FLOWPATH | PIPE-1 | 8 |
| POS-5 | FLOWPATH | PIPE-1 | 10 |
| POS-6 | FLOWPATH | PIPE-1 | 12 |
| POS-7 | FLOWPATH | PIPE-1 | 14 |
| POS-8 | FLOWPATH | PIPE-1 | 16 |
| POS-9 | FLOWPATH | PIPE-1 | 18 |
| POS-10 | FLOWPATH | PIPE-1 | 20 |
| POS-11 | FLOWPATH | PIPE-1 | 22 |
| POS-12 | FLOWPATH | PIPE-1 | 24 |
| POS-13 | FLOWPATH | PIPE-1 | 26 |

## 8. Signal Connections

| From | Out | To | In |
|---|---|---|---|
| TABLECONTROLLER-1 | ISACTIVE_1 | VALVE-1 | VALVESIG |

| | | | |
|---|---|---|---|
| TM-1 | OUTSIG_1 | TABLECONTROLLER-1 | INPSIG |
| TABLECONTROLLER-2 | ISACTIVE_1 | VALVE-2 | VALVESIG |
| TM-2 | OUTSIG_1 | TABLECONTROLLER-2 | INPSIG |
| TM-3 | OUTSIG_1 | TABLECONTROLLER-3 | INPSIG |
| TABLECONTROLLER-3 | ISACTIVE_1 | VALVE-3 | VALVESIG |
| TM-5 | OUTSIG_1 | TABLECONTROLLER-5 | INPSIG |
| TABLECONTROLLER-5 | ISACTIVE_1 | VALVE-5 | VALVESIG |
| TM-6 | OUTSIG_1 | TABLECONTROLLER-6 | INPSIG |
| TABLECONTROLLER-6 | ISACTIVE_1 | VALVE-6 | VALVESIG |
| TM-7 | OUTSIG_1 | TABLECONTROLLER-7 | INPSIG |
| TM-8 | OUTSIG_1 | TABLECONTROLLER-8 | INPSIG |
| TABLECONTROLLER-8 | ISACTIVE_1 | VALVE-8 | VALVESIG |
| TM-9 | OUTSIG_1 | TABLECONTROLLER-9 | INPSIG |
| TABLECONTROLLER-9 | ISACTIVE_1 | VALVE-9 | VALVESIG |
| TM-10 | OUTSIG_1 | TABLECONTROLLER-10 | INPSIG |
| TABLECONTROLLER-10 | ISACTIVE_1 | VALVE-10 | VALVESIG |
| TM-11 | OUTSIG_1 | TABLECONTROLLER-11 | INPSIG |
| TABLECONTROLLER-11 | ISACTIVE_1 | VALVE-11 | VALVESIG |
| TM-12 | OUTSIG_1 | TABLECONTROLLER-12 | INPSIG |
| TABLECONTROLLER-12 | ISACTIVE_1 | VALVE-12 | VALVESIG |
| TM-13 | OUTSIG_1 | TABLECONTROLLER-13 | INPSIG |
| TABLECONTROLLER-13 | ISACTIVE_1 | VALVE-13 | VALVESIG |
| TM-4 | OUTSIG_1 | TABLECONTROLLER-4 | INPSIG |
| TABLECONTROLLER-4 | ISACTIVE_1 | VALVE-4 | VALVESIG |
| TABLECONTROLLER-7 | ISACTIVE_1 | VALVE-7 | VALVESIG |